Graduate School Form 30
(Revised 08/14)

PURDUE UNIVERSITY
GRADUATE SCHOOL
Thesis/Dissertation Acceptance

This is to certify that the thesis/dissertation prepared

By Sourav Pramanik

Entitled
CHARGE OPTIMIZATION OF LITHIUM-ION BATTERIES FOR ELECTRIC-VEHICLE APPLICATION

For the degree of Master of Science in Engineering

Is approved by the final examining committee:

Sohel Anwar

Tamar Wasfy

Lingxi Li

To the best of my knowledge and as understood by the student in the Thesis/Dissertation Agreement, Publication Delay, and Certification/Disclaimer (Graduate School Form 32), this thesis/dissertation adheres to the provisions of Purdue University's "Policy on Integrity in Research" and the use of copyrighted material.

Sohel Anwar

Approved by Major Professor(s): _____

_____

Approved by: Sohel Anwar 02/18/2015

Head of the Department Graduate Program Date

CHARGE OPTIMIZATION OF LITHIUM-ION BATTERIES FOR ELECTRIC-VEHICLE APPLICATION

A Thesis

Submitted to the Faculty

of

Purdue University

by

Sourav Pramanik

In Partial Fulfillment of the

Requirements for the Degree

of

Master of Science in Engineering

May 2015

Purdue University

Indianapolis, Indiana

I would like to dedicate this work to my family and my wife Neha Ratnalikar.

ACKNOWLEDGMENTS

I would like to express my deepest appreciation to my committee chair, Professor Sohel Anwar, who has always been instrumental and articulate in guiding me throughout the course of this research. He has continuously and persuasively conveyed the spirit of adventure in regard to research, and an excitement in regard to teaching. Without his supervision and constant help this thesis would not have been possible.

I would like to thank my committee members, Professor Tamar Wasfy and Professor Lingxi Li, whose work demonstrated to me that concern for global affairs supported by an engagement in comparative literature and modern technology, should always transcend academia and provide a quest for our times.

I would like to thank my wife Neha Ratnalikar for her support and motivation throughout the course of this work. I would also like to thank Ms. Valerie Lim Diemer, Mr. Mark Senn and Ms. Sara Vitaniemi for their help and assistance throughout the tenure of my masters program. Last but not the least, I would like to thank all my co-workers and friends who have always been a source of knowledge and inspiration to me.

PREFACE

With the advent of time and recent achievements in technology, there is a need for efficient source and use of energy. Apart from conventional and traditional forms of energy sources, there is a tremendous need for mobile high density energy sources to provide sustainable forms of energy. Lithium Ion is one such promising technology which has vast potentials to suffice the need of ever increasing energy demands. Lithium ion has certain added benefits over other energy sources which gives it a higher edge over other sources.

Thus said, there is a urge to design better controls to charge and discharge the energy cells. In this work the challenges and methods of charging a Lithium Ion cell is studied and a better method is proposed to add some benefit to the process. The work is done to achieve a better performance in whole, rather than achieving only a specific goal. In this work a method to charge a Lithium Ion cell is described which is designed to charge the battery in shortest time while maintaining the chemistry and structure of the battery intact, so that the battery is not degraded beyond a specific limit. This helps in achieving a balanced performance while delivering efficiency along with longevity.

TABLE OF CONTENTS

Page

LIST OF TABLES

LIST OF FIGURES

Figure Page

Appendix Figure

SYMBOLS

a	inter-facial surface area
A	cross-sectional area of an electrochemical cell
$C_{e,i}$	concentration in electrolyte phase
$C_{s,i}$	concentration in solid phase
D_e	diffusion coefficient of electrolyte
D_s	diffusion coefficient of solid
$f_{+/-}$	mean molar activity coefficient of electrolyte
F	Faraday's constant
i_n	transfer current at the surface of active material
i_o	exchange current density
L_i	thickness of electrode/separator
Q	charge capacity
R	universal gas constant
T	temperature
α_a, α_c	anodic and cathodic transfer coefficient
ϵ_i	volume fraction
κ_i	ionic conductivity in electrolyte
σ_i	ionic conductivity in solid matrix
$\phi_{s,i}$	potential in solid matrix
$\phi_{e,i}$	potential in electrolyte
ρ	material density

ABBREVIATIONS

DOH	degree of hybridization
EV	electric vehicle
PHEV	plug-in hybrid electric vehicle
GHG	green house gases
ICE	internal combustion engine
KKT	Karush-Kuhn-Tucker
OCP	open circuit potential
SEI	solid electrolyte interface
SOC	state of charge
DOD	depth of discharge
SQP	sequential quadratic programming
SNOPT	Sparse Nonlinear OPTimizer
EUL	End of Useful Life
PMP	Pontryagin's Minimum Principle
CEC	Constant Electrolyte Concentration
MEC	Modeled Electrolyte Concentration
PDAE	Partial Differential Algebraic Equation
NMPC	Non-Linear Model Predictive Control
EKF	Extented Kalman Filter
ODE	Ordinary Differential Equation
PDE	Partial Differential Equation
SPM	Single Particle Model
ROM	Reduced Order Model
NOx	Oxides of Nitrogen

SOx	Oxides of Sulphur
HC	Hydrocarbons
BMS	Battery management System
PWM	Pulse Width Modulation
HJB	Hamilton-Jacobi-Bellman
RC	Resistance Capacitance

NOMENCLATURE

subscript i	Refers to Positive/Negative Electrode
subscript n	Refers to Negative Electrode
subscript p	Refers to Positive Electrode
subscript s	Refers to Separator Region
subscript e	Refers to Electrolyte Phase
subscript s	Refers to Solid Phase when not referring to separator
space node	Refers to the iterative space steps
time node	Refers to iterative time steps at which the numerical solution is done

GLOSSARY

Cathode	The Negative Terminal of the Battery. Electrons move from this terminal to the Positive terminal during regeneration process.
Anode	The positive Terminal of the Battery. Lithium Ions move from this terminal to the Negative Terminal during regeneration of the battery.
Regeneration	This is a term used to denote the state when energy is supplied to the Battery. This is the state when the battery is charged. It is called regeneration since the cell is regenerated from a depleted state to a charged state.
Regeneration Current	This is the current which is applied to the cell during a Battery Regeneration. This supplied current is responsible to charge the battery.
Load Current	This is the current which is drawn from the battery during a discharge process. The battery can only supply a rated load current for a rated time period which is stated by the C Rate of the battery.

ABSTRACT

Pramanik, Sourav. M.S.E., Purdue University, May 2015. Charge Optimization of Lithium-Ion Batteries for Electric-Vehicle Application. Major Professor: Sohel Anwar.

In recent years Lithium-Ion battery as an alternate energy source has gathered lot of importance in all forms of energy requiring applications. Due to its overwhelming benefits over a few disadvantages Lithium Ion is more sought off than any other Battery types. Any battery pack alone cannot perform or achieve its maximum capacity unless there is some robust, efficient and advanced controls developed around it. This control strategy is called Battery Management System or BMS. Most BMS performs the following activity if not all - Battery Health Monitoring, Temperature Monitoring, Regeneration Tactics, Discharge Profiles, History logging, etc. One of the major key contributor in a better BMS design and subsequently maintaining a better battery performance and EUL is Regeneration Tactics.

In this work, emphasis is laid on understanding the prevalent methods of regeneration and designing a new strategy that better suits the battery performance. A performance index is chosen which aims at minimizing the effort of regeneration along with a minimum deviation from the rated maximum thresholds for cell temperature and regeneration current. Tuning capability is provided for both temperature deviation and current deviation so that it can be tuned based on requirement and battery chemistry and parameters. To solve the optimization problem, Pontryagin's principle is used which is very effective for constraint optimization with both state and input constraints.

Simulation results with different sets of tuning shows that the proposed method has a lot of potential and is capable of introducing a new dynamic regeneration tactic

for Lithium Ion cells. With the current optimistic results from this work, it is strongly recommended to bring in more battery constraints into the optimization boundary to better understand and incorporate battery chemistry into the regeneration process.

1. INTRODUCTION

1.1 Motivation and Major Contribution of this Thesis

In the last few centuries there has been a huge technological leap in all spheres of human development. Transportation and automobile technologies have manifolded along with this race for technological improvements. Due to modern high speed transportation system, traveling across states and even overseas have become a piece of cake. While these means of transportation allow us to reach all corners of the world, they are energy intensive and depend primarily on fossil fuels. In the past half century or so, our demand for fossil fuels has steadily climbed, as both the larger population and their economic prosperity has increased [1].

These newer generation of automobiles consumes a large amount of fossil fuels and along with increases the emission of green house gasses and other toxic life threatening oxides (NOx, SOx, HCs, etc). GHG have been blamed as the main cause of anthropogenic global warming. In 2011, transportation accounted for 28% of US primary energy consumption, 93% of which came from petroleum [2]. This directly translates to 28% of GHG emissions [3]. The ability to control the amount and the sources of energy used for transportation can result in a significant reduction which accounted for GHG release into the atmosphere as well.

The difficulties in controlling the GHG emissions and the over-dependence of fossil fuels play major roles in shaping the future of transportation and pushed our limits to venture out into other technological advancements to find alternative energy solutions. The initiative to find alternative energy sources apart from conventional fossil fuels for transport use, therefore, arises from the need to address the following concerns:

- **Energy security:** Reducing dependency on fossil fuels from foreign nations. There is also the global risk of depleting the decreasing natural storage of fos-

sil fuels. There is a need to secure the future of fossil fuels and use it more conservatively.

- **Conservation:** Sustain development without negatively impacting the environment. Technological advancement and urbanization always push the natural resources to limits. There has to be trade off between conserving the nature and technological growth.

- **Revenue protection:** Maintain profitability and reduce the operating costs by insulating against fluctuating fuel prices.

To address these issues, various green technologies, such as EVs and HEVs, advanced battery technology, and alternative fuel systems, du fuel systems and even nuclear technologies have gained prominence. The development has been most obvious in the automotive industry, due to the need to improve vehicle fuel efficiency and to satisfy increasingly stringent emission standards. Spurred by the feasibility of hydrogen fuel cells and development of higher energy density batteries, EVs have been demonstrated as possible successors of traditional vehicles operating with an internal combustion engine (ICE). Various energy carriers are available to power EV of different architecture. Section 1.2 will explain various types of EVs and HEV's, while Section 1.3, talks more about Lithium Ion Cell Structure as an energy storage device. One of the main advantages of electric-powered vehicles is the significantly lower operating costs compared to ICE powered vehicles.

With this increasing trend towards utilizing more cleaner and alternate forms of energy, Lithium Ion cells showcases a very high potential in the future years. Thus there is a need to to develop a better controls around the usage and maintenance of Lithium Ion battery management systems. This Thesis work is focused on understanding and studying Lithium Ion cell as an energy storage device, developing a robust numerical framework to solve the reformulated 1-D model and verifying with a published 1-D physics based cell model, and finally developing a robust charging

algorithm to charge the Lithium Ion cell in an efficient way. The major parts of the Thesis are:

- Develop a robust 1-D Lithium Ion cell Model, which can replicate accurately the battery reactions and phenomenon. The model is so chosen so that it is fast enough in terms of computational speed along with maintaining the details of chemistry so as not to lose any performance measures,
- Develop a robust algorithm to numerically solve the governing equations,
- Develop an efficient charging scheme which will not stress the battery beyond its limits and will also charge it at a fast rate,

1.2 Hybrid/Electric Vehicle Design

Thus said, the need for alternate energy source to drive commercial vehicles is widespread. There is a huge trend towards hybridization of automobile as well as off road engines. Hybridization is also considered seriously these days for high volume engines as well, along with light duty engines (passenger cars/ pickup vans). Hybrid electric vehicles (HEVs) combine the benefits of gasoline engines and electric motors and can be configured to meet different objectives such as improved fuel economy, increased power, or additional auxiliary power for electronic devices and power tools. HEVs run on fuel alone and do not plug in to an electrical outlet to recharge the battery. The battery pack is charged utilizing engine power during regenerative braking. Though off course there are Plug-in HEV available which can be charged via, an external charging outlet.

Automobile designers follow two major conventional strategies:-

- A fully Electric configuration where the engine power is completely driven by Battery energy. Fig. 1.1
- A Hybrid configuration, where the engine is driven by both ICE and Battery Energy.

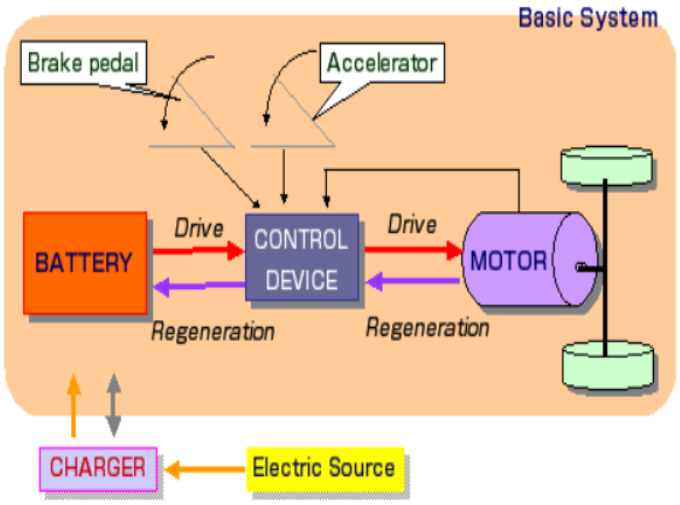

Fig. 1.1. Electric Vehicle Configuration. [4]

Hybrid electric vehicles are powered by both internal combustion engine and electric motor independently or jointly, doubling the fuel efficiency compared with a conventional vehicle. Hybrid passenger cars are achieving a substantial success in sales in Japan and in the U.S. due to the features of high fuel efficiency, low emissions and affordable price.

- **Series Hybrid System:** This configuration is designed to deliver maximum range for a single charge. The ICE is solely used to generate electricity.
- **Parallel Hybrid System:** Designed to increase fuel efficiency of ICE and to decrease exhaust emissions. The engine provides main propulsion, and the generator works in parallel to assist the engine to drive.
- **Series-Parallel Hybrid System:** Combination of series and parallel hybrid systems. The vehicle is powered by both ICE and a motor either independently or jointly.

Fig. 1.2 shows the different Hybrid Electric Vehicle system configurations. All these configurations need a robust and efficient Management System to monitor and maintain the battery source.

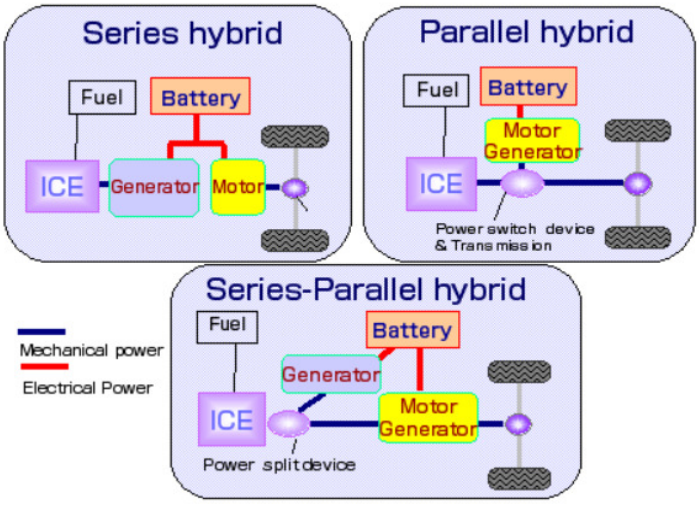

Fig. 1.2. Hybrid Electric Vehicle Configuration. [4]

1.3 Lithium-Ion Cell structure

The focus of this thesis work is to develop a Lithium-Ion cell model and design a robust charging scheme for the same. Before going into the details of charging technique and algorithm ,a brief study of the Lithium-Ion cell is done in this section. Lithium-ion has not yet reached its full maturity and the technology is continually improving. The anode in today's cell is made up of a graphite mixture and the cathode is a combination of lithium and other choice of metals. All battery materials has a theoretical energy density. With lithium-ion, the anode is well optimized and little improvements can be gained in terms of design changes. The cathode, however, shows promise for further enhancements. Battery research is therefore focusing on the cathode material. Another scope of improvement in the battery cell is the electrolyte. The electrolyte serves as a reaction medium between the anode and the cathode.

The battery industry is making incremental capacity gains of 8-10% per year. This trend is expected to continue. This, however, is a far cry from Moore's Law that specifies a doubling of transistors on a chip every 18 to 24 months. Translating this increase to a battery would mean a doubling of capacity every two years. In-

stead of two years, lithium-ion has doubled its energy capacity in 10 years. Today's lithium-ion comes in many "flavors" and the differences in the composition are mostly related to the cathode material. Fig. 1.3, below summarizes the most commonly used lithium-ion on the market today. For simplicity, we summarize the chemistry into four groupings, which are Cobalt, Manganese, NCM and Phosphate.

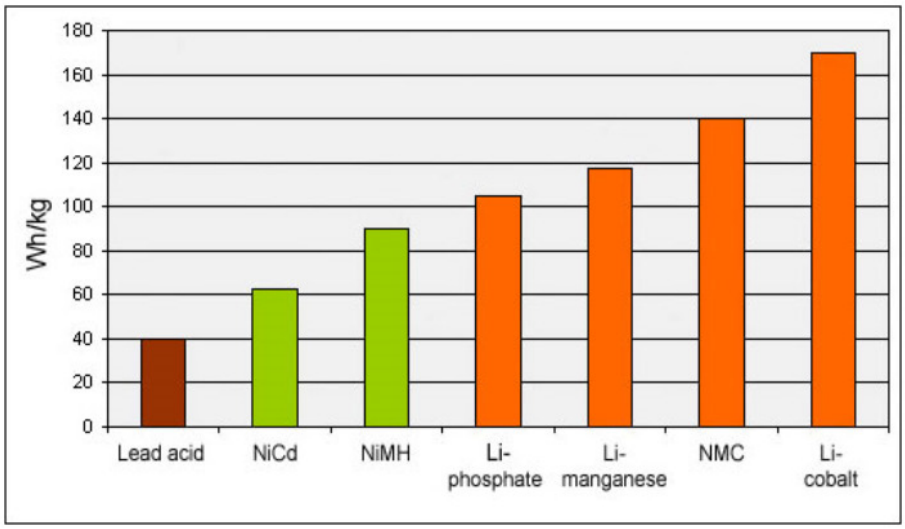

Fig. 1.3. Typical energy densities of lead, nickel and lithium-based batteries. [5]

Fig. 1.3 shows the typical energy density of different batteries as compared to Lithium-Ion.

Table. 1.1 shows the different Lithium Ion types. It states the materials used for each type along with the short names and abbreviations. It also mentions about the usage of each type.

1.3.1 Battery Chemistry

Lithium ion batteries have gained significant importance and popularity these days. The popularity of the Li-ion battery is due to the advantages offered over other secondary (or rechargeable) batteries:

Table 1.1
Reference names for Li-ion batteries. [5]

Chemical Name	Material	Abbreviation	Short Form	Notes
Lithium Cobalt Oxide	$LiCoO_2$	LCO	Li-cobalt	High capacity for cell phone laptop, camera
Lithium Manganese Oxide	$LiMn_2O_4$	LMO	Li-manganese, spinel	Most safe lower capacity than Li-cobalt but high specific power and long life
Lithium Iron Phosphate	$LiFePO_4$	LFP	Li-phosphate	
Lithium Nickel manganese Cobalt Oxide	$LiNiMnCoO_2$	NMC	NMC	
Lithium Nickel Cobalt Aluminium Oxide	$LiNiCoAlO_2$	NCA	NCA	Gaining importance in electric power-train and grid storage
Lithium Titanate	$Li_4Ti_5O_{12}$	LTO	Li-titanate	

- For the same given capacity Lithium Ion Batteries are much lighter than its counterparts,
- Lithium ion chemistry delivers a high open-circuit voltage,
- Low self-discharge rate (about 1.5% per month),
- Do not suffer from battery memory effect,
- Environmental benefits: rechargeable and reduced toxic landfill.

Even though Lithium Ion Batteries have a lot of advantage over other rechargeable batteries, they have certain disadvantages as well. Lithium Ion batteries have the inherent issues such as:

- Poor cycle life, particularly in high current applications,
- Increase in internal resistance with cycling and aging,
- Safety concerns if overheated or overcharged,
- Applications which require a higher capacity are not designed to use Lithium Ion Batteries,
- In Lithium Ion batteries, lithium ions move from the anode to cathode during discharge, and from cathode to anode when charging. The materials used for the anode and cathode can dramatically affect a number of aspects of the batterys performance, including capacity,
- New higher capacity materials are urgently required in order to address the need for greater energy density, cycle life and charge lifespan, among other issues faced by Li-ion batteries.

The Lithium Ion goes thorough a chemical process during charge and discharge cycles. During charge/regeneration process Lithium Ions move prom the Positive Electrode to Negative electrode thereby increasing the concentration and SOC at the

Negative Electrode. The reverse process happens during a discharge cycle. Overall reaction on a Lithium ion cell is given below as:

$$C + LiCoO_2 \leftrightarrow LiC_6 + Li_{0.5}CoO_2 \tag{1.1}$$

At the Cathode:

$$LiCoO_2 - Li^+ - e^- \leftrightarrow Li_{0.5}CoO_2 \Rightarrow 143mAh/g \tag{1.2}$$

At the Anode:

$$6C + Li^+ + e^- \leftrightarrow LiC_6 \Rightarrow 372mAh/g \tag{1.3}$$

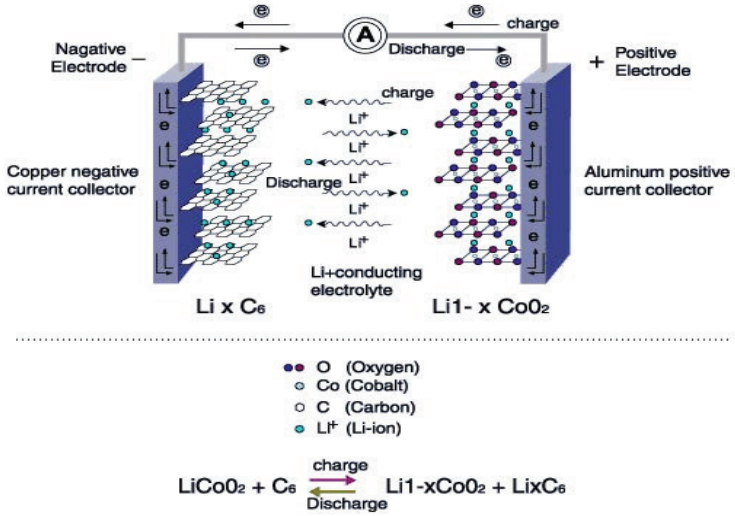

Fig. 1.4. Lithium Ion Battery Chemistry. [6]

Materials other than graphite have been investigated with silicon offering the highest gravimetric capacity (mAh/g). The volumetric capacity of silicon (Wh/cc), i.e. the capacity of silicon taking into account volume increases, resulting from lithium insertion, is still significantly higher than that associated with carbon anode materials. The potential contained within silicon holds great promise for the future of Li-ion batteries, if it can be used without compromising the battery cycle life. When charging a lithium ion battery, lithium is inserted into the silicon, causing a dramatic

increase in volume (up to 400%). On discharge, lithium is extracted from the silicon which returns to a smaller size. Repeated expansion and contraction places great strain on the silicon, causing silicon material to fracture or pulverize. This, in turn, leads to the electrical isolation of silicon fragments from nearest neighbors and a loss of conductivity in the anode of the battery. For this reason, charge-discharge cycle life for conventional silicon-based anodes is typically short.

1.3.2 Li Ion Battery Model

Mathematical modeling of lithium-ion batteries involves the specification of the dependent variables of interest (e.g., solution- phase concentration) and the first principles based derivation of governing equations for these dependent variables (based on the physics of the battery system) with specification of boundary/initial conditions and nonlinear expressions for transport/kinetic parameters. Doyle et al. [7] developed a model for a lithium-ion sandwich that consists of a porous electrode, separator, and a current collector. This model is based on the concentrated solution theory. This important effort paved the way for a number of similar models, because it is general enough to incorporate further developments in a battery system. Fig. 1.5 shows the Lithium Ion structure for the 1-D Model.

For analysis and control of lithium-ion batteries in hybrid environments (with a fuel cell, capacitor, or electrical components), there is a need to simulate state of charge, state of health, and other parameters of lithium-ion batteries in milliseconds. Rigorous physics-based models take a few seconds up to a few minutes to simulate discharge curves, depending on the solvers, routines, computers, etc. Circuit-based or empirical models (based on the past data) can be simulated in milliseconds. However, these models fail at various operating conditions, and use of these models might cause abuse or under-utilization of electrochemical power sources. This paper presents the mathematical analysis for reformulation of physics-based models and utilize this models as baseline for the battery plant to further study the charging techniques.

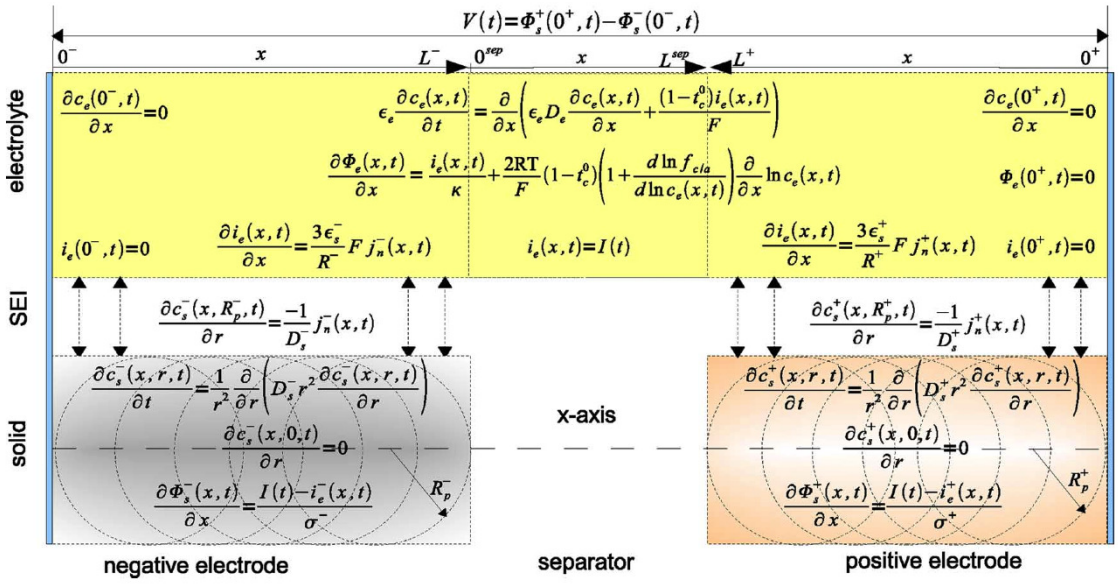

Fig. 1.5. Lithium Ion Cell Structure. [8]

Governing Equations

The state variables of the macro-homogeneous 1-D electrochemical model of a lithium ion battery are the lithium concentration $c_e(x,t)$ in the electrolyte, the lithium concentration $c_s(x,r,t)$ in the positive and negative electrodes, the potential $\phi_e(x,t)$ in the electrolyte, the potential $\phi_s(x,t)$ in the positive and negative electrodes, the ionic current $i_e(x,t)$ in the electrolyte, and the molar ionic flux $j_n(x,t)$ between the active material in the electrodes and the electrolyte. The governing equations are given by (see also [1], [7], [8])

$$\epsilon_p \frac{\partial C(x,t)}{\partial t} = D_{eff,p} \frac{\partial C(x,t)^2}{\partial x} + a_p(1-t_+^0) j_p \tag{1.4}$$

Reordering the equation we get:

$$\epsilon_e \frac{\partial C_e(x,t)}{\partial t} = \frac{\partial}{\partial x}(\epsilon_e D_e \frac{\partial C_e(x,t)}{\partial x} + \frac{1-t_+^0}{F} i_e(x,t)) \tag{1.5}$$

$$\frac{\partial C_{s,i}(x,r,t)}{\partial t} = \frac{1}{r^2}\frac{\partial}{\partial r}(D_{s,i}r^2\frac{\partial C_{s,i}(x,r,t)}{\partial r}) \tag{1.6}$$

This is further reformulated as with more simplifications as:

$$\frac{\partial C_s(t)}{\partial t} = -\frac{3}{R_p}J(t), \tag{1.7}$$

$$\frac{\partial \phi_e(x,t)}{\partial x} = -\frac{i_e(x,t)}{\kappa} + \frac{2RT}{F}(1-t_+^0)\times(1+\frac{dlnf_{c/a}(x,t)}{dlnC_e(x,t)})\frac{\partial lnC_e(x,t)}{\partial x} \tag{1.8}$$

$$\frac{\partial \phi_s(x,t)}{\partial x} = \frac{i_e(x,t)-I(t)}{\sigma} \tag{1.9}$$

$$\frac{\partial i_e(x,t)}{\partial x} = \frac{3\epsilon_s}{R_p}Fj_n(x,t) \tag{1.10}$$

$$j_n(x,t) = \frac{i_0(x,t)}{F}(e^{\frac{\alpha_a F}{RT}\eta(x,t)} - e^{\frac{\alpha_c F}{RT}\eta(x,t)}) \tag{1.11}$$

In Equation 1.11, the exchange current density $i_0(x,t)$ and the over potential $\eta(x,t)$ for the main reaction are modeled as:

$$i_0(x,t) = r_{eff}C_e(x,t)^{\alpha_c}(C_s^{max} - C_{ss}(x,t))^{\alpha_a}C_s(x,t)^{\alpha_c}, \tag{1.12}$$

$$\eta(x,t) = \phi_s(x,t) - \phi_e(x,t) - U(C_{ss}) - FR_f j_n(x,t), \tag{1.13}$$

where $c_{ss}(x,t) \approx c_s(x,R_p,t), U(c_{ss}(x,t))$ is the open circuit potential of the active material and c_s^{max} is the maximum concentration in the active material of each electrode.

The internal temperature is described by:

$$\begin{aligned}\rho^{avg}c_p\frac{dT(t)}{dt} &= h_{cell}(T_{amb}(t) - T(t)) + I(t)V(t) \\ &\quad - \int_{0^-}^{0^+}\frac{3\epsilon_s}{R_p}Fj_n(t)(U(\bar{c}_s(x,t)) - T(t)\frac{\partial U(\bar{c}_s(x,t))}{\partial T})dx,\end{aligned} \tag{1.14}$$

where, T_{amb} is the ambient temperature and $\bar{c}(x,t)$ represents the volume averaged concentration of a particle in the solid phase defined as:

$$\bar{c_s}(x,t) = \frac{3}{R_p^3}\int_0^{R_p} r^2 c_s(x,r,t)dr, \tag{1.15}$$

The initial conditions of the battery model are given by:

$c_e(x,0) = c_e^0(x)$, $c_s(x,r,0) = c_s^0(x,r)$, $T(0) = T^0$,

and the boundary conditions are given by:

$$\frac{\partial c_e(0^-,t)}{\partial x} = \frac{\partial c_e(0^+,t)}{\partial x} = 0, \tag{1.16}$$

$$c_e(L^-,t) = c_e(0^{sep},t), c_e(L^{sep},t) = c_e(L^+,t), \tag{1.17}$$

$$\epsilon_e^- D_e \frac{\partial c_e(L^-,t)}{\partial x} = \epsilon_e^{sep} D_e \frac{\partial c_e(0^{sep},t)}{\partial x}, \tag{1.18}$$

$$\epsilon_e^{sep} D_e \frac{\partial c_e(L^{sep},t)}{\partial x} = -\epsilon_e^+ D_e \frac{\partial c_e(L^+,t)}{\partial x}, \tag{1.19}$$

$$\frac{\partial c_s(x,0,t)}{\partial r} = 0, \frac{\partial c_s(x,R_p,t)}{\partial r} = -\frac{j_n(x,t)}{D_s}, \tag{1.20}$$

$$\phi_e(L^-,t) = \phi_e(0^{sep},t), \phi_e(L^{sep},t) = \phi_e(L^+,t), \tag{1.21}$$

$$\phi_e(0^+,t) = 0, \tag{1.22}$$

$$i_e(0^-,t) = i_e(0^+,t) = 0, i_e(x^{sep},t) = -I(t), \tag{1.23}$$

$$i_e(L^-,t) = -i_e(L^+,t) = -I(t), \tag{1.24}$$

where, $x^{sep} \in [0^{sep}, L^{sep}]$ represents the entire separator domain of the battery. In general, it is difficult to provide consistent initial conditions for the battery model,

hence we always initialize the model at some equilibrium state where consistent initial conditions are easily obtained.

In the above equations, ϵ_e, ϵ_s, σ, R, R_p, F, α_a, α_c, ρ_{avg}, c_p, h_{cell} and t_c^0 are model parameters and are constant in each region of the cell, while κ, $f_{c/a}$ and D_e are known functions of the electrolyte concentration. Additionally, r_{eff} ,R_f , D_s, κ, $f_{c/a}$ and D_e have an Arrhenius-like temperature dependency of the form:

$$\Theta(T) = \Theta_{T_0} e^{A_\theta \frac{T(t)-T_0}{T(t)T_0}}, \tag{1.25}$$

where, T_0 is some standard temperature and A_θ is a constant. The voltage is given by the potential difference in the solid phase at the boundaries of the electrodes:

$$V(t) = \phi_s(0^+, t) - \phi_s(0^-, t), \tag{1.26}$$

The model parameters are chosen such that the battery mimics the behavior of a mixed high energy/ high power cell. The main feature of energy cells are thicker electrodes of approximately 200m, compared to 50m in power cells. Based on the model parameters, the designed cell has a nominal capacity of 3.5Ah.

2. LITERATURE SURVEY

2.1 Introduction

In this section a comparative study of the available techniques of charging a Lithium-Ion battery is done. The Lithium-Ion charger is a voltage-limiting device that is similar to the lead acid system. The difference lies in a higher voltage per cell, tighter voltage tolerance and the absence of trickle or float charge at full charge. While lead acid offers some flexibility in terms of voltage cutoff, manufacturers of Lithium-Ion cells are very strict on the correct setting because Li-ion cannot accept overcharge. The so-called miracle charger that promises to prolong battery life and methods that pump extra capacity into the cell do not exist here. Li-ion is a clean system and only takes what it can absorb. Anything extra causes stress. Most cells charge to 4.20V/cell with a tolerance of +/50mV/cell. Higher voltages could increase the capacity, but the resulting cell oxidation would reduce service life. More important is the safety concern if charging beyond 4.20V/cell. Figure 1 shows the voltage and current signature as lithium-ion passes through the stages for constant current and topping charge.

The charge rate of a typical consumer Li-ion battery is between 0.5 and 1C in Stage 2, which is the initial constant current charge stage, and the charge time is about three hours. Usually the battery is not subjected to this current right from the beginning of charging, which is Stage 1. In stage 1, a small current is supplied to get the Lithium ions settle and adjust to the charging process. Manufacturers recommend charging at 0.8C or less. Charge efficiency is 97 to 99 percent and the cell remains cool during charge. Some Li-ion packs may experience a temperature rise of about 5C (9F) when reaching full charge. This could be due to the protection circuit and/or elevated internal resistance. After the constant current charge, at

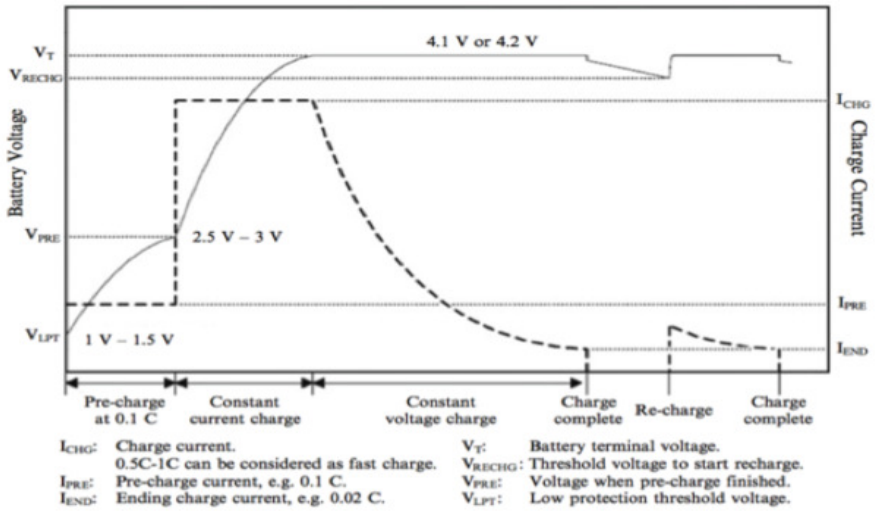

Fig. 2.1. Constant Current - Constant Voltage Charging. [9]

Stage 3, the battery is subjected to a constant Voltage charge with an exponentially decaying current supply. Full charge occurs when the battery reaches the voltage threshold and the current drops to three percent of the rated current. A battery is also considered fully charged if the current levels off and cannot go down further. Elevated self-discharge might be the cause of this condition.

Increasing the charge current does not hasten the full-charge state by much. Although the battery reaches the voltage peak quicker with a fast charge, the saturation charge will take longer accordingly. The amount of charge current applied simply alters the time required for each stage; Stage 2 will be shorter but the saturation Stage 3 will take longer. A high current charge will, however, quickly fill the battery to about 70%. Li-ion does not need to be fully charged, as is the case with lead acid, nor is it desirable to do so. In fact, it is better not to fully charge, because high voltages stresses the battery. Choosing a lower voltage threshold, or eliminating the saturation charge altogether, prolongs battery life but this reduces the runtime. Since the consumer market promotes maximum runtime, these chargers go for maximum capacity rather than extended service life.

Table 2.1
Typical charge characteristics of lithium-ion [5]

Charge V/cell	Capacity at cut-off voltage	Charge Time	Capacity with full saturation
3.80	60%	120min	∼65%
3.90	70%	135min	∼75%
4.00	75%	150min	∼80%
4.10	80%	165min	∼90%
4.20	85%	180min	100%

2.2 Available Options

Some low cost consumer chargers may use the simplified charge-and-run method that charges a lithium-ion battery in one hour or less without going to the saturation charge. Ready appears when the battery reaches the voltage threshold at Stage 1. Since the state-of-charge (SoC) at this point is only about 85%, the user may complain of short runtime, not knowing that the charger is to blame. Many warranty batteries are being replaced for this reason, and this phenomenon is especially common in the cellular industry.

Battery charge thresholds are set to a lower value often to prevent the battery from getting fully charged thereby aging the battery more aggressively. The above Table. 2.1 illustrates the estimated capacities when charged to different voltage thresholds with and without saturation charge [5]. There are some other charging methods being investigated at but none in commercial use though [8] [9]. One such method is the NMPC scheme. The proposed state-feedback NMPC scheme is computationally less prohibitive and feasible for real-time control. The time-optimal charging profiles are compared with the standard CC/CV method for charging Li-ion batteries. While the CC/CV method is very simple to realize in hardware, this method is far from being optimal. Furthermore, considering aging of the battery, the CC currents are

in general chosen very conservative, such that safety can be guaranteed during the lifetime of the battery.

3. METHODOLOGY

3.1 Introduction

Lithium Ion battery can be modeled in a variety of techniques. Equivalent Circuit Model, 1-D Electrochemical Model, 2-D Electrochemical Model, Multi Dimensional - Multi Particle Model are some of the techniques used to model the Battery Dynamics. No one model can be used to suffice the need of different applications. Some model provide higher computational speed where some other provide more accurate performance. The choice of a particular model depends on the usage and the requirements. Like, R-C models are simple and computationally fast but lag the accurate performance required for a charge/discharge characterization study. On the contrary a full order multi dimensional, multi particle model is accurate to the level of details but is super slow for ordinary application needs. Hence the choice of a model requires good amount of insight into the requirements and application it will be used at. If a high speed medium accurate model is good enough for a particular application then that is the best choice.

3.2 Cell Model

One of the primary objective of designing an optimal control for Lithium Ion battery is the creation of a robust, high fidelity battery plant model. Generally, the effort of developing a detailed multi-scale and multi-physics model with high predictive ability is very expensive, so model development efforts begin with a simple model and then add more physics until the model predictions are sufficiently accurate.That is, model development starts from the simplest form and increases in complexity until the satisfying performance is achieved as per the objective and requirement. The

best possible physics-based model can depend on the type of issue being addressed, the systems requirement objectives and accuracy desired and on the available computational resources. This section describes various types of models available in the literature, the modeling efforts being undertaken so far and the difficulties in using the most comprehensive models in all scenarios. Fig. 3.1 shows the basic approach in designing a system for a battery model.

An important task is to experimentally validate the chosen model to ensure that the model predicts the experimental data to the required precision with a reasonable confidence. This task is typically performed in part for experiments designed to evaluate the descriptions of physio-chemical phenomena in the model whose validity is less well established. However, in a materials system such as a lithium-ion battery, most variables in the system are not directly measurable during charge-discharge cycles, and hence are not available for comparison to the corresponding variables in the model to fully verify the accuracy of all of the physio-chemical assumptions made in the derivation of the model. Also, model parameters that cannot be directly measured experimentally typically have to be obtained by comparing the experimental data with the model predictions.

Models for the prediction of battery performance can be roughly grouped into four categories: empirical models, electrochemical engineering models, multi-physics models, and molecular/atomic models [10].

- **Empirical models:** Empirical models employ past experimental data to predict the future behavior of lithium-ion batteries without consideration of physio-chemical principles. Polynomial, exponential, power law, logarithmic, and trigonometric functions are commonly used as empirical models. The computational simplicity of empirical models enables very fast computations, but since these models are based on fitting experimental data for a specific set of operating conditions, predictions can be very poor for other battery operating

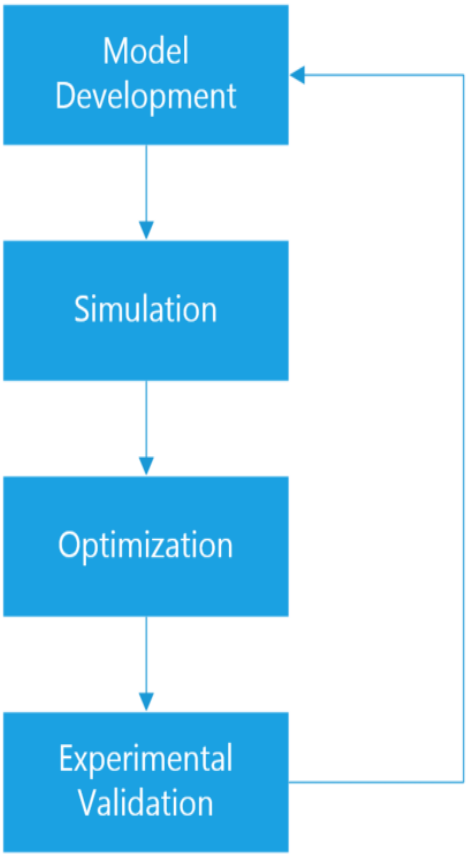

Fig. 3.1. Schematic of Battery Modeling

- **Electrochemical engineering models:** The electrochemical engineering field has long employed continuum models that incorporate chemical/ electrochemical kinetics and transport phenomena to produce more accurate predictions than empirical models. Electrochemical engineering models of lithium-ion batteries have appeared in the literature for more than twenty years [7].
  Below is a summary of electrochemical engineering models, presented in order of increasing complexity.

  – **Single-particle model:** SPM incorporates the effects of transport phenomena in a simple manner. Zhang et al [11]. developed a model of diffusion and intercalation within a single electrode particle. This is ex-

panded to a sandwich model by considering the anode and cathode each as a single particle with the same surface area as the electrode [12]. Diffusion and intercalation are considered within the particle in this model. Concentration and potential effects in the solution phase between the particles are neglected

- **Ohmic porous-electrode models:** Next in complexity order, porous electrode model is studied. This model uses the solid and electrolyte phase potentials and current but neglect the spatial variation in the concentrations. The model assumes either linear, Tafel or exponential kinetics for the electrochemical reactions and incorporates some additional phenomena, such as the dependency on conductivity as a function of porosity. Optimization studies have been performed using this model to design the separator and electrode thicknesses [13], [14] and ideal spatial variations of porosity within electrodes.
- **Pseudo-two-dimensional models:** The pseudo-two-dimensional (P2D) model expands on the ohmic porous-electrode model by including diffusion in the electrolyte and solid phases, as well as Butler-Volmer kinetics (1.5). Doyle et al [7]. developed a P2D model based on concentrated solution theory to describe the internal behavior of a lithium-ion sandwich consisting of positive and negative porous electrodes, a separator, and a current collector. This model was generic enough to incorporate further advancements in battery systems understanding, leading to the development of a number of similar models [12], [15–25]. This physics-based model is by far the most used by battery researchers, and solves for the electrolyte concentration, electrolyte potential, solid-state potential, and solid-state concentration within the porous electrodes and the electrolyte concentration and electrolyte potential within the separator

- **Multiphysics models:** Multi-scale, multidimensional, and multi-physics electrochemical, thermal coupled models are necessary to accurately describe all of the important phenomena that occur during the operation of lithium-ion batteries for high power/energy applications such as in electric/hybrid vehicles.
  - **Thermal models:** Including temperature effects into the P2D model adds to the complexity, but also to the validity, of the model, especially in high power/energy applications. Due to the added computational load required to perform thermal calculations, many researchers have decoupled the thermal equations from the electrochemical equations by using a global energy balance, which makes it impossible to monitor the effects on the performance of the cells due to temperature changes [26–30]. Other researchers have similarly decoupled the thermal simulation of the battery stack from the thermal/electrochemical simulation of a single cell sandwich [31, 32].
  - **Stack models:** In order to simulate battery operation more accurately, battery models are improved by considering multiple cells arranged in a stack configuration. Simulation of the entire stack is important when thermal or other effects cause the individual cells to operate differently from each other. Since it is often not practical or possible to measure each cell individually in a stack, these differences can lead to potentially dangerous or damaging conditions such as overcharging or deep-discharging certain cells within the battery, which can cause thermal runaway or explosions.
- **Molecular/atomistic models:** Kinetic Monte Carlo method :- The Kinetic Monte Carlo (KMC) method is a stochastic approach that has been used to model the discharge behavior of lithium ions during intercalation. Such models [33–36] have been used to simulate diffusion of lithium from site to site within an active particle to aid in understanding on how different crystal structures affect lithium mobility [37] and how the activation barrier varies with lithium-ion concentration [35,36]. Additionally, Monte Carlo methods have been used to

predict thermodynamic properties [38]. KMC has also been applied to simulate the growth of the passive SEI-layer across the surface of the electrode particle, to simulate one of the mechanisms for capacity fade

In this work, a reformulated 1-D electrochemical model is used which is computationally fast as well as accurate to the level of details required for the work. A brief overview of the RC Model is given in the below section and a detailed analysis of the physics based electrochemical model is presented in the following subsections.

3.2.1 Equivalent Circuit Model

The Battery cell can be modeled as a simplistic RC model. The RC model is good enough in many applications but not very accurate and detailed to the level this literature requires. Various equivalent circuit models such as the **Rint model**, the **RC model**, the **Thevenin model** or the **PNGV model** are now widely used in Electric Vehicle studies. In order to refine the polarization characteristics of a battery, an improved Thevenin circuit model named DP (for dual polarization) model is proposed herein. Further, comparisons between the model-based simulation data and the experimental data are carried out to evaluate the validity of the foregoing models, which provides a foundation for the model-based SOC estimation.

The below Fig. 3.2, shows the SOC estimate by the different Equivalent Circuit Models

3.2.2 Physics Based Cell Model

Doyle et al. and Fuller et al. [7] published a physics-based model for a lithium-ion cell, which has been used or modified by others [39–43]. These models are computationally very expensive to be considered as a potential optimal candidate for battery simulations. Consequently, several simplifications of their model have been published to reduce the computation time associated with diffusion of lithium ions

Table 3.1
The statistical analysis of the absolute values of terminal voltage errors

$Model$	$Maximum(V)$	$Mean(V)$	$Variance(V^2)$	$Max.\ ErrorRate(\%)$
$RintModel$	1.6229	0.3945	0.0762	2.8176
$RCModel$	1.0785	0.2336	0.0463	2.0337
$TheveninModel$	0.2967	0.0455	0.0220	0.5151
$PNGVModel$	0.5772	0.0875	0.0243	1.0020
$DPModel$	0.2183	0.0429	0.0021	0.3790

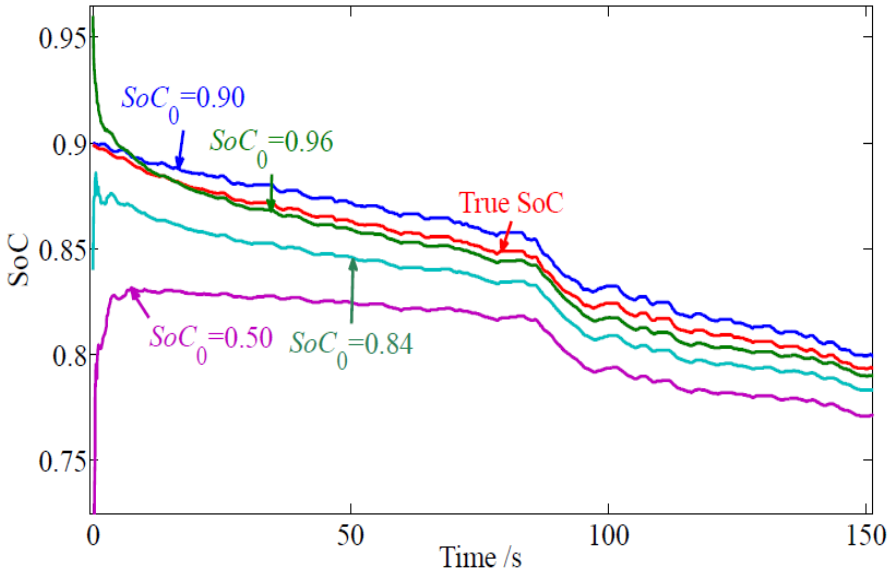

Fig. 3.2. The SOC estimation profiles with different SOC initial values

in the solid phase [44–46]. Also, Subramanian et al. [45] developed a real-time simulation model using a combination of perturbation techniques, volume averaging, and intuition-based simplification. Although they reported that the computational time for their real-time simulation model for a single process was around 100 ms, to derive the lower-order model by using this method one needs to carry out preprocessing and have a prior knowledge of the behavior of the system under different conditions, which makes their method less flexible than desired. Other methods have also been used to derive ROMs for lithium-ion batteries, including Chebyshev polynomial methods [47] and a residue grouping method [48] [49]. The state variables are approximated by linear combinations of different Chebyshev polynomials and then an approximated model is projected onto a subspace formed by these ortho-normal Chebyshev polynomials to form an ROM. This model is then solved for unknown coefficients in the truncated expressions. Smith et al. [50] developed a control-oriented one-dimensional 1-D electrochemical model by using the method of residue grouping. Their transfer functions are represented by a truncated series of grouped residues with similar

eigenvalues. A single Particle Model which is a reduced version of a full Physics based model is used in this thesis.

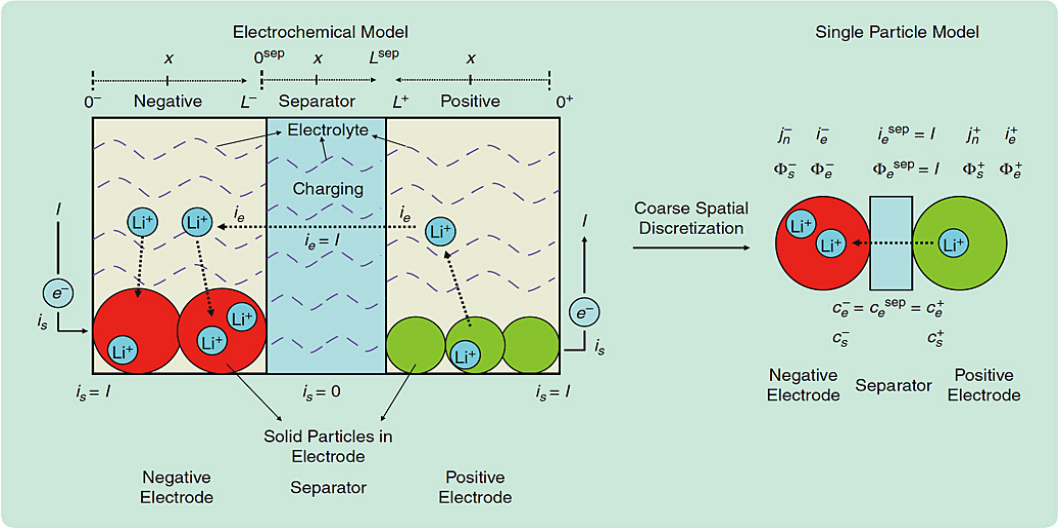

Fig. 3.3. Single particle model. Since only one node is chosen in the electrode, there is only one solid spherical particle. Furthermore, we can consider the value at each node to be an averaged quantity over the electrode. This simplification holds only for small currents or for an electrolyte with a high ionic conductance. [51]

Fig. 3.3 and Fig. 3.4 shows the single particle model.

3.2.3 Numerical Treatment of the Physics Based Cell Model

In this literature Finite Difference Method has been used to discretize the 1-D electrochemical cell model. The finite difference approximations for derivatives are one of the simplest and one of the oldest methods to solve differential equations. It was already known by L. Euler (1707-1783) ca. 1768, in one dimension of space and was probably extended to 2 dimension by C. Runge (1856-1927) ca. 1908. The advent of finite difference techniques in numerical applications began in the early 1950s and their development was stimulated by the emergence of computers that offered a convenient framework for dealing with complex problems of science and technology.

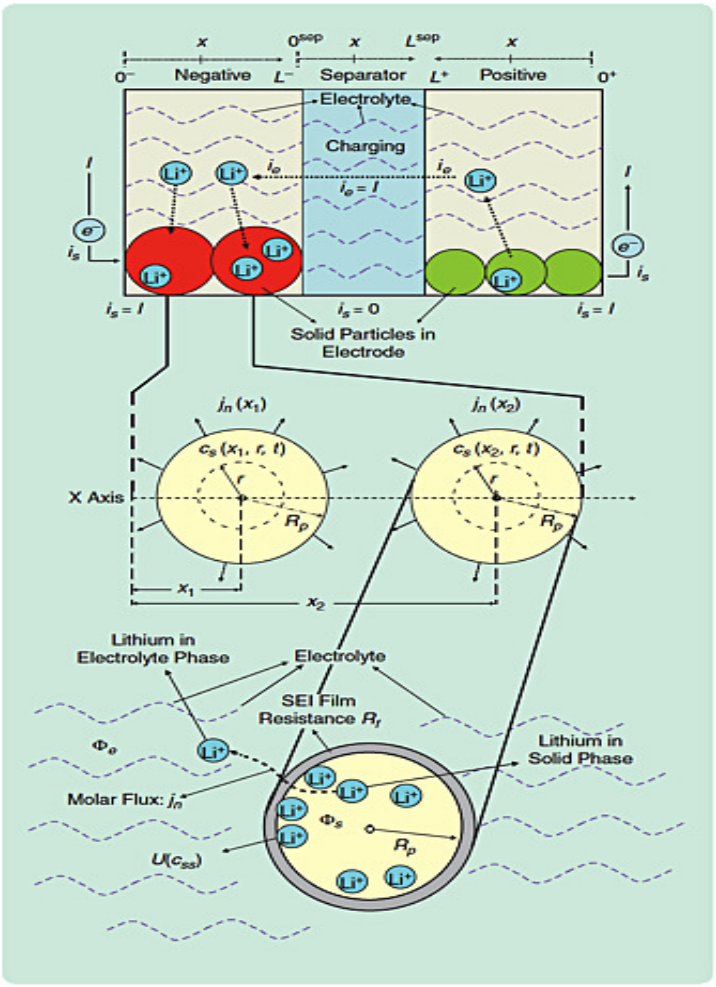

Fig. 3.4. Single particle model detailed structure. [51]

Theoretical results have been obtained during the last five decades regarding the accuracy, stability and convergence of the finite difference method for partial differential equations. In this work the reformulated battery governing equations are discretized at their time and space grid points using FDM. The Equations are then solved for their value at the next grid point. While solving the equations for the grid points the boundary and initial values are applied to maintain the equation limits. This process is followed until a convergence is reached with a given degree of accuracy.

Finite difference approximations

The principle of FDM is very similar to numerical methods used to solve ODEs. In this method the differential operator is approximated by replacing it with the derivatives in the equation using differential quotients. The solution domain is divided into space and time nodes and the differentiation is approximated at each node. The difference between the solved numerical solution and the exact analytical solution is determined by the error that is committed by going from a differential operator to a difference operator. This error is called the quantization error or truncation error. The truncation error proves the fact that a finite part of the Taylor series is used in the approximation.

Here we have considered one-dimensional space only for simplicity. The main concept behind any finite difference scheme is related to the definition of the derivative of a smooth function u at a point $x \in R$:

$$u'(x) = \lim_{h \to 0} \frac{u(x+h) - u(x)}{h},$$

and, to the fact that when h tends to 0 (without vanishing), the quotient on the right-hand side provides a good approximation of the derivative. In other words, h should be sufficiently small to get a good approximation. It remains to indicate what exactly is a good approximation, in what sense. Actually, the approximation is good when the error committed in this approximation (i.e. when replacing the derivative by the differential quotient) tends towards zero when h tends to zero. If the function u is sufficiently smooth in the neighborhood of x, it is possible to quantify this error using a Taylor expansion.

Finite Difference Method

$$1D: \qquad \Omega = (0, X), \qquad u_i \approx u(x_i), \qquad i = 0, 1, \ldots, N$$

$$grid\ \ points: \qquad x_i = i\Delta x \qquad mesh\ \ size: \qquad \Delta x = \frac{X}{N}$$

First-Order derivatives:

$$\begin{aligned}\frac{\partial u}{\partial x}(\bar{x}) &= \lim_{\Delta x \to 0} \frac{u(\bar{x}+\Delta x) - u(\bar{x})}{\Delta x} = \lim_{\Delta x \to 0} \frac{u(\bar{x}) - u(\bar{x}-\Delta x)}{\Delta x} \\ &= \lim_{\Delta x \to 0} \frac{u(\bar{x}+\Delta x) - u(\bar{x}-\Delta x)}{\Delta x},\end{aligned} \tag{3.1}$$

The first order derivatives are approximated in the following 3 ways.

- Forward difference:

$$(\frac{\partial u}{\partial x})_i \approx \frac{u_{i+1} - u_i}{\Delta x} \tag{3.2}$$

- Backward difference:

$$(\frac{\partial u}{\partial x})_i \approx \frac{u_i - u_{i-1}}{\Delta x} \tag{3.3}$$

- Central difference:

$$(\frac{\partial u}{\partial x})_i \approx \frac{u_{i+1} - u_{i-1}}{2\Delta x} \tag{3.4}$$

To better understand the different forms of Finite Difference Methods, a geometric visual representation is provided in Figure 3.5.

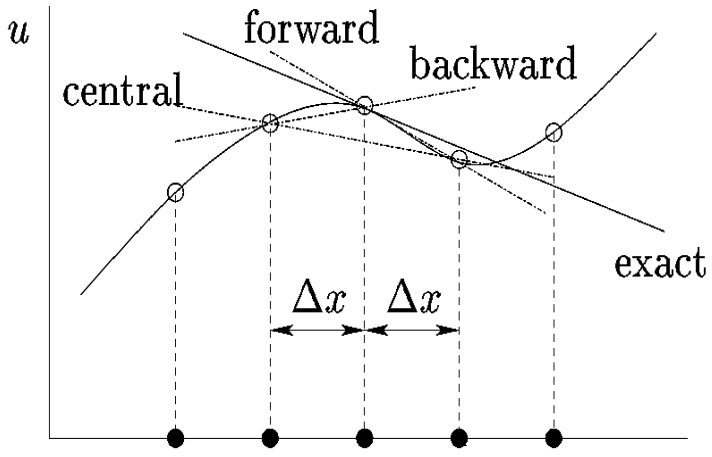

Fig. 3.5. Geometric Interpretation of FDM

Taylor series expansion $u(x) = \sum_{n=0}^{\infty} \frac{(x-x_i)^n}{n!}(\frac{\partial^n u}{\partial x^n})_i,\ u \in C^{\infty}([0, X])$

$T_1 : u_{i+1} = u_i + \Delta x(\frac{\partial u}{\partial x})_i + \frac{(\Delta x)^2}{2}(\frac{\partial^2 u}{\partial x^2})_i + \frac{(\Delta x)^3}{6}(\frac{\partial^3 u}{\partial x^3})_i + \ldots$

$T_2 : u_{i-1} = u_i - \Delta x(\frac{\partial u}{\partial x})_i + \frac{(\Delta x)^2}{2}(\frac{\partial^2 u}{\partial x^2})_i - \frac{(\Delta x)^3}{6}(\frac{\partial^3 u}{\partial x^3})_i + \ldots$

Analysis of truncation error: The following lines shows the accuracy of the finite difference approximations for forward, backward and central difference.

- $T_1 \Rightarrow= (\frac{\partial u}{\partial x})_i = \frac{u_{i+1}-u_i}{\Delta x} - \frac{\Delta x}{2}(\frac{\partial^2 u}{\partial x^2})_i - \frac{(\Delta x)^2}{6}(\frac{\partial^3 u}{\partial x^3})_i + \ldots$

  Forward Difference truncation error $\mathcal{O}(\Delta x)$

- $T_2 \Rightarrow= (\frac{\partial u}{\partial x})_i = \frac{u_i-u_{i-1}}{\Delta x} - \frac{\Delta x}{2}(\frac{\partial^2 u}{\partial x^2})_i - \frac{(\Delta x)^2}{6}(\frac{\partial^3 u}{\partial x^3})_i + \ldots$

  Backward Difference truncation error $\mathcal{O}(\Delta x)$

- $T_1 - T_2 \Rightarrow= (\frac{\partial u}{\partial x})_i = \frac{u_{i+1}-u_{i-1}}{\Delta 2x} - \frac{(\Delta x)^2}{6}(\frac{\partial^3 u}{\partial x^3})_i + \ldots$

  Central Difference truncation error $\mathcal{O}(\Delta x)^2$

This gives the leading truncation error as:
$\epsilon_\tau = \alpha_m(\Delta x)^m + \alpha_{m+1}(\Delta x)^{m+1} + \ldots \approx \alpha_m(\Delta x)^m$
Similarly approximation of Second Order Derivatives are given as:
Central Difference Scheme: $T_1 + T_2 \Rightarrow= (\frac{\partial^2 u}{\partial x^2})_i = \frac{u_{i+1}-2u_i+u_{i-1}}{(\Delta x)^2} + \mathcal{O}(\Delta x)^2$
Alternative derivation gives:

$$
\begin{aligned}
(\frac{\partial^2 u}{\partial x^2})_i = [\frac{\partial}{\partial x}(\frac{\partial u}{\partial x})]_i &= \lim_{\Delta x \to 0} \frac{(\frac{\partial u}{\partial x})_{i+\frac{1}{2}} - (\frac{\partial u}{\partial x})_{i-\frac{1}{2}}}{\Delta x} \\
&\approx \frac{\frac{u_{i+1}-u_i}{\Delta x} - \frac{u_i-u_{i-1}}{\Delta x}}{\Delta x} = \frac{u_{i+1} - 2u_i + u_{i-1}}{(\Delta x)^2}
\end{aligned}
\tag{3.5}
$$

Simulation

The 1-D Lithium Ion battery model is simulated in a Macintosh machine and the results are validated against a published paper. The simulation results showed good accuracy. The simulation took around 20 real time seconds to simulate 10000 simulation seconds.

Fig. 3.6, shows the flow chart for the battery simulation process.

The Battery Parameters are chosen from one of the published papers by Subramanian et. al. [52].

Table. 3.2.3 shows the parameter values with the 1-D model is simulated.

The model is simulated at a frequency of $1Hz$. The space node is chosen so as to make the simulation computational time fast as well as not to compromise on any accuracy. The below observations and analysis are made to decide the space nodes for Negative, Positive and Separator regions.

- The reaction coefficient at the electrolyte is much faster as compared to the solid phase reactions.
- The state parameters take longer time to modify in the solid phase as compared to the separator.
- Diffusivity in the electrodes is much slower than the separator.
- Reaction rate is faster by the order of 10^3 in the separator.

Fig. 3.7 shows the representation of the transport coefficient. Thus said, to mimic the battery reactions accurately with out loosing any measurable performance, the negative and positive electrodes are divided into more spatial grid points than the separator. Though increasing the points slows down the computational speed, it is required to follow a certain grid spacing to maintain the required performance. Thus there is a trade off between the computational load and the performance accuracy. In this work we have used 88 points for the negative electrode, 80 points for the positive

Parameters	Symbols	Units	Negative Electrode	Separator	Positive Electrode
Thickness	L	m	88×10^{-6}	35×10^{-6}	80×10^{-6}
Node Points	N	-	88	35	80
Particle Radius	R_i	m	2×10^{-6}	-	2×10^{-6}
Active Material Volume Fraction	ϵ_s	-	0.4824	-	0.5
Electrolyte Phase Volume Fraction (Porosity)	ϵ_e	-	0.485	0.724	0.385
Conductivity of Solid Active Material	σ	$\Omega^{-1}m^{-1}$	100	-	100
Effective Conductivity of Solid Active Material	σ^{eff}	-	$\epsilon_s\sigma$	-	$\epsilon_s\sigma$
Transference Number	${t_+}^0$	-	0.363	0.363	0.363
Electrolyte Phase Ionic Conductivity	κ	$\Omega^{-1}m^{-1}$	$0.0158c_{e,n}e^{(0.85c_{e,n}^{1.4})}$	$0.0158c_{e,s}e^{(0.85c_{e,s}^{1.4})}$	$0.0158c_{e,p}e^{(0.85c_{e,p}^{1.4})}$
Effective Electrolyte Phase Ionic Conductivity	κ^{eff}	$mol(molm^{-3})^{-1.5}$	$\epsilon_e^{1.5}\kappa$	$\epsilon_e^{1.5}\kappa$	$\epsilon_e^{1.5}\kappa$
Effective Electrolyte Phase Diffusivity	K_D^{eff}	-	$[\frac{2RT\kappa^{eff}}{F}](t_+^0-1)$	$[\frac{2RT\kappa^{eff}}{F}](t_+^0-1)$	$[\frac{2RT\kappa^{eff}}{F}](t_+^0-1)$
Electrolyte Phase Diffusion Coefficient	D_e	m^2s^{-1}	4.1498×10^{-11}	7.5×10^{-10}	1.6478×10^{-11}
Effective Electrolyte Phase Diffusion Coefficient	D_e^{eff}	-	$\epsilon_e^1.5D_e$	$\epsilon_e^1.5D_e$	$\epsilon_e^1.5D_e$
Solid Phase Diffusion Coefficient	D_s	m^2s^{-1}	3.9×10^{-14}	-	1.0×10^{-14}
Maximum Solid Phase Concentration	$Cs_{max,i}$	$molm^{-3}$	30555	-	51554
Stoichiometry @ 0%	-	-	0.4955	-	0.8551
Stoichiometry @ 100%	-	-	0.8551	-	0.4955
Electrolyte Concentration	$c_{e,i}$	$molm^{-3}$	1000	1000	1000
Charge Transfer Coefficients	α_a, α_c	-	0.5, 0.5	-	0.5, 0.5
Universal Gas Constant	R	$jmol^{-1}K^{-1}$	8.314	8.314	8.314
Farraday's Constant	F	$Cmol^{-1}$	96487	96487	96487
Electrode Plate Area	A	m^2	30	-	30
Active Surface Area	a_s	m^{-1}	$\frac{3\epsilon}{R}$	-	$\frac{3\epsilon}{R}$

electrode and 35 points for the separator, when using the 1-D model with constant electrolyte concentration. When using modeled electrolyte concentration (where the physics based model of C_e is used), we used a generic 10 point grids for Negative, Positive and separator region. The performance is verified from the simulation results. A simplistic way of describing the FDM approach to numerically solve the 1-D model is presented below, in Fig. 3.8.

Model Validation Plots

The plant model is validated against a published paper by Subramanian et. al. [52] The 1-D Model is also verified with MEC.

Fig. 3.9 and Fig.3.10 shows the discharge curves for CEC as well as MEC for C/2 and C discharge rates. The subsequent plot shows the discharge voltage curves from the published paper.

Fig. 3.11 and Fig. 3.12 shows the Discharge Voltage Curves at different C rates for CEC and MEC.

Fig. 3.13, shows the electrolyte concentration for MEC Battery Model Simulation. Electrolyte concentration starts from the constant initial value and decreases/increases on the positive/negative electrode with time and space nodes.

Fig. 3.14 and Fig. 3.15 shows the HPPC Voltage profiles with temperature and current. In this cycle the battery is simulated with alternating charge and discharge cycles with Pulsed regeneration/load currents. The battery voltage shows a charge/discharge trend whereas the temperature shows a gradual increasing trend.

Fig. 3.17 and Fig. 3.18, Fig. 3.16 shows the Battery state parameters for CEC and MEC simulations at 1C discharge rate.

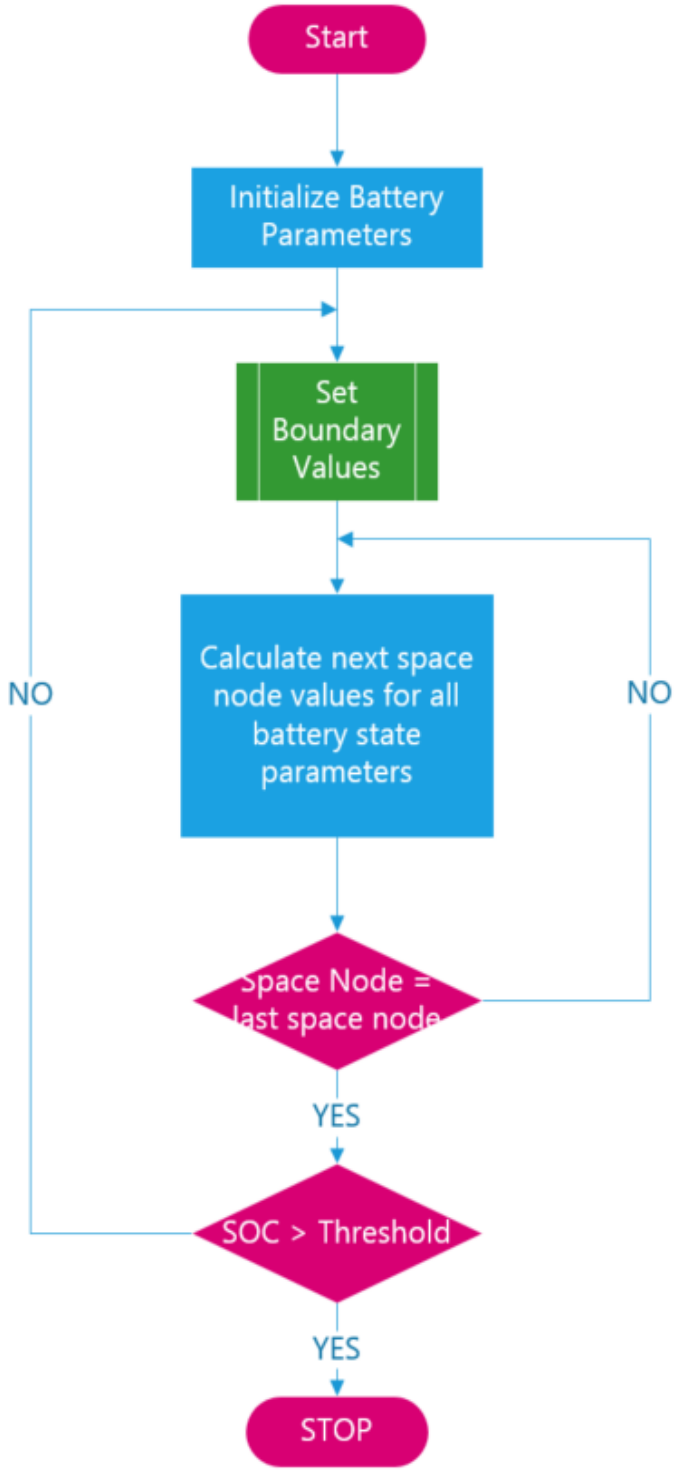

Fig. 3.6. Flow Chart for Battery Model Simulation

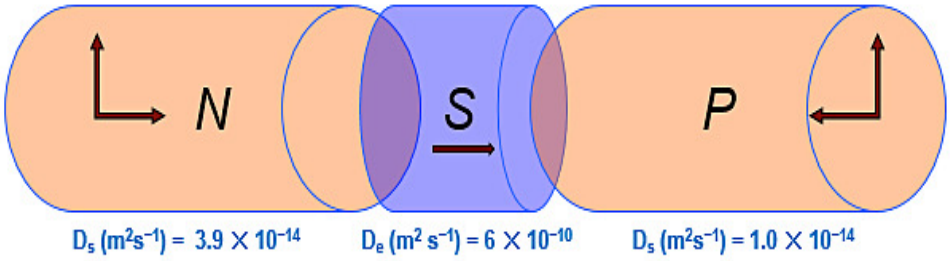

Fig. 3.7. Reaction Rate in Cell

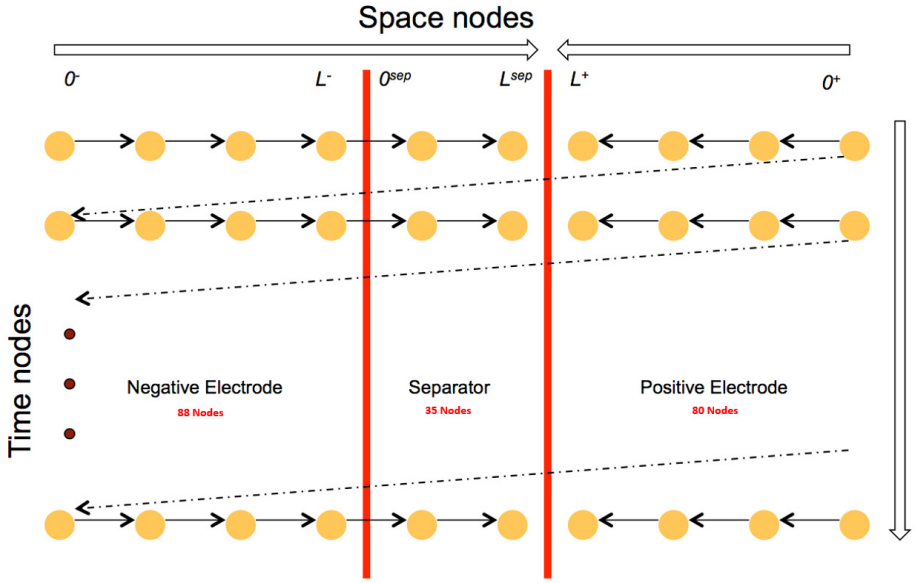

Fig. 3.8. Numerical approach for Battery Model

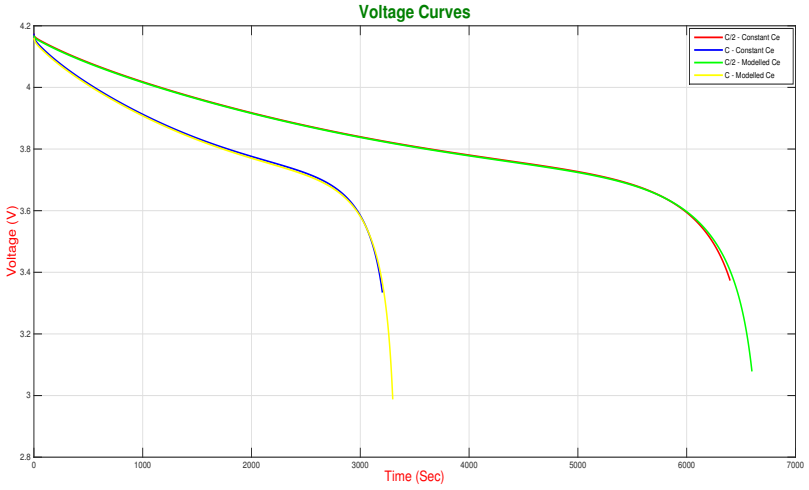

Fig. 3.9. Discharge Voltage Curves for MEC and CEC at C/2 and C Rate

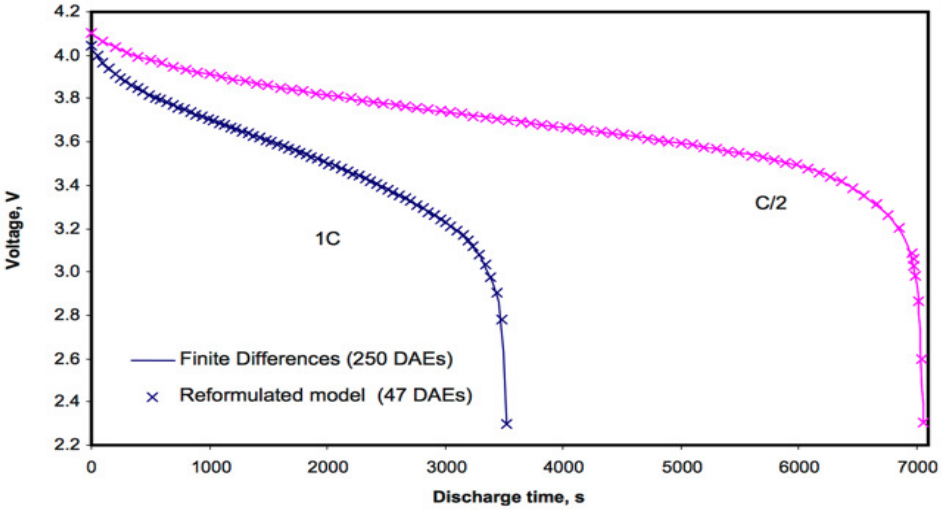

Fig. 3.10. Discharge Voltage Curves from Published Paper. [45]

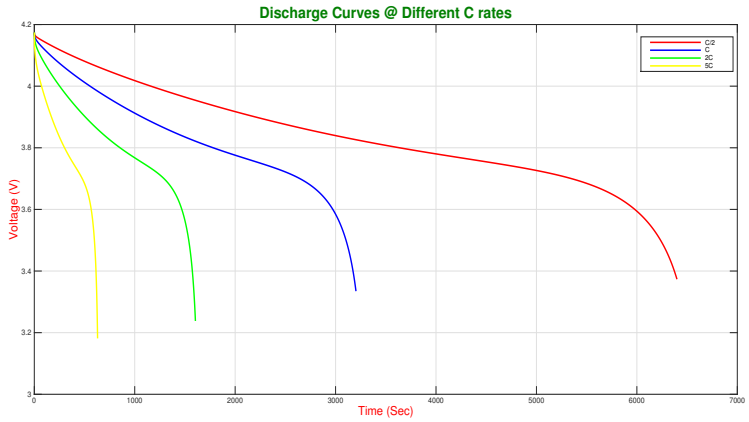

(a) CEC Simulation.

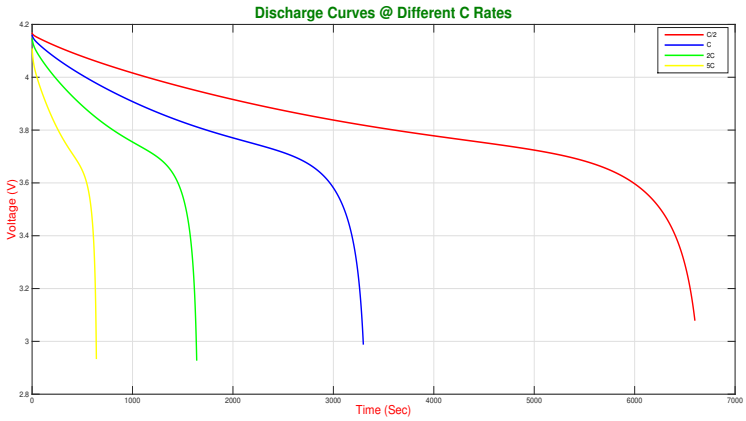

(b) MEC Simulation.

Fig. 3.11. Discharge Voltage Curves at different C Rates

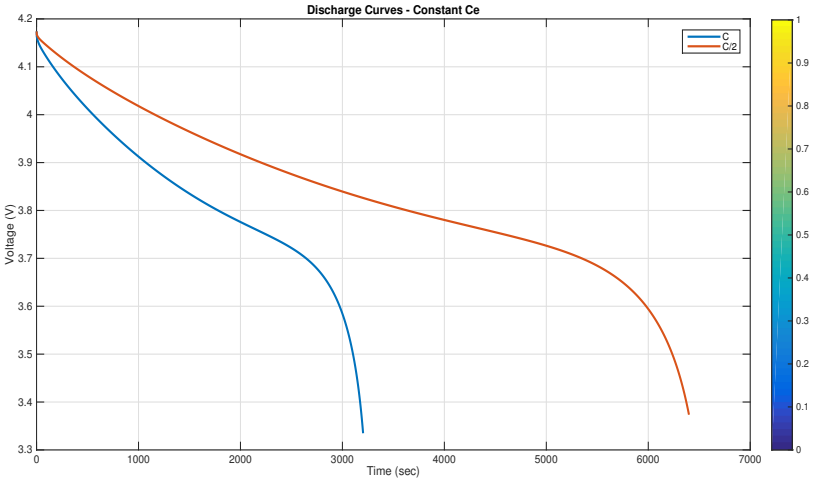

Fig. 3.12. Discharge Voltage Curves for CEC

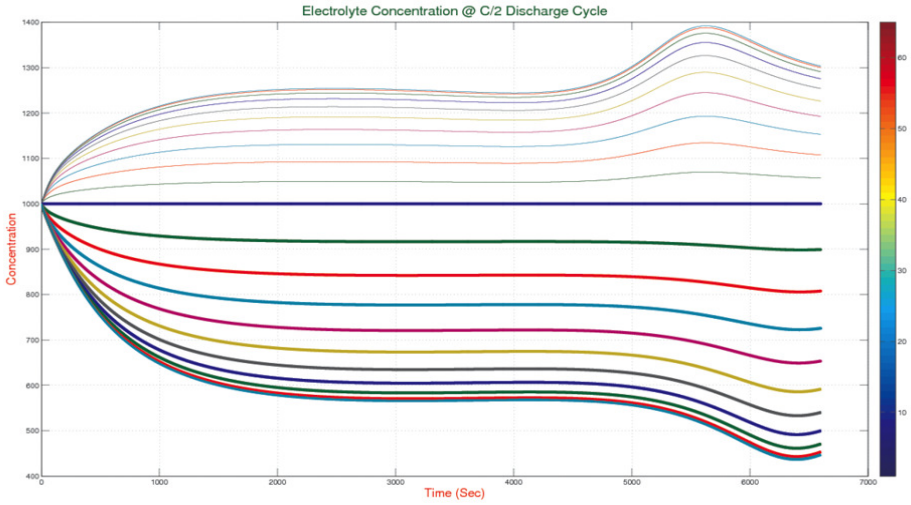

Fig. 3.13. HPPC Results for CEC

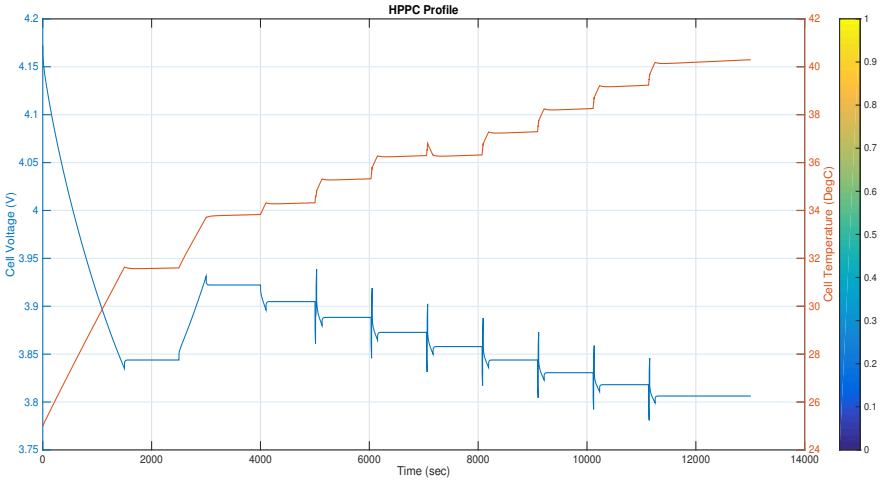

Fig. 3.14. HPPC Results for CEC

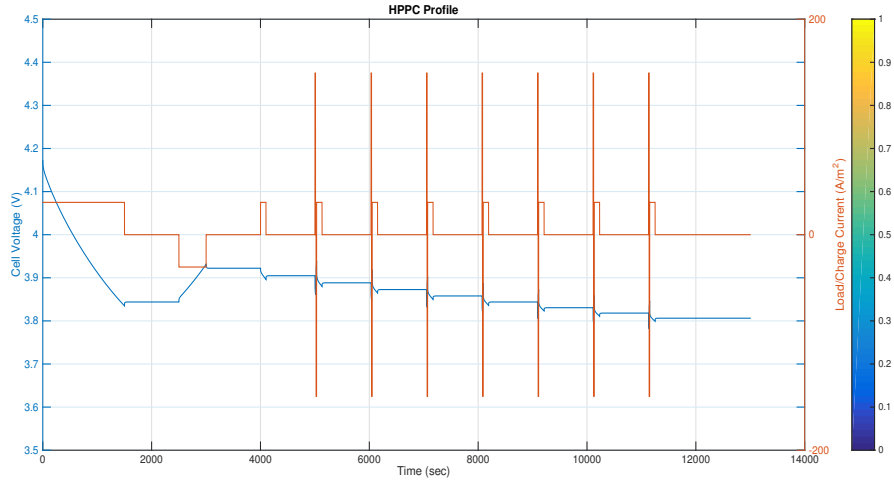

Fig. 3.15. HPPC Current Profile for CEC

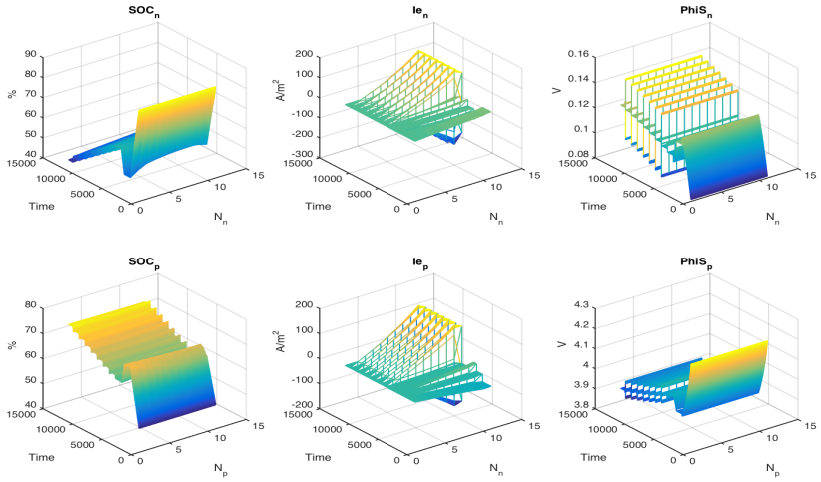

Fig. 3.16. Battery State Parameters at HPPC run for MEC

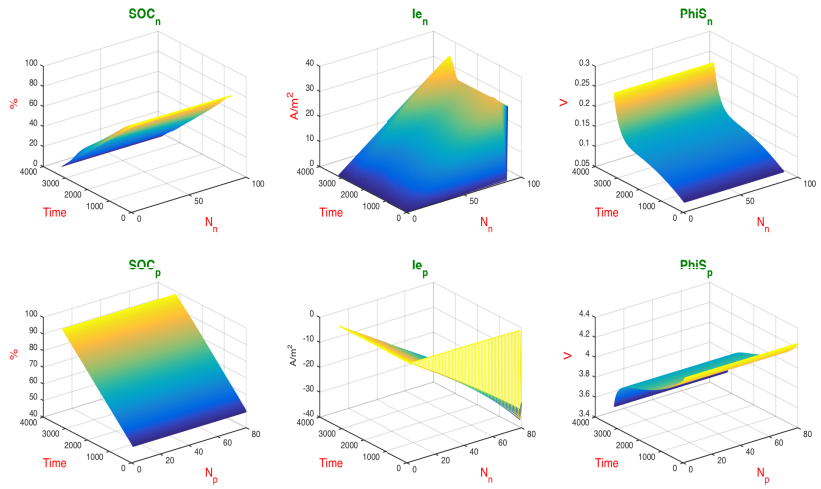

Fig. 3.17. Battery State Parameters for CEC

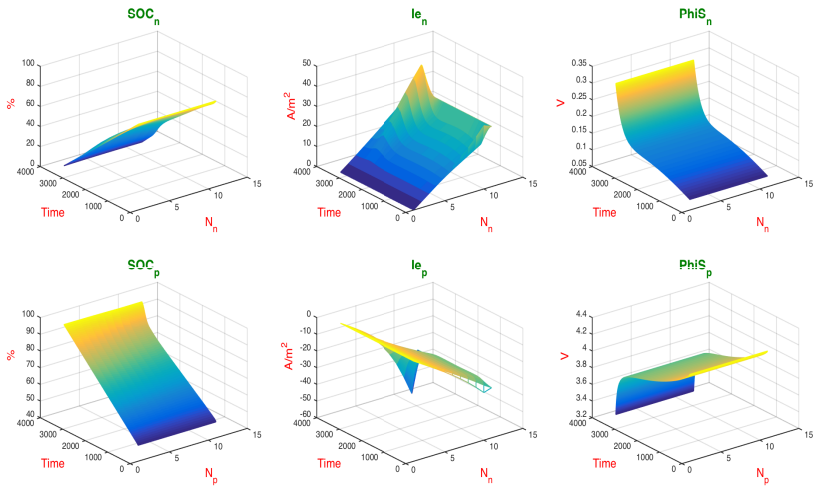

Fig. 3.18. Battery State Parameters for MEC

4. OPTIMIZATION METHODS

4.1 Introduction

Any control system design can be approached in two different ways, an open loop method or a closed loop method. While in open loop method an initial calculated input is provided to the system, in closed loop the system is constantly monitored by a set of feedback signals which are often state parameters. Depending on the feedback and calculating the error in the required state trajectory the driving input signal is modified. Different optimization methods are applied to open loop and closed loop systems to achieve a required performance. The method is also bounded by different state and input constraints which gives rise to different other forms of control. An optimal control is a set of differential equations describing the paths of the control variables that minimize the cost function or performance index. The optimal control can be derived using Pontryagin's maximum principle (a necessary condition also known as Pontryagin's minimum principle or simply Pontryagin's Principle [53]), or by solving the HJB equation (a sufficient condition).

In this work we focussed on Lev Pontryagin's work. His work showcases a way to optimize a given cost function utilizing the state and co-state trajectories.

4.2 Pontryagin's Maximum/Minimum Principle

Optimal Control Problem states, given a system dynamics, find a control law which provides a controlled input u(t) over an interval $[t_0, T]$ to minimize/maximize a performance index

Basic Principles are prescribed as below:

Systems Model:

$$\dot{x} = f(x, u, t), t >= t_0, t_0 is fixed \tag{4.1}$$

Performance Index:

$$J = \phi(x(T), T) + \int_{t_0}^{T} (x(t), u(t), t)dt \tag{4.2}$$

Terminal Constraint:

$$\psi(x(T), T) = 0 \tag{4.3}$$

Now once we have the system and constraints described we write the Hamiltonian as

$$H(x, u, \lambda, t) = L(x, u, t) + \lambda^T(t) f(x, u, t) \tag{4.4}$$

Optimal input u^* minimizes $H(x, u, \lambda, t)$ among all admissible inputs u. If u is unconstrained then $H_u = L_u + \lambda^T f_u = 0$

The state and co-sate equations are given as:

$$\dot{x} = H_\lambda = f(x, u^*, t) \tag{4.5}$$

$$\frac{d\lambda^T}{dt} = -H_x = -\lambda^T f_x(x, u^*, t) - L_x(x, u^*, t) \tag{4.6}$$

The boundary conditions are describes as:

$$x(t_0) = x_0(given) \tag{4.7}$$

$$\lambda^T(T) = \phi_x(x(T), T) + \upsilon^T \psi_x(x(T), T) \tag{4.8}$$

$$\psi(x(T), T) = 0 \tag{4.9}$$

Terminal Value of the co-state is described as:

$$\lambda^T(T) = \frac{\partial J^*(x(T), T)}{\partial x} = \bar{\phi_x}(x(T), \upsilon, T) \tag{4.10}$$

The control u^* causes a relative minimum of H if, $H(u) - H(u^*) = \Delta H$

In most optimal control problems we have the following three cases:

1. No terminal constraint: $\lambda^T(T) = \upsilon_x(x(T), T)$
2. Fixed final state: $x(T)$ is fully specified, $\lambda(T)$ need not be specified.
3. Partial state constraint.

Optimal control problems are generally nonlinear and therefore, generally do not have analytic solutions (e.g., like the linear-quadratic optimal control problem). Hence it is essential to use numerical techniques to solve optimal control problems. In the early years of optimal control (circa 1950s to 1980s) the favored approach for solving optimal control problems was that of indirect methods. Calculus of variation is used in the indirect method to obtain the first order optimality conditions. These conditions result in a two-point (or, in the case of a complex problem, a multi-point) boundary-value problem. This boundary-value problem actually has a special structure because it arises from taking the derivative of a Hamiltonian. Thus, the resulting dynamical system is a Hamiltonian system of the form:

$$\dot{x} = \frac{\partial H}{\partial \lambda} \tag{4.11}$$

$$\dot{\lambda} = -\frac{\partial H}{\partial x} \tag{4.12}$$

where,

$$H = \mathcal{L} + \lambda^T a - \mu^T b \tag{4.13}$$

is the augmented Hamiltonian and in an indirect method, the boundary-value problem is solved using the appropriate boundary or transversality conditions. The advantage of using an indirect method is that the state and adjoin ($i.e., \boldsymbol{\lambda}$) are solved

and the resulting solution is readily verified to be an extremal trajectory. The disadvantage of indirect method is that the boundary-value problem is often extremely difficult to solve (particularly for problems that span large time intervals or problems with constraints interior points).

The approach that has risen to prominence in numerical optimal control over the past three decades (i.e., from the 1980s to the present) is that of so-called direct methods. In a direct method, the state and/or control are approximated using an appropriate function approximation (e.g., polynomial approximation or piece wise constant parameterization). Simultaneously, the cost functional is approximated as a cost function. Then, the coefficients of the function approximations are treated as optimization variables and the problem is "transcribed" to a nonlinear optimization problem of the form:

Minimize $F(\mathbf{z})$ subject to the algebraic constraints $\begin{aligned} \mathbf{g}(\mathbf{z}) &= \mathbf{0} \\ \mathbf{h}(\mathbf{z}) &\leq \mathbf{0} \end{aligned}$

5. PROBLEM FORMULATION AND SOLUTION TECHNIQUES

5.1 Design Objectives

In this work we tried to find an optimal state trajectory for the state of charge (SOC^*) and the optimal input trajectory I^* to achieve the optimal state trajectory.

The input current is constraint to change only between 0 and a maximum set value, $0 <= I(t) <= I_{max}$. The final state is also constraint to saturate to a final state of charge, which is the value when the battery is considered to be fully charged.

The other non linear constraints are bulk cell temperature $T(t)$ which is restricted to below 40°C and over-potential η which is restricted to have a positive value. These non linear constraints helps to reduce aging and protects from increasing the formation of resistance films across the electrodes.

The ultimate design objective and performance goal is to achieve an input charging current which will take the battery state of charge to a low (discharged) state to a final high (charged) state in minimum time without adversely affecting the battery performance and thereby reducing the lifespan of the battery or degraded performance before the EUL.

5.2 Problem Statement

The cost function defined in this work is to minimize the time required to take the battery from one initial (discharged) SOC to another final (charged) SOC, following an optimum state trajectory. To achieve this, the control law is to find the optimum input current profile.

The Performance Index is designed minimize time by coupling the effort required and keeping the input as close to the maximum value as possible without violating the boundary conditions.

We define Performance index is defined as:

$$P.I. = \int_0^{T_f} [\alpha(I_{max} - I(t))^2 + \beta(T_{max} - T(t))^2 + \delta I^2(t)]dt \tag{5.1}$$

Subjected to:

- Input Constraint:- $I(t) <= I_{max}$
- State Constraints:- $T(t) <= T_{max}$
- Model Equations:-
  - $\frac{\partial C_s(t)}{\partial t} = \frac{-3J(t)}{Rp}$
  - $\rho^{avg} c_p \frac{\partial T(t)}{\partial t} = h_{cell}[T_{max} - T(t)] + I(t)V(t)$
    $- \sum_{i=1}^{n} [\int_{0^-}^{0^+} \frac{3\epsilon}{R} \times FJ(t)(U_i(t) - T(t)\frac{\partial U}{\partial T})dx]$

The Performance Index is chosen such as to minimize the effort and to keep the Regeneration current and Bulk Cell Temperature close to the maximum set thresholds. This helps in maintaining a fast charge rate. The term which minimizes the effort keeps the Regeneration current and the Bulk Cell Temperature within the set thresholds.

With the above statement we construct the Hamiltonian, including the constraints and the model equations:

$$\begin{aligned} H(C_s, T, \lambda_1, \lambda_2, t) = {} & \alpha(I_{max} - I(t))^2 + \beta(T_{max} - T(t))^2 + \delta I^2 \\ & + \lambda_1(-\frac{6i_0}{RF} sinh(\frac{\alpha F}{RT}\eta(t)) + \lambda_2(\frac{1}{\rho^{avg} c_p}[h_{cell}(T_{max} - T(t)) + I(t)V(t)) \\ & - \sum_{i=1}^{n}[\int_{0^-}^{0^+} \frac{3\epsilon}{R} FJ(t)(U_i(t) - T(t)\frac{\partial U}{\partial T})dx]]) \end{aligned} \tag{5.2}$$

Next we find the optimal control law given by:

$$\frac{\partial H(\cdot)}{\partial I(t)} = 0 = 2\alpha I(t) - 2\alpha I_{max} + \lambda_2^* \frac{V(t)}{\rho} \tag{5.3}$$

So, from E.q: 5.3, we get:

$$\lambda_2^* = [2\alpha(I_{max} - I(t)] \times \frac{\rho^{avg} c_p}{V(t)} \tag{5.4}$$

Now we move on to find the state and co-state equations.
The state equations are given by:

$$\dot{C_s^*} = -\frac{\partial H(\cdot)}{\partial \lambda_1} = \frac{6i_0}{RF} sinh(\frac{\alpha F}{RT}\eta(t)), \tag{5.5}$$

$$\begin{aligned} \dot{T^*} = -\frac{\partial H(\cdot)}{\partial \lambda_2} = -[\frac{1}{\rho^{avg} c_p}[h_{cell}(T_{max} - T(t)) + I(t)V(t)) \\ - \sum_{i=1}^{n}[\int_{0^-}^{0^+} \frac{3\epsilon}{R} FJ(t)(U_i(t) - T(t)\frac{\partial U}{\partial T})dx]]], \end{aligned} \tag{5.6}$$

The co-state equations are given by:

$$\dot{\lambda_1^*} = \frac{\partial H(\cdot)}{\partial C_s} = 0, \tag{5.7}$$

$$\begin{aligned} \dot{\lambda_2^*} = \frac{\partial H(\cdot)}{\partial T} &= 2\beta(T_{max} - T) + \lambda_2^* \frac{h}{\rho^{avg} c_p} \\ &- \lambda_2^* \frac{1}{rho^{avg} c_p}[\sum_{i=1}^{n}[\int_{0^-}^{0^+} \frac{3\epsilon}{R} FJ(t)(U_i(t) - T(t)\frac{\partial U}{\partial T})dx]] \\ &+ \lambda_1^* \frac{\alpha F}{RT^2}\eta[\frac{6i_0}{RF} cosh(\frac{\alpha F}{RT}\eta)], \end{aligned} \tag{5.8}$$

The above equations are solved using a 2 point Boundary Value problem using an initial shooting method.

Using the above scheme we find the optimal current trajectory at each time step is given as:

$$I(t) = I_{max} - \lambda_2 \frac{V(t)}{\rho^{avg} c_p} \times \frac{1}{2\alpha} \tag{5.9}$$

Now following 2-point boundary value method, we calculate the value of λ_1^* at the initial time step, which is the boundary condition.

At the initial time step, we assume, the complete electrode for the spatial derivative, thus we use the below equations:

$$\dot{C_s} = -\frac{3}{Rp} J(t), \tag{5.10}$$

$$J(t) = \frac{I(t)}{3} \times \frac{Rp}{\epsilon} \times \frac{1}{FL_n}, \tag{5.11}$$

Thus at the first time step, we get the optimal law as:

$$\frac{\partial H(\cdot)}{\partial I(t)} = 0 = I(t) + 2\alpha I(t) - 2\alpha I_{max} - \frac{\lambda_1^*}{\psi} + \lambda_2^* \frac{V(t)}{\rho}, \tag{5.12}$$

Where, $\psi = \epsilon L_n F$

This gives λ_1^* calculated at the initial time step.

$$\lambda_1^* = [I(t)(1 + 2\alpha) - 2\alpha I_{max} + \lambda_2^* \frac{V(t)}{\rho^{avg} c_p}] \times \psi, \tag{5.13}$$

The below Fig. 5.1, shows the flow chart of the Charging Algorithm.

5.3 Performance Results

The 2-Point Boundary Value Problem is solved at each time step and the performance results are analyzed.

The below Fig. 5.2, shows the optimal charging trajectory. Looking at the current trajectory it is noticed that the Charging starts at set value and then follows the control law to take the battery to the final charged state in minimum time maintaining the state and input constraints.

Fig. 5.3 shows the Regeneration current at different α and β settings.

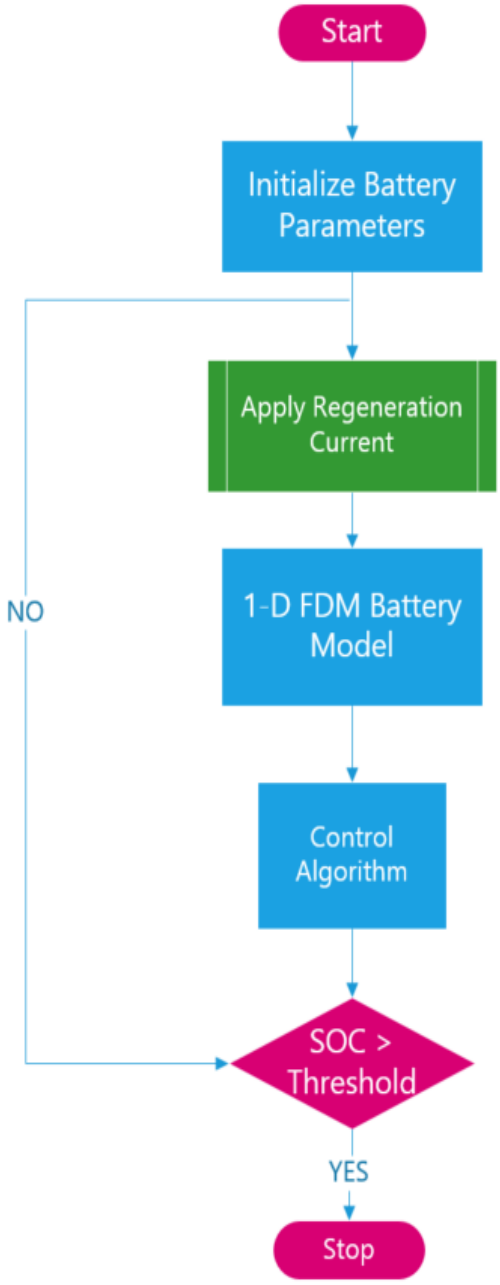

Fig. 5.1. State Flow of the Optimized Regeneration Controller Algorithm

The rate of increase of Cell Temperature is monitored to make sure that the rate is conserved within a limit. This is to make sure that the battery is not subjected

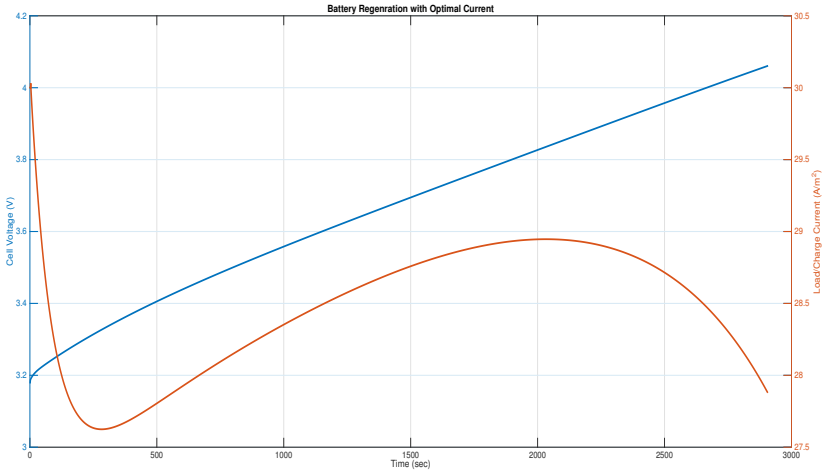

Fig. 5.2. Optimum Current Trajectory

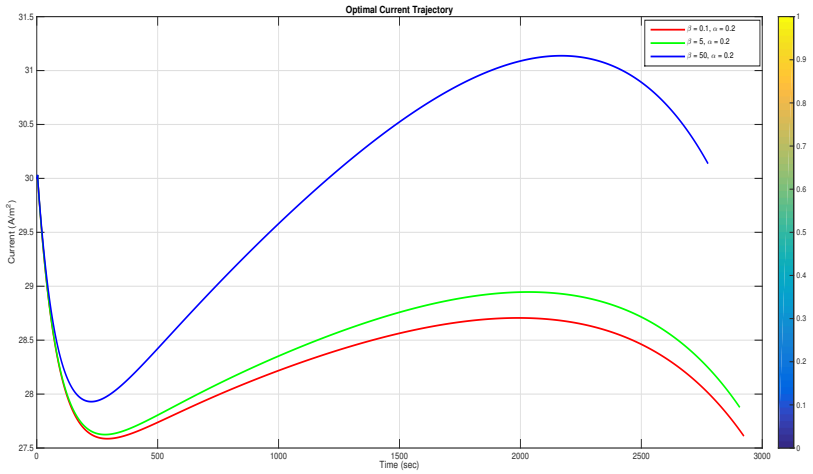

Fig. 5.3. Optimum Current Trajectory for Different α and β settings

to excessive temperature rise which adversely affect the battery performance and decreases its EUL. Temperature is a key factor in battery performance and also is point of safety issue. Hence, it is to be noted that a high charge current can try to charge the battery in a shortest time possible but will compromise of battery performance, life and safety. In this work cell bulk temperature is measured and fed

as a feedback to the controller which is a deciding factor in increasing or decreasing the charge current.

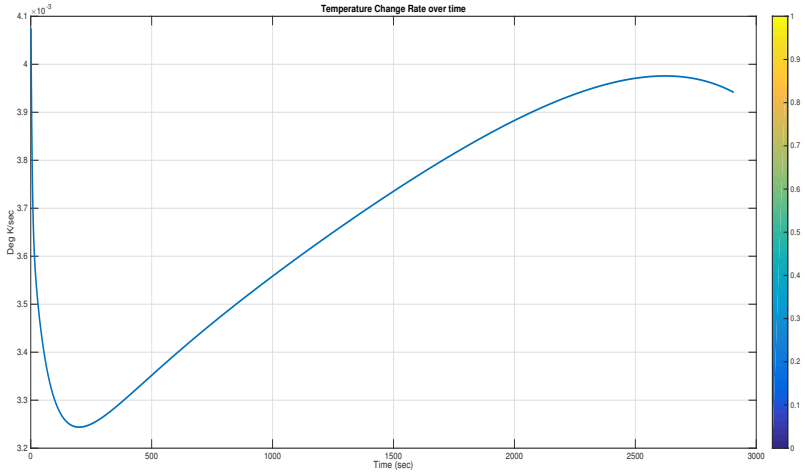

Fig. 5.4. Cell Temperature Rate

The tunable parameter β is to be adjusted such that both fast charge rate and low degradation is achieved. This parameter provide the manufacturers with an option of tuning the controller in terms of cell temperature. The above Fig. 5.4 shows the rate of increase of cell temperature.

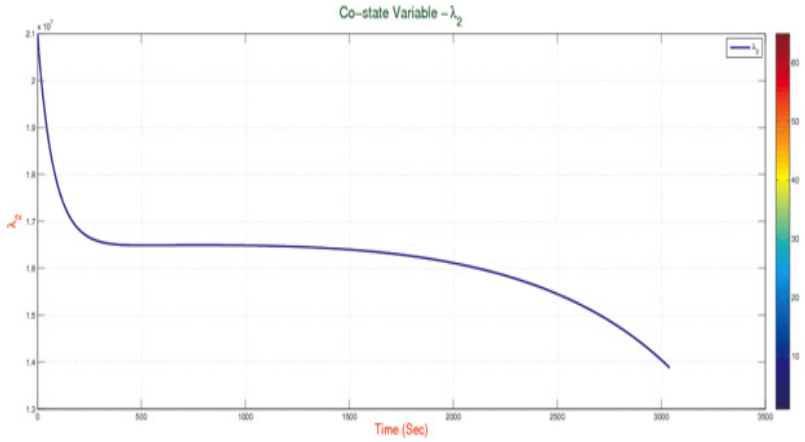

Fig. 5.5. Co-state Plot

The Co-state plots are shown in Fig. 5.5 for λ_2. λ_1 is constant throughout.

The different current rates are also analyzed to see the difference between the constant current regeneration Vs. optimal rate regeneration.

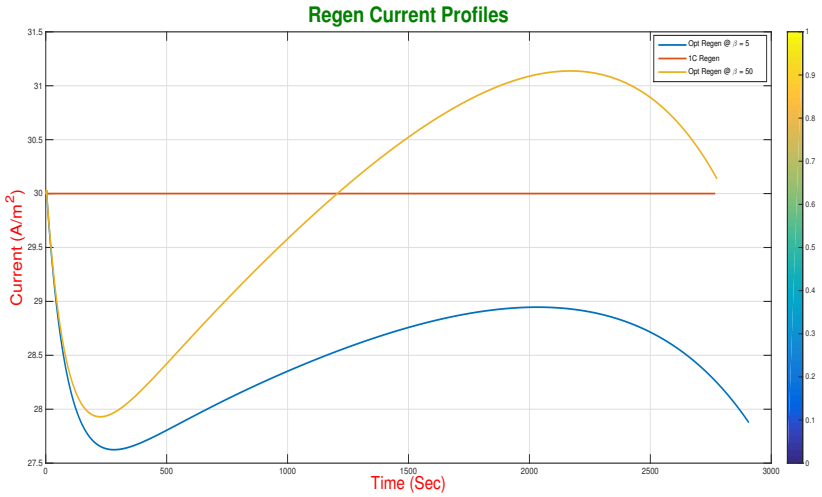

Fig. 5.6. Different Current Profiles for Regeneration

Fig. 5.6 shows that the regeneration times are quite similar but the big difference is in the battery parameter conservation which increases the performance and longevity.

A comparative study between the 1C Regeneration and the Optimal Regeneration with $\beta = 5$ is shown below. From the plot it is quite obvious that the ramp rate of cell temperature is kept at the required limit. While the constant 1C rate increases the cell temperature ramp rate without a check.

A quick look at the optimal current rate with a β value of 50. This shows that the regeneration time is reduced but there is no compromise on the temperature increase rate.

The over potential is also monitored to make sure that it is positive.

The implications of these study proves that in case of constant current regeneration, charging time can be reduced by increasing the current but this will adversely affect the battery performance and will cause aging, thereby reducing the Battery EUL. In case the regeneration current is lowered it will increase the charging time

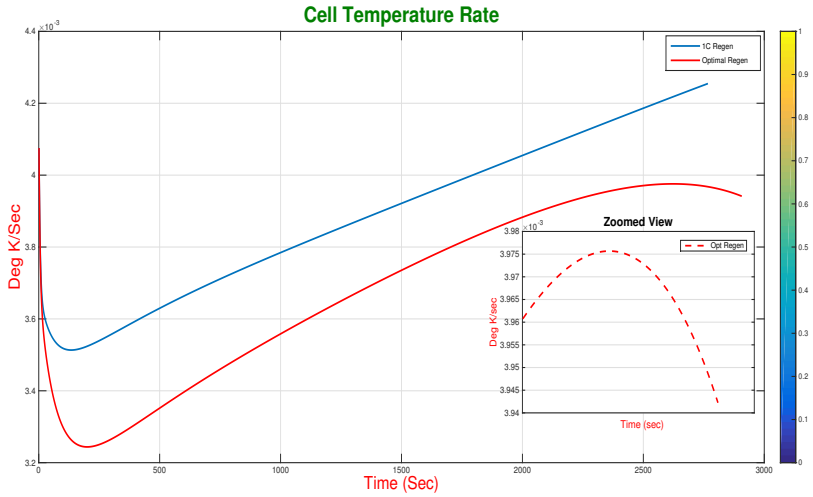

Fig. 5.7. Cell Temperature Rate: 1C Regen Vs. Optimal Regen

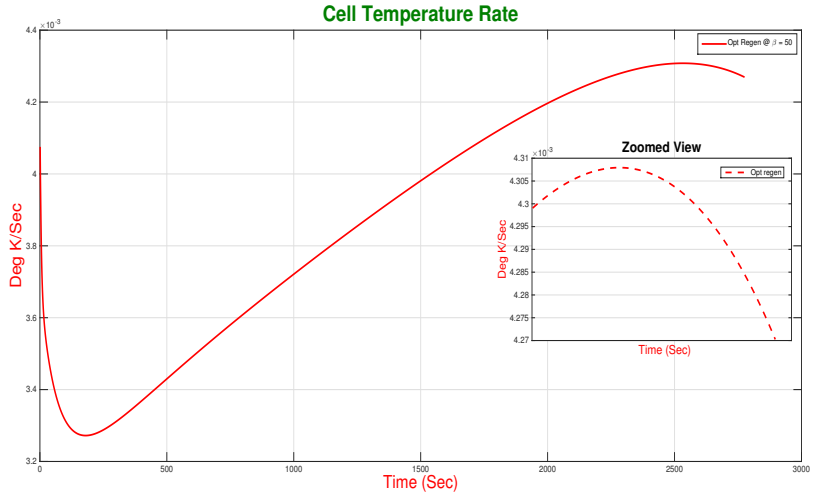

Fig. 5.8. Cell Temperature Rate: Optimal Regeneration at $\beta = 50$

without any significant reduction in temperature ramp rate.

A set of values for α, β and δ is selected and simulation results were compared to analyze the effect of each values. The results also shows the trend that must be followed to in selecting the correct settings. So, these parameters can be chosen in such

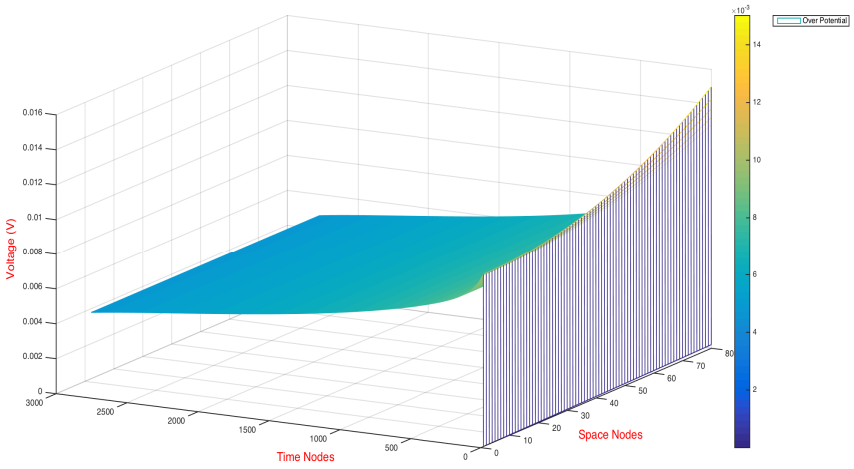

Fig. 5.9. Over Potential: Optimal Regeneration at $\beta = 50$

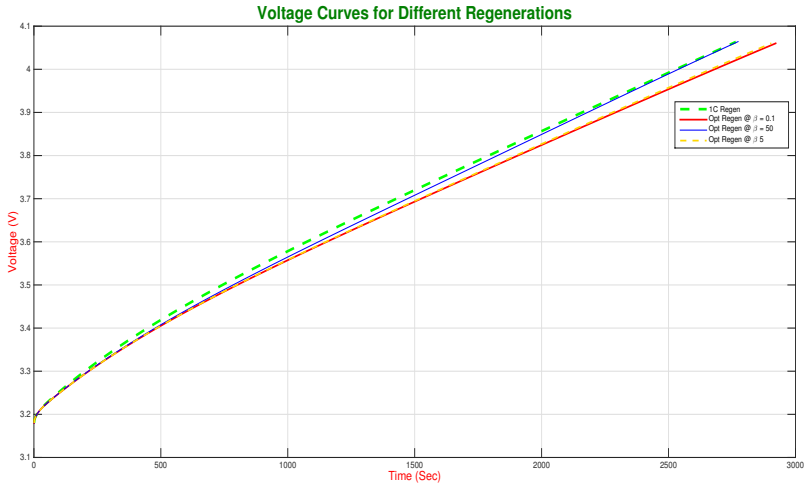

Fig. 5.10. Voltage Plots for all Regeneration Profiles

a way to achieve a balance between fast charge rate and limiting the cell degradation by keeping a watch on cell temperature. The results are shown in Appendix. A.2

The regeneration time with each settings are analyzed and it is seen that the time is not improved by a large margin. Two examples are shown below.

Table 5.1
Typical regeneration time for different β and δ : $\alpha = 0.01$

-	$\beta = 0.5$	$\beta = 5$	$\beta = 50$
$\delta = 0.1$	3072	2980	2422
$\delta = 1$	3108	3097	2996
$\delta = 10$	3112	3111	3100

Table 5.2
Typical regeneration time for different β and δ : $\alpha = 1$

-	$\beta = 0.5$	$\beta = 5$	$\beta = 50$
$\delta = 0.1$	2798	2789	2706
$\delta = 1$	2946	2941	2891
$\delta = 10$	3083	3082	3072

Table 5.3
Typical regeneration time for different β and δ : $\alpha = 10$

-	$\beta = 0.5$	$\beta = 5$	$\beta = 50$
$\delta = 0.1$	2769	2768	2758
$\delta = 1$	2799	2798	2789
$\delta = 10$	2947	2946	2941

Table. 5.1 shows the regeneration time for different β and δ with a fixed $\alpha = 0.01$. All time measurements are in seconds.

Table. 5.2 shows the regeneration time for different β and δ with a fixed $\alpha = 1$. All time measurements are in seconds.

Table. 5.3 shows the regeneration time for different β and δ with a fixed $\alpha = 10$. All time measurements are in seconds. As compared to a constant current regeneration with a 1C charge rate it took 2941 seconds for the model to charge to its final capacity.

The final SOC after the simulation is analyzed as well.

Table. 5.4 shows the final saturated SOC for different β and δ with a fixed $\alpha = 0.01$.

Table. 5.5 shows the final saturated SOC for different β and δ with a fixed $\alpha = 1$

Table 5.4
Final SOC saturation level at the end of simulation for different β and δ : $\alpha = 0.01$

-	$\beta = 0.5$	$\beta = 5$	$\beta = 50$
$\delta = 0.1$	95.40%	95.57%	96.74%
$\delta = 1$	95.36%	95.38%	95.54%
$\delta = 10$	95.36%	95.36%	95.38%

Table 5.5
Final SOC saturation level at the end of simulation for different β and δ : $\alpha = 1$

-	$\beta = 0.5$	$\beta = 5$	$\beta = 50$
$\delta = 0.1$	95.77%	95.79%	95.97%
$\delta = 1$	95.56%	95.57%	95.68%
$\delta = 10$	95.38%	95.38%	95.40%

Table 5.6
Final SOC saturation level at the end of simulation for different β and δ: $\alpha = 10$

-	$\beta = 0.5$	$\beta = 5$	$\beta = 50$
$\delta = 0.1$	95.83%	95.83%	95.84%
$\delta = 1$	95.77%	95.77%	95.79%
$\delta = 10$	95.57%	95.56%	95.57%

Table. 5.6 shows the final saturated SOC for different $\boldsymbol{\beta}$ and $\boldsymbol{\delta}$ with a fixed $\boldsymbol{\alpha = 10}$.

Thus, we have seen that the present results are quite promising. The two tuning parameters $\boldsymbol{\alpha}$ and $\boldsymbol{\beta}$ can be used to their fullest potential to achieve better results for all variety of battery state parameters. It is also noted that the regeneration current is not following a conventional steady state trends but rather it follows a continuous and smooth curve. While this increases a bit of hard wire change but with the current PWM switching frequency oscillators this is not impossible. Also, with a constant current - constant voltage there is a chance of pushing the batteries to its limits with out any feedback monitoring system of the battery internal states. In this scheme the battery states are continuously monitored in terms of temperature and its co-states. This gives a better internal state management system of the battery.

The cell model assumes an ideal electro-chemical cell and ignores any cell degradation mechanisms that may result from any extreme cell designs. These mechanisms are important when considering the overall life cycle performance. A cell design that has maximum initial energy density or performance only to suffer catastrophic capacity loss or power fade within a small number of cycles would be a poor design. Additional constraints that set lower bounds on the end-of-life energy density or modifications to the objective function that accounts for cumulative useful energy over the entire lifetime should be included. Another important aspect is the volume fraction change. Volume fraction change in the graphite anode and manganese spinel cathode is small and is neglected in the cell model, however it is not the case for some of the other materials, such as silicon in anodes. Volume change up to factors of 3 4 can be expected during intercalation. The large volume increase means that the ion transport equation in the solid phase cannot be simplified to the diffusion equation.

Volume change in electrode causes [54]:

- Change in porosity
- Cell impedance

- Loss of power
- Contact loss of active materials
- Capacity fade

Accounting for the effects of volume expansion in the cell model requires coupling of a physics-based degradation model to determine how design variables, such as particle size and volume fraction, contribute to contact loss. Factors such as particle packing density and size influence the effect of volume change [55] needs to be considered as well.

One of the primary causes of lithium loss in the cell is the decomposition of electrolyte at the negative electrode/electrolyte interface to form a passive SEI layer during the initial cycles [54]. This is due to the anode operating at voltages that are outside the electrochemical stability window of electrolyte components. SEI formation is an irreversible process that consumes reusable lithium. However the SEI layer is also beneficial in preventing further decomposition of solvent and at the same time allows lithium ions to pass through. To accurately model the formation, growth and subsequent stabilization of SEI layer, physics-based interaction between electrode active material and electrolyte and influence of SEI thickness on electrolyte diffusivity should be included in the cell model [56].

Volume change in the cell and SEI formation affects the intercalation induced stress on the solid particles. The amount of stress depends on the shape and size of particles, and it is interrelated through the local surface flux, and ion concentration gradient [57]. Multi-scale modeling has shown that lithium intercalation for large particles is diffusion limited and that the resulting diffusion-stress coupling causes mismatching strains and stresses [58]. High stress is also experienced in nano-scale particles due to surface stress effect [59].

6. CONCLUSIONS AND RECOMMENDATIONS

6.1 Concluding Summary

The 1-D Cell model is validated against published papers to substantiate its performance against all operating regions.The different C-Rate charge/discharge cycles shows promising results.

The optimal charging algorithm developed in this literature is based on the following battery state parameters:

- State of charge - $\boldsymbol{SOC(t)}$
- Solid Phase concentration - $\boldsymbol{C_s(t)}$
- Molar Flux - $\boldsymbol{J(t)}$
- Cell Temperature - $\boldsymbol{T(t)}$
- Over potential - $\boldsymbol{\eta(t)}$

The control law behaved well with both, input and state constraints. Though battery internal degradation is not dynamically modeled, but it is observed that neglecting these factors did not affect the simulation result much.

A set of 3 point values were used for each $\boldsymbol{\alpha}$, $\boldsymbol{\beta}$ and $\boldsymbol{\delta}$ and the simulation results are presented in Appendix B.
Based on the current and voltage profile along with the cell temperature rate 2 sets of optimized and tuned values are proposed. Table. 6.1 shows the tuned set of proposed values.

Table 6.1
Tuned values of $\boldsymbol{\alpha}$, $\boldsymbol{\beta}$ and $\boldsymbol{\delta}$

Parameters	Tuned Set 1	Tuned Set 2
$\boldsymbol{\alpha}$	**0.01**	**1**
$\boldsymbol{\beta}$	**5**	**50**
$\boldsymbol{\delta}$	**0.01**	**1**

6.2 Major contribution on the Thesis

This thesis work is focused to improve two major aspects of 1-D Lithium Battery BMS system. Though many small factors are touched upon and discussed in this work like cell volume change, stresses in the cell and resistance formation and their relation to bulk cell temperature, the primary two major improvements discussed and supported in this work are:

- Robust numerical solution framework for reformulated physics based 1-D model.
- A dynamic closed loop efficient optimization technique for battery regeneration.

The numerical framework designed in this work is a multi purpose model which is capable of running all battery cycles with high fidelity. Simulation of the numerical method showed that the model replicates the actual cell characteristics and behavior for almost any cycle. Cell bulk temperature which is one of the key contributor to many other battery states and its performance is also modeled very accurately in this model. The numerical method of solving the battery equations can be used to solve battery dynamics required in any application where a physics based model is desired.The next big improvement is obviously the optimization method and the performance achieved. Contrary to the conventional CC-CV method this is more dynamical and more close to following the battery internal chemistry. In traditional CC-CV process apart from the basic safety feature which tends to switch the charging current from one level to the other so as to keep a check on the temperature there is no other close loop action or monitoring of the internal battery kinetics. With this proposed optimization scheme there is a huge leap towards including the cell temperature and other battery internal states into the calculation of charging current. This brings in a balance between both performance and battery degradation and performs an optimized charging action. This is a big improvement when battery life and aging is considered.

6.3 Recommendations for Future Work

As stated earlier, future work is to include physical measurable state parameters from the battery and manipulate the optimal law to include only those parameters. The next big step shall be to include the control algorithm into hardware in loop and quantify the performance of the algorithm. Experiments with actual battery cell along with battery pack is required to come up with optimized tuned values for $\boldsymbol{\alpha}$, $\boldsymbol{\beta}$ and $\boldsymbol{\delta}$ parameters. This simulations with actual cell will also indicate the level of improvements based on aging and degradation of the battery. Future work shall focus deeply on the effects of battery state parameters on resistive film formation across the electrodes. It is also require to analyze the effects of these resistive films on battery performance, especially when the battery reaches it EUL. A more advanced study is recommended to analyze the effects of altering the battery internal states by external perturbation so as to increase the battery performance. This is a very abstract level notion which could be pondered upon to get beneficial results.

LIST OF REFERENCES

LIST OF REFERENCES

[1] N. Xue, *Design and Optimization of Lithium-Ion Batteries for Electric-Vehicle Applications*. PhD thesis, University of Michigan, 2014.

[2] E. I. Administration and U. D. of Energy, "Eia. annual energy review," 2011.

[3] U. S. E. P. Agency, "Eia. inventory of u.s. greenhouse gas emissions and sinks:," 2013.

[4] T. K. S. of Automotive Engineers (KSAE), "Electric vehicles in asia pacific: What is electric vechicle?." `http://www.evaap.org/electric/electric.html?sgubun=1` (Last Accessed: 21 January 2015).

[5] B. University, "Charging lithium ion batteries." Last Accessed: 21 January 2015.

[6] D. X. Chen, "Illustration of the charge/discharge processes in rechargeable lithium ion." `http://cas.umkc.edu/chemistry/chen.asp` (Last Accessed: 21 January 2015).

[7] M. Doyle, T. F. Fuller, and J. Newman, "Modeling of galvanostatic charge and discharge of the lithium/polymer/insertion cell," *Journal of The Electrochemical Society*, vol. 140, no. 6, pp. 1526–1533, 1993.

[8] R. Klein, N. A. Chaturvedi, J. Christensen, J. Ahmed, R. Findeisen, and A. Kojic, "Optimal charging strategies in lithium-ion battery," *American Control Conference*, 2011.

[9] N. Chaturvedi, R. Klein, J. Christensen, J. Ahmed, and A. Kojic, "Algorithms for advanced battery management systems: Modeling, estimation, and control challenges for lithium-ion batteries," *IEEE Control Systems Magazine*, vol. 30, no. 3, 2010.

[10] V. Ramadesigan, P. W. C. Northrop, S. De, S. Santhanagopalan, R. D. Braatz, and V. R. Subramanian, "Modeling and simulation of lithium-ion batteries from a systems engineering perspective," *Journal of The Electrochemical Society*, vol. 159, no. 3, pp. 31–45, 2012.

[11] D. Zhang, B. N. Popov, and R. E. White *Journal of The Electrochemical Society*, vol. 147, p. 831, 2000.

[12] S. Santhanagopalan, Q. Z. Guo, P. Ramadass, and R. E. White *Journal of The Electrochemical Society*, vol. 156, p. 620, 2006.

[13] M. Doyle and J. Newman, "Effects of diffusive charge transfer and salt concentration gradient in electrolyte on li-ion battery energy and power densities," *Journal of The Electrochemical Society*, vol. 40, p. 2191, 1995.

[14] J. Newman *Journal of The Electrochemical Society*, vol. 142, p. 97, 1995.

[15] P. Arora, M. Doyle, A. S. Gozdz, R. E. White, and J. Newman *Journal of The Electrochemical Society*, vol. 88, p. 219, 2000.

[16] G. G. Botte, V. R. Subramanian, and R. E. White *Journal of The Electrochemical Society*, vol. 45, p. 2595, 2000.

[17] M. Doyle, J. Newman, A. S. Gozdz, C. N. Schmutz, and J. M. Tarascon *Journal of The Electrochemical Society*, vol. 143, p. 1890, 1996.

[18] T. F. Fuller, M. Doyle, and J. Newman *Journal of The Electrochemical Society*, vol. 141, p. 982, 1994.

[19] T. F. Fuller, M. Doyle, and J. Newman *Journal of The Electrochemical Society*, vol. 141, p. 1, 1994.

[20] P. M. Gomadam, J. W. Weidner, R. A. Dougal, and R. E. White *Journal of The Electrochemical Society*, vol. 110, p. 267, 2002.

[21] J. Newman and W. Tiedemann *AIChE*, vol. 21, p. 25, 1975.

[22] G. Ning, R. E. White, and B. N. Popov *Electrochim Acta*, vol. 51, p. 2012, 2006.

[23] P. Ramadass, B. Haran, P. M. Gomadam, R. White, and B. N. Popov, "Development of first principles capacity fade model for li-ion cells," *Journal of The Electrochemical Society*, vol. 151, p. A196, 2004.

[24] P. Ramadass, B. Haran, R. White, and B. N. Popov *J Power Sources*, vol. 123, p. 230, 2003.

[25] K. E. Thomas and J. Newman *Journal of The Electrochemical Society*, vol. 150, p. A176, 2003.

[26] S. A. Hallaj, H. Maleki, J. S. Hong, and J. R. Selman *J Power Sources*, vol. 83, p. 1, 1999.

[27] T. I. Evans and R. E. White, "A thermal analysis of a spirally wound battery using a simple mathematical model," *Journal of The Electrochemical Society*, vol. 136, p. 2145, 1989.

[28] D. Bernardi, E. Pawlikowski, and J. Newman *Journal of The Electrochemical Society*, vol. 132, p. 5, 1985.

[29] Y. Chen and J. W. Evans *Journal of The Electrochemical Society*, vol. 140, p. 1833, 1993.

[30] Y. F. Chen and J. W. Evans *Journal of The Electrochemical Society*, vol. 141, p. 2947, 1994.

[31] C. R. Pals and J. Newman *Journal of The Electrochemical Society*, vol. 142, p. 3274, 1995.

[32] C. R. Pals and J. Newman, "The effect of battery design parameters on heat generation and utilization in a li-ion cell," *Journal of The Electrochemical Society*, vol. 142, p. 3282, 1995.

[33] J. Bhattacharya and A. V. der Ven, "Understanding li diffusion in li-intercalation compounds," *Phys Rev B*, vol. 81, 2010.

[34] A. B. Bortz, M. H. Kalos, and J. L. Lebowitz, "A new algorithm for mote carlo simulation of ising spin systems," *J Comput Phys*, vol. 17, no. 12, 1975.

[35] A. V. der Ven and G. Ceder *Electrochem Solid St*, vol. 3, p. 301, 2000.

[36] A. V. der Ven, J. C. Thomas, Q. C. Xu, B. Swoboda, and D. Morgan *Phys Rev B*, vol. 78, 2008.

[37] P. W. C. Northrop, V. Ramadesigan, S. De, and V. R. Subramanian, "Efficient simulation and reformulation of lithium-ion battery models for enabling electric transportation," *Journal of The Electrochemical Society*, vol. 158, no. 12, p. 1461, 2011.

[38] M. Wagemaker, A. V. D. Ven, D. Morgan, G. Ceder, F. M. Mulder, and G. J. Kearley *Chem Phys*, vol. 317, p. 130, 2005.

[39] W. B. Gu and C. Y. Wang *Journal of The Electrochemical Society*, vol. 147, p. 2910, 2000.

[40] M. Doyle, Y. Fuentes, and J. Newman *Journal of The Electrochemical Society*, vol. 150, p. 706, 2003.

[41] S. Santhanagopalan, Q. Guo, R. Ramadass, and R. E. White, "Review of models for predicting the cycling performance of lithium ion batteries," *J. Power Sources*, vol. 156, p. 620, 2006.

[42] P. Ramadass, B. Haran, P. M. Gomadam, R. E. White, and B. N. Popov *Journal of The Electrochemical Society*, vol. 151, p. 196, 2004.

[43] V. Srinivasan and C. Y. Wang, "Analysis of electrochemical and thermal behavior of li-ion cells," *Journal of The Electrochemical Society*, vol. 150, p. 98, 2003.

[44] C. Y. Wang, W. B. Gu, and B. Y. Liaw *Journal of The Electrochemical Society*, vol. 145, p. 3407, 1998.

[45] V. R. Subramanian, V. D. Diwakar, and D. Tapriyal, "Efficient macro-micro scale coupled modeling of batteries," *Journal of The Electrochemical Society*, vol. 152, p. 2002, 2005.

[46] S. Liu *Solid State Ionics*, vol. 177, p. 53, 2006.

[47] L. Cai and R. E. White, "Reduction of model order based on proper orthogonal decomposition for lithium-ion battery simulations," *Journal of The Elctrochemical Society*, vol. 156, no. 3, pp. A154–A161, 2009.

[48] K. A. Smith, C. D. Rahn, and C.-Y. Wang, "Model-based electrochemical estimation and constraint management for pulse operation of lithium ion batteries," *Control Systems Technology, IEEE Transactions*, vol. 18, no. 3, pp. 654–663, 2009.

[49] T.-S. Dao and C. P. V. J. McPhee, "Simplification and order reduction of lithium-ion battery model based on porous-electrode theory," *Joournal of Power Sources*, vol. 198, no. 15, pp. 329–337, 2012.

[50] K. A. Smith, C. D. Rahn, and C.-Y. Wang, "Control oriented 1d electrochemical model of lithium ion battery," *Science Direct*, vol. 48, no. 9, pp. 2565–2578, 2007.

[51] N. A. Chaturvedi, R. Klein, J. Christensen, J. Ahmed, and A. Kojic, "Algorithms for advanced battery management systems - modeling, estimation and control challenges for lithium ion batteries," *IEEE Control Systems Magazine*, 2010.

[52] V. R. Subramanian, V. Boovaragavan, V. Ramadesigan, and M. Arabandi, "Mathematical model reformulation for lithium-ion battery simulations: Galvanostatic boundary conditions," *Journal of The Electrochemical Society*, vol. 156, no. 4, pp. 260–271, 2009.

[53] L. M. Ross in *A Primer on Pontryagin's Principle in Optimal Control*, vol. 1, Collegiate Publishers, 2009.

[54] J. Vetter, P. Novak, M. Wagner, C. Veit, K.-C. Moller, J. Besenhard, M. Winter, M. Wohlfahrt-Mehrens, C. Vogler, and A. Hammouche, "Ageing mechanisms in lithium-ion batteries," *Journal of Power Sources*, vol. 147, no. 1, pp. 269–281, 2005.

[55] J. Besenhard, J. Yang, and M. Winter, "Will advanced lithium-alloy anodes have a chance in lithium-ion batteries?," *Journal of Power Sources*, vol. 68, no. 1, pp. 87–90, 1997.

[56] X. Lin, J. Park, L. Liu, Y. Lee, A. Sastry, and W. Lu, "A comprehensive capacity fade model and analysis for li-ion batteries," *Journal of The Electrochemical Society*, vol. 160, no. 10, pp. A1701–A1710, 2013.

[57] X. Zhang, W. Shyy, and A. M. Sastry, "Numerical simulation of intercalation-induced stress in li-ion battery electrode particles," *Journal of the Electrochemical Society*, vol. 154, no. 10, pp. A910–A916, 2007.

[58] S. Golmon, K. Maute, and M. L. Dunn, "Multiscale design optimization of lithium ion batteries using adjoint sensitivity analysis," *International Journal for Numerical Methods in Engineering*, vol. 92, no. 5, pp. 475–494, 2012.

[59] C. M. DeLuca, K. Maute, and M. L. Dunn, "Effects of electrode particle morphology on stress generation in silicon during lithium insertion," *Journal of Power Sources*, vol. 196, no. 22, pp. 9672–9681, 2011.

APPENDICES

A. REFERENCE FIGURES

A.1 1-D Battery Model Numerical Solution Results

This section shows the 1-D Lithium Ion Battery model state parameter plots. The plots below shows the parameter development over space and time node.

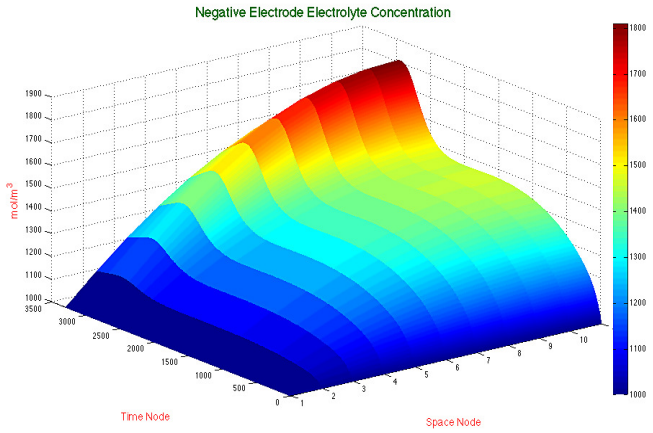

(a) Electrolyte Concentration at Negative Electrode

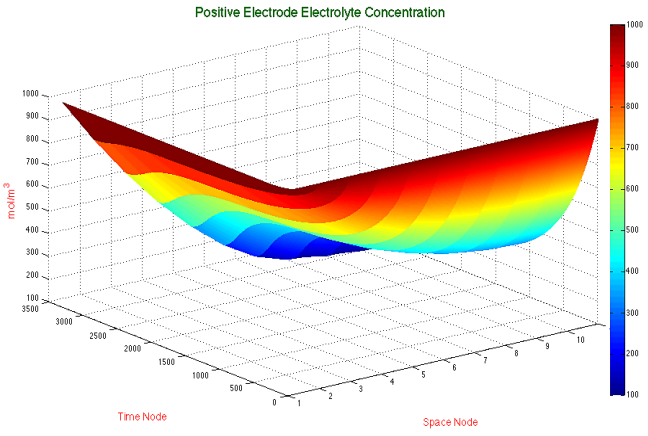

(b) Electrolyte Concentration at Positive Electrode

Fig. A.1. Electrolyte Phase Concentration

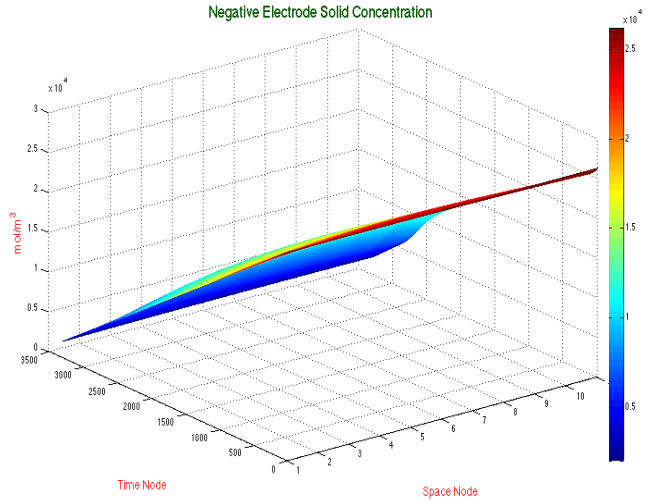

(a) Solid Phase Concentration at Negative Electrode

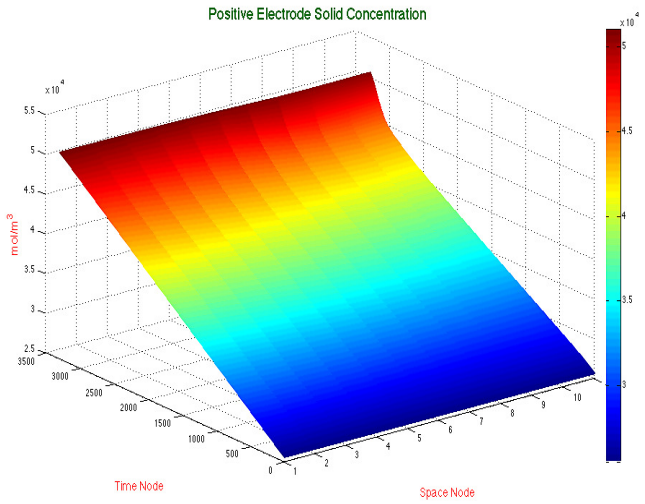

(b) Solid Phase Concentration at Positive Electrode

Fig. A.2. Solid Phase Concentration

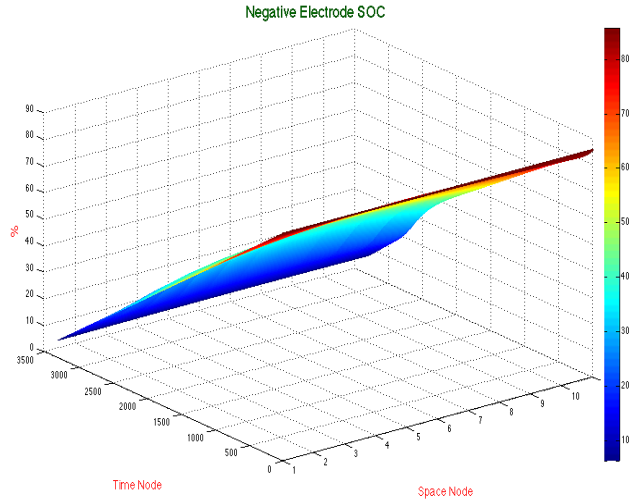

(a) State of Charge at Negative Electrode

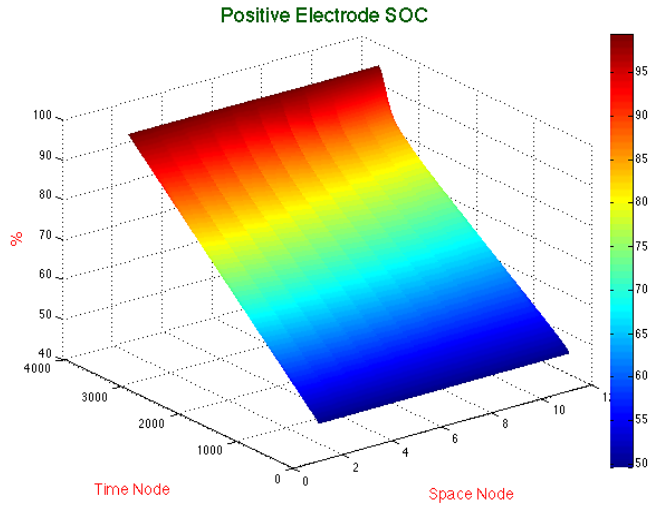

(b) State of Charge at Positive Electrode

Fig. A.3. State of Charge

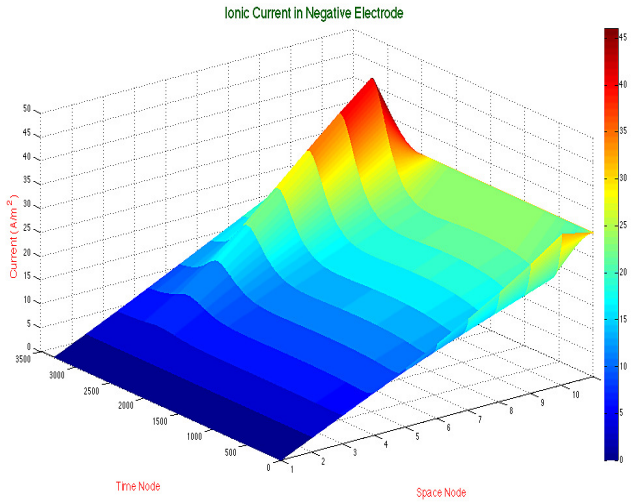

(a) Ionic Current - Negative Electrode

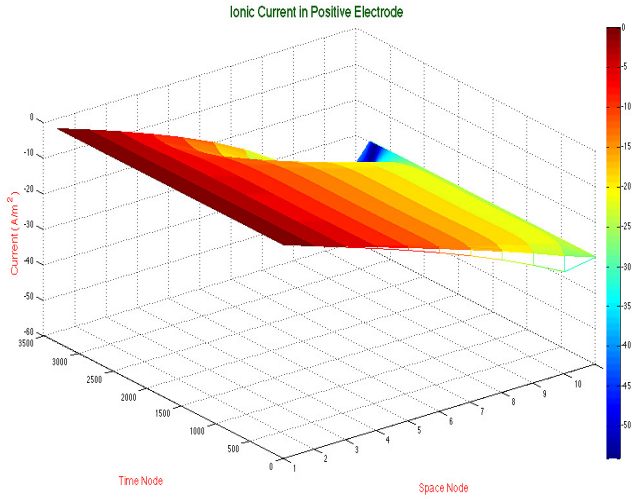

(b) Ionic Current - Positive Electrode

Fig. A.4. Ionic Current

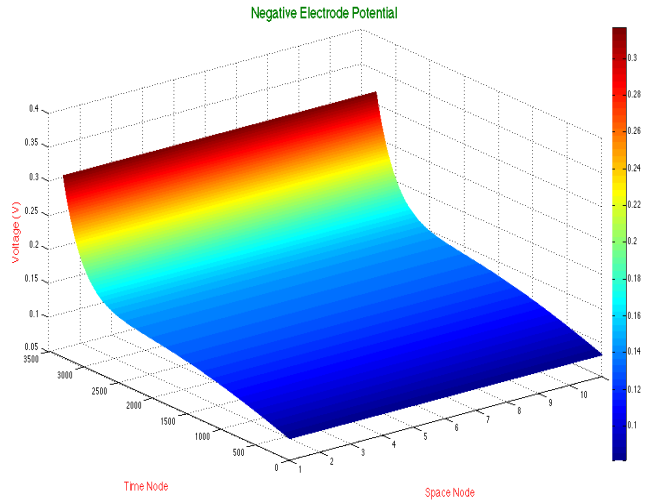

(a) Solid Potential - Negative Electrode

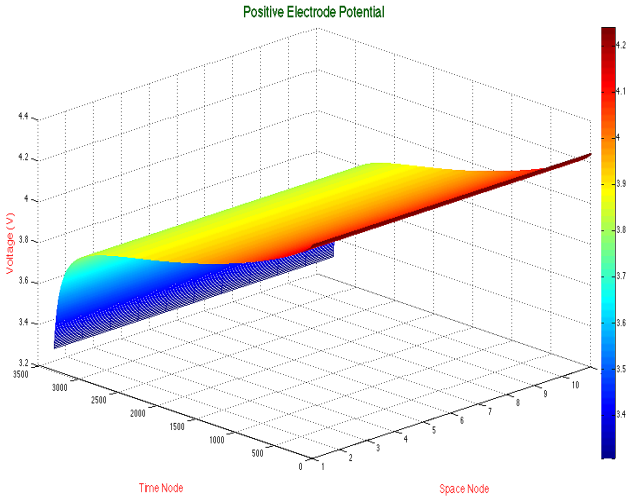

(b) Solid Potential - Positive Electrode

Fig. A.5. Solid Phase Potential

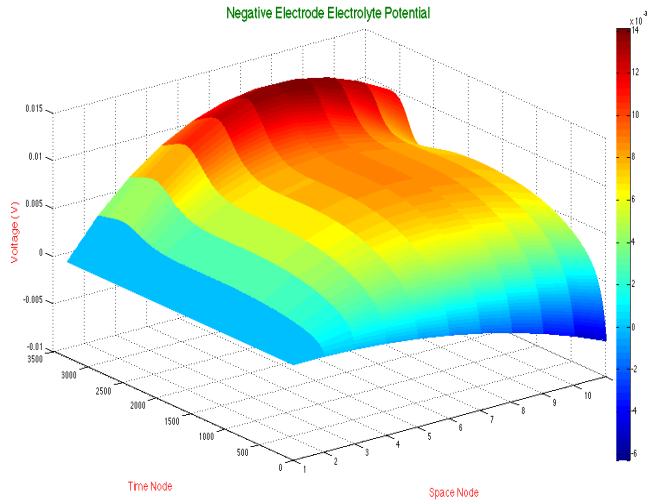

(a) Electrolyte Potential - Negative Electrode

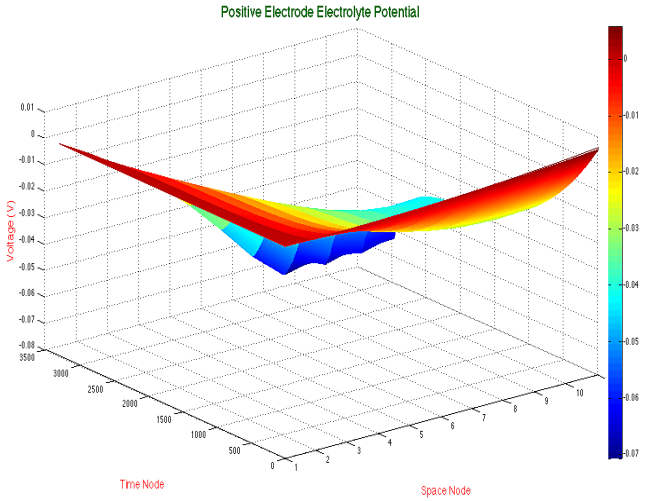

(b) Electrolyte Potential - Positive Electrode

Fig. A.6. Electrolyte Phase Potentials

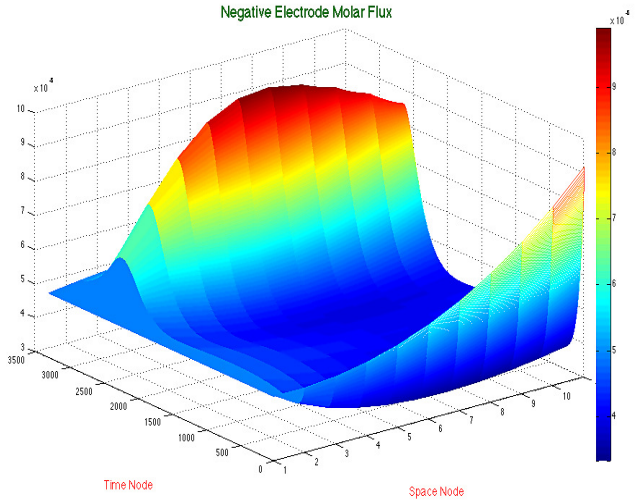

(a) Molar Flux - Negative Electrode

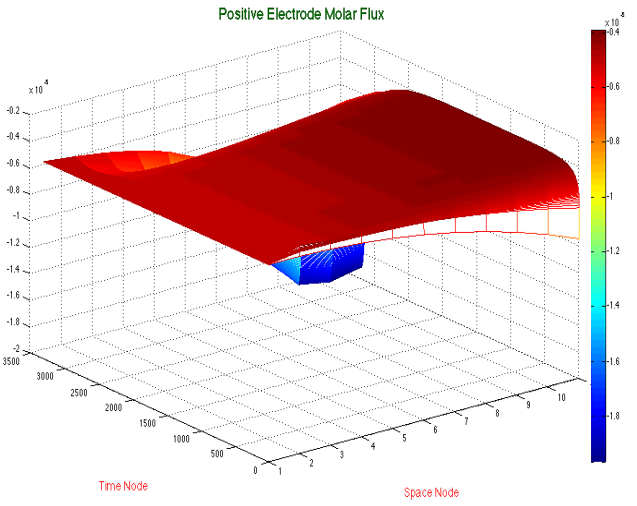

(b) Molar Flux - Positive Electrode

Fig. A.7. Molar Flux

A.2 Tuning Results - Different α, β and δ Settings

A set of values is chosen for $\boldsymbol{\alpha}$, $\boldsymbol{\beta}$ and $\boldsymbol{\delta}$, which are the corresponding weights of temperature and current. The following figures shows the simulation results for different $\boldsymbol{\alpha}$ and $\boldsymbol{\beta}$ with 3 $\boldsymbol{\delta}$ values of 0.1, 1 and 10 for each simulation run.

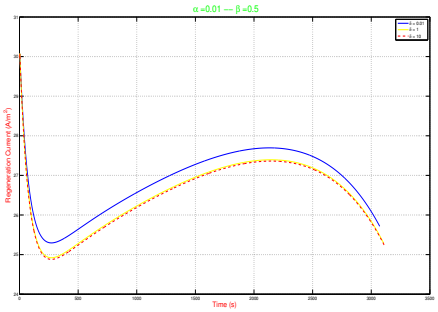

(a) Regeneration Current - $\boldsymbol{\alpha = 0.01}$, $\boldsymbol{\beta = 0.5}$

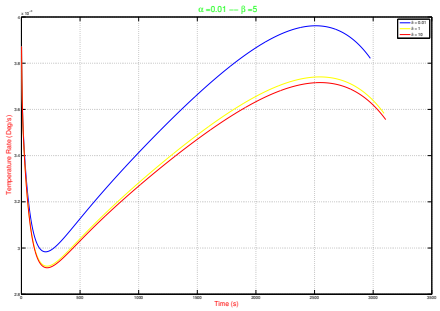

(b) Temperature Rate - $\boldsymbol{\alpha = 0.01}$, $\boldsymbol{\beta = 0.5}$

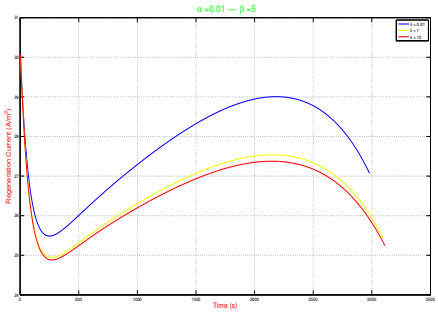

(c) Regeneration Current - $\boldsymbol{\alpha = 0.01}$, $\boldsymbol{\beta = 5}$

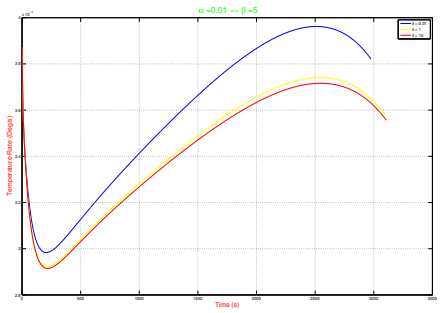

(d) Temperature Rate - $\boldsymbol{\alpha = 0.01}$, $\boldsymbol{\beta = 5}$

Fig. A.8. Tuning Results - $\boldsymbol{\alpha = 0.01}$, $\boldsymbol{\beta = 0.5, 5}$ - $\boldsymbol{\delta = 0.1, 1, 10}$

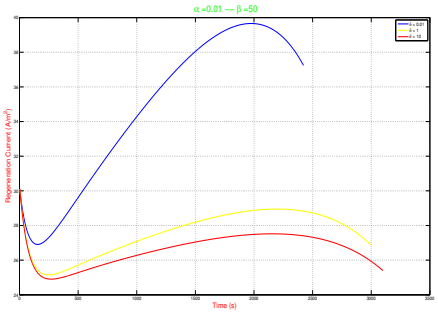

(a) Regeneration Current - $\boldsymbol{\alpha = 0.01}$, $\boldsymbol{\beta = 50}$

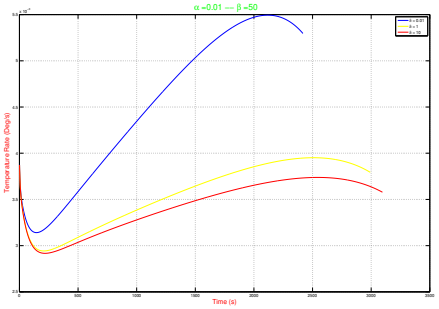

(b) Temperature Rate - $\boldsymbol{\alpha = 0.01}$, $\boldsymbol{\beta = 50}$

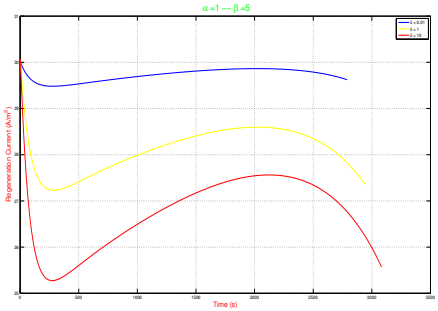

(c) Regeneration Current - $\boldsymbol{\alpha = 1}$, $\boldsymbol{\beta = 0.5}$

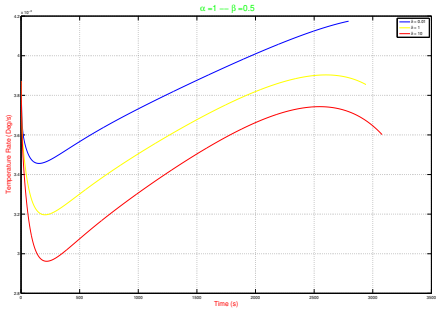

(d) Temperature Rate - $\boldsymbol{\alpha = 1}$, $\boldsymbol{\beta = 0.5}$

Fig. A.9. Tuning Results - $\boldsymbol{\alpha = 0.01, 1}$, $\boldsymbol{\beta = 0.5, 50}$ - $\boldsymbol{\delta = 0.1, 1, 10}$

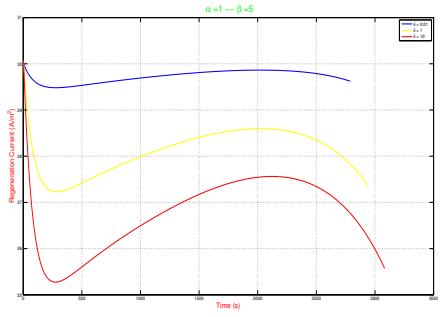

(a) Regeneration Current - $\boldsymbol{\alpha = 1}$, $\boldsymbol{\beta = 5}$

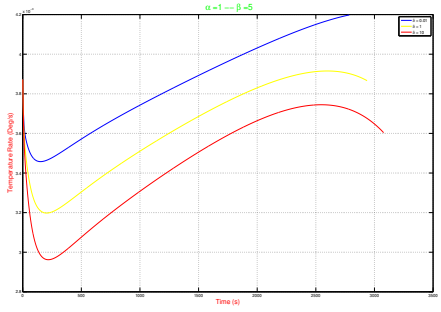

(b) Temperature Rate - $\boldsymbol{\alpha = 1}$, $\boldsymbol{\beta = 5}$

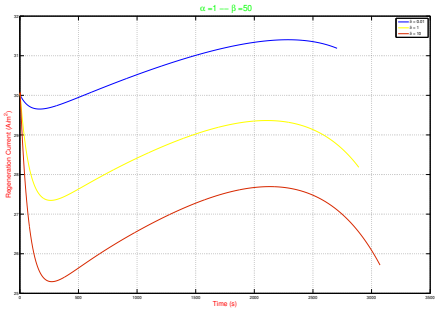

(c) Regeneration Current - $\boldsymbol{\alpha = 1}$, $\boldsymbol{\beta = 50}$

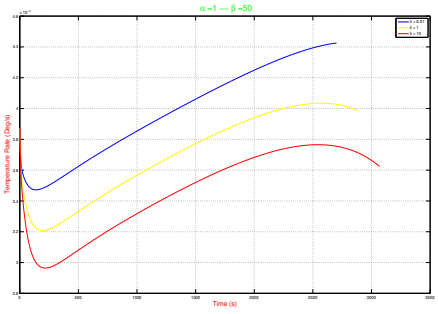

(d) Temperature Rate - $\boldsymbol{\alpha = 1}$, $\boldsymbol{\beta = 50}$

Fig. A.10. Tuning Results - $\boldsymbol{\alpha = 1}$, $\boldsymbol{\beta = 5, 50}$ - $\boldsymbol{\delta = 0.1, 1, 10}$

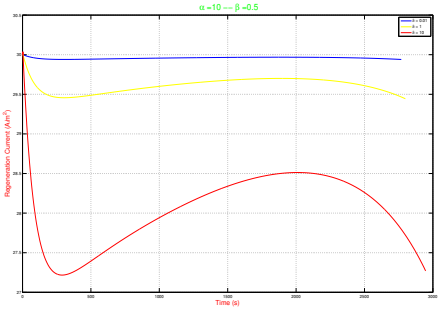

(a) Regeneration Current - $\boldsymbol{\alpha = 10}$, $\boldsymbol{\beta = 0.5}$

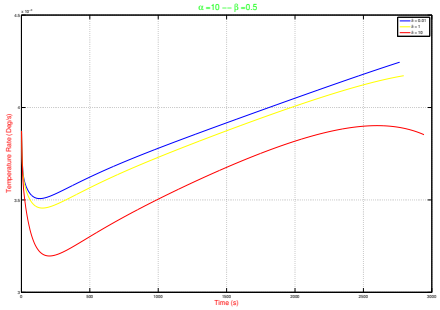

(b) Temperature Rate - $\boldsymbol{\alpha = 10}$, $\boldsymbol{\beta = 0.5}$

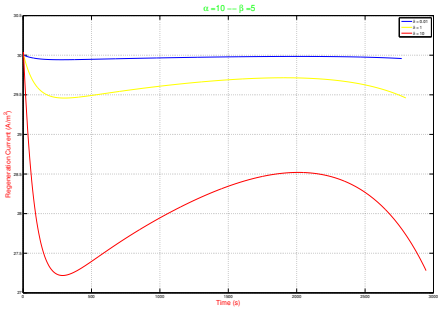

(c) Regeneration Current - $\boldsymbol{\alpha = 10}$, $\boldsymbol{\beta = 5}$

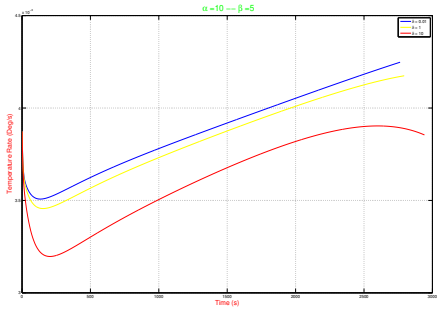

(d) Temperature Rate - $\boldsymbol{\alpha = 10}$, $\boldsymbol{\beta = 5}$

Fig. A.11. Tuning Results - $\boldsymbol{\alpha = 10}$, $\boldsymbol{\beta = 0.5, 5}$ - $\boldsymbol{\delta = 0.1, 1, 10}$

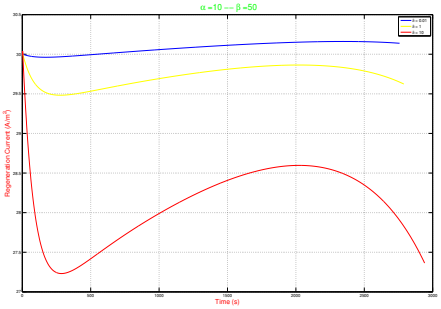

(a) Regeneration Current - $\boldsymbol{\alpha = 10}$, $\boldsymbol{\beta = 50}$

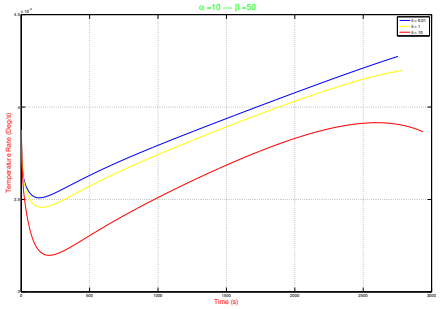

(b) Temperature Rate - $\boldsymbol{\alpha = 10}$, $\boldsymbol{\beta = 50}$

Fig. A.12. Tuning Results - $\boldsymbol{\alpha = 10}$, $\boldsymbol{\beta = 50}$ - $\boldsymbol{\delta = 0.1, 1, 10}$

B. 1-D LITHIUM-ION BATTERY MODEL CODE

********** Battery Model **********

1D Li Ion Electrochemical Battery Model

****

Contents

- Positive Electrode
- Temperature Calculation
- Controller Settings
- Post Processing

```
% Author :: Sourav Pramanik


% Course :: Master of Science - Thesis
%
% Date :: 20th November 2014
%
% Department :: Mechanical Engineering
%
% Institution :: Indiana University Purdue University Indianapolis
%
% Description :: This is the initialization file for all
%                battery parameters and setup configuration.
%                Simulation setup information is selected
%                from user input.
```

```
%
%               Ce_n, Ce_p, Ce_s are Electrolyte concentrations
%               for the Negative, Positive and separator regions.
%               They are kept constant at 1000 throughout.
%
%               Cs_n, Cs_p are Solid Phase concentration
%               qs_n, qs_p are concentration flux
%               Css_n, Css_p are surface concentrations
%
%               J_n, J_p are molar flux
%               Ke_n, Ke_p, Ke_s are ionic conductivity used in
%               calculation of Electrolyte potentials
%
%               Us_n, Us_p are solid phase potentials
%               Ue_n, Ue_p, Ue_s are electrolyte phase potentials
%
%               U_eq_n, U_eq_p are over-potentials


% ****************************************************************
clear all;
clc
tic
Li_Ion_1D_Model_Parameter_Determination_Draft09_09_rev2;

% Ce_n,Ce_p,Ce_s are Electrolyte concentrations for the Negative,
% Positive and separator regions. They are kept constant at 1000
% throughout.
```

```
% Cs_n, Cs_p are Solid Phase concentration
% qs_n, qs_p are concentration flux
% Css_n, Css_p are surface concentrations

% J_n, J_p are molar flux
% Ke_n, Ke_p, Ke_s are ionic conductivity used in calculation of
% Electrolyte potentials

% Us_n, Us_p are solid phase potentials
% Ue_n, Ue_p, Ue_s are electrolyte phase potentials

% U_eq_n, U_eq_p are overpotentials



% ###################################################################
% Equations -
% ###################################################################
%
```

——— Initial and Boundary Conditions ———-

```
            Applying the initial conditions
------------------------------------------------------------------
Negative Electrode at time t = 0 [Start]
------------------------------------------------------------------

 T_n(init_time_node, :) = T_amb;
 Ie_n(init_time_node, 1) = 0;
 Ie_n(init_time_node, N_n) = I;
% Effective R_eff
```

```
 K_n(init_time_node, 1) = r_eff_n*exp(-30000/R ...
                        *(1/celltmptr(init_time_node) ...
                        - 1/T_amb));
% Effective Electrolyte Diffusivity
 De_n(init_time_node, 1) = diffu_E_n*exp(-10000/R ...
                        * (1/celltmptr(init_time_node) ...
                        - 1/T_amb))*0.21331;
% Electrolyte Concentration is assumed to be constant
 Ce_n(init_time_node, 1:N_n) = Ce_init;
% Solid Phase Negative Electrode Concentration
 Cs_n(init_time_node, 1:N_n) = stoic_n * Cs_max_n;
 Css_n(init_time_node, 1:N_n) = stoic_n * Cs_max_n;
 qs_n(init_time_node, 1:N_n) = stoic_n * Cs_max_n;
 SOC_n(init_time_node, 1:N_n) = ...
      Css_n(init_time_node, 1)/Cs_max_n;
% Electrolyte Conductivity
 Ke_n_0(init_time_node, 1:N_n) = ...
      (-1.6018e-014) ...
     * Ce_n(init_time_node, 1)^4 ...
     + 1.5094e-010*Ce_n(init_time_node, 1)^3 ...
     - 4.7212e-007*Ce_n(init_time_node, 1)^2 ...
     + 0.0005007 * Ce_n(init_time_node, 1) ...
     + 0.041253;
% Effective Solid Phase Diffusivity
 Ds_n(init_time_node, 1) = diffu_S_n*exp(-20000/R ...
                        * (1/celltmptr(init_time_node) ...
                        - 1 / T_amb));

% ------------------------------------------------------------
```

```
% Separator Region at time t = 0 [Start]
% ------------------------------------------------------------
 T_s(init_time_node, :) = T_amb;
 Ce_s(init_time_node, 1:N_s) = Ce_init;
 Ke_s_0(init_time_node, 1:N_s) = ...
      (- 1.6018e-014) ...
       * Ce_s(init_time_node, 1)^4 ...
       + 1.5094e-010 * Ce_s(init_time_node, 1)^3 ...
       - 4.7212e-007 * Ce_s(init_time_node, 1)^2 ...
       + 0.0005007 * Ce_s(init_time_node, 1) ...
       + 0.041253;
 Ie_s(init_time_node, 1:N_s) = I;

% ------------------------------------------------------------
% Positive Electrode at time t = 0 [Start]
% ------------------------------------------------------------

% Effective R_eff
 K_p(init_time_node, 1) = r_eff_p*exp(-30000/R ...
                       * (1/celltmptr(init_time_node) ...
                         - 1/T_amb));
% Effective Electrolyte Diffusivity
 De_p(init_time_node, 1) = diffu_E_p*exp(-10000/R ...
                        * (1/celltmptr(init_time_node) ...
                        - 1/T_amb))*0.29585;
% Effective Solid Phase Diffusivity
 Ds_p(init_time_node, 1) = diffu_S_p*exp(-4000/R* ...
                          (1/celltmptr(init_time_node)-1/T_amb));
 Ce_p(init_time_node, 1:N_p) = Ce_init;
```

```
Cs_p(init_time_node, 1:N_p) = stoic_p * Cs_max_p;
Css_p(init_time_node, 1:N_p) = stoic_p * Cs_max_p;
qs_p(init_time_node, 1:N_p) = stoic_p * Cs_max_p;
SOC_p(init_time_node, 1:N_p) = Css_p(init_time_node, 1)/Cs_max_p;
Ke_p_0(init_time_node, 1:N_p) = ...
     (- 1.6018e-014) ...
   * Ce_p(init_time_node, 1)^4 ...
   + 1.5094e-010 ...
   * Ce_p(init_time_node, 1)^3 ...
   - 4.7212e-007 ...
   * Ce_p(init_time_node, 1)^2 ...
   + 0.0005007 * Ce_p(init_time_node, 1) ...
   + 0.041253;

% -----------------------------------------------------------------
% Negative Electrode
% -----------------------------------------------------------------
 J_n(init_time_node, 1) =  (I/L_n)*(Rp_n/(3*epss_neg))*(1/F);

 Ke_n(init_time_node, 1) = Ke_n_0(init_time_node, 1)*exp(-20000/R* ...
                          (1/celltmptr(init_time_node)-1/T_amb));
 i0_n(init_time_node, 1)= 2 * K_n(init_time_node, 1) ...
                           * sqrt(Ce_n(init_time_node,1) ...
                           * (Cs_max_n - Css_n(init_time_node,1)) ...
                           * Css_n(init_time_node,1));

 T_n(init_time_node, 1:N_n) = T_amb;
 T_neg(init_time_node, 1:N_n) = T_amb;
 eta_neg(init_time_node, 1) = ...
```

```
       ((R*celltmptr(init_time_node))/(0.5*F)) ...
       *asinh((J_n(init_time_node, 1)) ...
       /(i0_n(init_time_node, 1)));

Ue_n(init_time_node, 1) = 0;

if charge == true && mode ~= 3
U_eq_n(init_time_node, 1) = ...
         0.15 - 0.10*SOC_n(init_time_node, 1) ...
       + (0.00578/SOC_n(init_time_node, 1));
else
U_eq_n(init_time_node, 1) = ...
          0.7222 + 0.1387*SOC_n(init_time_node, 1) ...
        + 0.029*(SOC_n(init_time_node, 1))^0.5 ...
        - (0.0172/SOC_n(init_time_node, 1)) ...
        + (0.0019/(SOC_n(init_time_node, 1))^1.5) ...
        + (0.2808*exp(0.90 - 15 ...
        * SOC_n(init_time_node, 1))) ...
        - (0.7984*exp(0.4465 ...
       * SOC_n(init_time_node, 1) - 0.4108));
end
Us_n(init_time_node, 1) = eta_neg(init_time_node, 1) ...
                       + Ue_n(init_time_node, 1) ...
                       + U_eq_n(init_time_node, 1);

qn_lump(init_time_node, 1) = (3 * epss_neg * F ...
                          * J_n(init_time_node, 1))/Rp_n ...
                          * (U_eq_n(init_time_node, 1) ...
                          - (dudt * celltmptr(init_time_node)));
```

```
space_node = 2;

while (space_node <= N_n)
K_n(init_time_node, space_node) = ...
          r_eff_n * exp(-30000 / R * ...
         (1 / celltmptr(init_time_node) ...
          - 1/T_amb));

De_n(init_time_node, space_node) = ...
         diffu_E_n * exp(-10000/R* ...
        (1/celltmptr(init_time_node) ...
        - 1/T_amb))*0.21331;

Ds_n(init_time_node, space_node) = ...
        diffu_S_n * exp(-20000 / R * ...
       (1 / celltmptr(init_time_node) ...
        - 1/T_amb));

if space_node ~= N_n
Ie_n(init_time_node, space_node) = ...
      ((3*epss_neg ...
      * J_n(init_time_node, space_node-1) ...
      * F*grid_n)/Rp_n) ...
      + Ie_n(init_time_node, space_node-1);
end

Us_n(init_time_node, space_node) = ...
       ((Ie_n(init_time_node, space_node-1) - I)/sigma_n) ...
```

```
      * grid_n + Us_n(init_time_node, space_node-1);

Ke_n(init_time_node, space_node) = ...
       Ke_n_0(init_time_node, space_node)*exp(-20000/R* ...
       (1/celltmptr(init_time_node)-1/T_amb));

Ue_n(init_time_node, space_node) = ...
      (-Ie_n(init_time_node, space_node-1) ...
       / Ke_n(init_time_node, space_node)*grid_n) ...
       + Ue_n(init_time_node, space_node-1);

if charge == true && mode ~= 3
U_eq_n(init_time_node, space_node) = ...
         0.15 - 0.10*SOC_n(init_time_node, space_node) ...
       + (0.00578/SOC_n(init_time_node, space_node));
else
U_eq_n(init_time_node, space_node) = ...
         0.7222 + 0.1387*SOC_n(init_time_node, space_node) ...
        +0.029*(SOC_n(init_time_node, space_node))^0.5 ...
        -(0.0172/SOC_n(init_time_node, space_node)) ...
        +(0.0019/(SOC_n(init_time_node, space_node))^1.5) ...
        +(0.2808*exp(0.90 - 15 ...
        *SOC_n(init_time_node, space_node))) ...
        -(0.7984*exp(0.4465*SOC_n(init_time_node, space_node) ...
        -0.4108));
end

eta_neg(init_time_node, space_node) = ...
         Us_n(init_time_node, space_node) ...
```

```
        - Ue_n(init_time_node, space_node) ...
        - U_eq_n(init_time_node, space_node);


 i0_n(init_time_node, space_node) = ...
       2 * K_n(init_time_node, space_node) ...
     *  sqrt(Ce_n(init_time_node,space_node) ...
     * (Cs_max_n - Css_n(init_time_node, space_node)) ...
     * Css_n(init_time_node, space_node));

 J_n(init_time_node, space_node) = ...
      i0_n(init_time_node, space_node) ...
    * sinh((0.5*F*eta_neg(init_time_node, space_node)) ...
    /(R*celltmptr(init_time_node)));

 q_n(init_time_node, space_node) = ...
      i_app*23.7*(-(3*epss_neg * F ...
    * J_n(init_time_node, space_node))/Rp_n ...
    * (eta_neg(init_time_node, space_node) ...
    - dudt * celltmptr(init_time_node)));
 qn_lump(init_time_node, space_node) = ...
         (3*epss_neg*F*J_n(init_time_node, space_node))/Rp_n ...
       * (U_eq_n(init_time_node, space_node) ...
       - (dudt * celltmptr(init_time_node)));
    space_node = space_node + 1;
 end

% Separator Region
```

```
De_s(init_time_node, 1) = ...
    diffu_E_s * exp(-10000 / R * ...
    (1 / celltmptr(init_time_node) - 1/T_amb));

Ke_s(init_time_node, 1) = ...
Ke_s_0(init_time_node, 1) * exp(-20000 / R ...
   * (1 / celltmptr(init_time_node) - 1/T_amb));

T_s(init_time_node, 1:N_s) = T_amb;
Ue_s(init_time_node, 1) = Ue_n(init_time_node, N_n);

space_node = 2;
while (space_node < N_s)
De_s(init_time_node, space_node) = ...
        diffu_E_s * exp(-10000 / R * ...
       (1 / celltmptr(init_time_node) ...
        - 1/T_amb));

Ke_s(init_time_node, space_node) = ...
         Ke_s_0(init_time_node, space_node) ...
        * exp(-20000/R*(1/celltmptr(init_time_node)-1/T_amb));
Ue_s(init_time_node, space_node) = ...
       (-Ie_s(init_time_node, space_node-1) ...
       /Ke_s(init_time_node, space_node) + ...
       (2*R*celltmptr(init_time_node)*(1-t_plus) ...
      *(log(Ce_s(init_time_node,space_node)) ...
      - log(Ce_s(init_time_node,space_node-1))) ...
      /(F*grid_s)))*grid_s ...
      + Ue_s(init_time_node, space_node-1);
```

```
    space_node = space_node + 1;
end

De_s(init_time_node, N_s) = ...
     diffu_E_s * exp(-10000 / R * ...
    (1 / celltmptr(init_time_node) - 1 / T_amb));

Ue_s(init_time_node, N_s) = ...
    (-Ie_s(init_time_node, N_s - 1) ...
    / Ke_n(init_time_node, N_n) + ...
    (2*R*celltmptr(init_time_node)*(1-t_plus) ...
   *(log(Ce_s(init_time_node,N_s)) ...
   - log(Ce_s(init_time_node,N_s-1))) ...
   /(F*grid_s))) ...
   * grid_s + Ue_s(init_time_node, N_s-1);
```

%

Positive Electrode

```
T_p(init_time_node, :) = T_amb;
T_p(init_time_node, 1:N_p) = T_amb;
Ue_p(init_time_node, 1) = 0;
Ie_p(init_time_node, 1) = 0;
Ie_p(init_time_node, N_p) = -I;
Ke_p(init_time_node, 1) = ...
      Ke_p_0(init_time_node, 1) ...
```

```
     * exp(-20000 / R ...
     * (1 / celltmptr(init_time_node) ...
     - 1 / T_amb));
J_p(init_time_node, 1) =  -(I/L_p)*(Rp_p/(3*epss_pos))*(1/F);

i0_p(init_time_node, 1)= ...
     2 * K_p(init_time_node, 1) ...
     * sqrt(Ce_p(init_time_node,1)...
     * (Cs_max_p - Css_p(init_time_node,1)) ...
     * Css_p(init_time_node,1));

eta_pos(init_time_node, 1) = ((R*celltmptr(init_time_node)) ...
                           / (0.5*F)) ...
                           * asinh((J_p(init_time_node, 1)) ...
                           / (i0_p(init_time_node, 1)));

if charge == true && mode ~= 3
U_eq_p(init_time_node, 1) = ...
         (-4.875 + (5.839*SOC_p(init_time_node, 1)) ...
       - (1.507*SOC_p(init_time_node, 1)^3) ...
       + (0.533*SOC_p(init_time_node, 1)^5)) ...
       / (SOC_p(init_time_node, 1) - 1.03);
else
U_eq_p(init_time_node, 1) = ...
         (-4.656+ 88.669*(SOC_p(init_time_node, 1))^2 ...
        - 401.119*(SOC_p(init_time_node, 1))^4 ...
        + 342.909*(SOC_p(init_time_node, 1))^6 ...
        - 462.471*(SOC_p(init_time_node, 1))^8 ...
        + 433.434*(SOC_p(init_time_node, 1))^10)/...
```

```
        (-1.0+18.933*(SOC_p(init_time_node, 1))^2 ...
        - 79.532*(SOC_p(init_time_node, 1))^4 ...
        + 37.311*(SOC_p(init_time_node, 1))^6 ...
        - 73.083*(SOC_p(init_time_node, 1))^8 ...
        + 95.96*(SOC_p(init_time_node, 1))^10);
 end

 Us_p(init_time_node, 1) = eta_pos(init_time_node, 1) ...
                         + Ue_p(init_time_node, 1) ...
                         + U_eq_p(init_time_node, 1);

 q_p(init_time_node, 1) = i_app*23.7*(-(3*epss_pos * F ...
                        * J_p(init_time_node, 1))/Rp_p ...
                        * (eta_pos(init_time_node, 1) ...
                        - dudt*celltmptr(init_time_node)) ...
                        - Ue_p(init_time_node, 1) ...
                        * Ie_p(init_time_node, 1) ...
                        + Us_p(init_time_node, 1) ...
                        *(I - Ie_p(init_time_node, 1)));

 qp_lump(init_time_node, 1) = (3 * epss_pos * F ...
                            * J_p(init_time_node, 1))/Rp_p ...
                            * (U_eq_p(init_time_node, 1) ...
                            - (dudt * celltmptr(init_time_node)));
space_node = 2;
while (space_node <= N_p)
 K_p(init_time_node, space_node) = ...
          r_eff_p*exp(-30000/R ...
         * (1/celltmptr(init_time_node) ...
```

```
        - 1/T_amb));

De_p(init_time_node, space_node) = ...
        diffu_E_p * exp(-10000 / R ...
       *(1/celltmptr(init_time_node) ...
       -1/T_amb))*0.29585;

Ds_p(init_time_node, space_node) = ...
        diffu_S_p * exp(-4000 / R ...
      * (1 / celltmptr(init_time_node) ...
      - 1 / T_amb));

if space_node ~= N_p
Ie_p(init_time_node, space_node) = ...
          ((3*epss_pos*J_p(init_time_node, space_node - 1) ...
            * F*grid_p)/Rp_p) ...
          + Ie_p(init_time_node, space_node - 1);
end

Us_p(init_time_node, space_node) = ...
       ((Ie_p(init_time_node, space_node - 1) ...
       - I)/sigma_p)*grid_p ...
       + Us_p(init_time_node, space_node - 1);

Ke_p(init_time_node, space_node) = ...
        Ke_p_0(init_time_node, space_node) ...
      * exp(-20000 / R * (1 / celltmptr(init_time_node) ...
      - 1 / T_amb));
Ue_p(init_time_node, space_node) = ...
```

```
        (-Ie_p(init_time_node, space_node-1) ...
        / Ke_p(init_time_node, space_node))*grid_p ...
        + Ue_p(init_time_node, space_node-1);

if charge == true && mode ~= 3
 U_eq_p(init_time_node, space_node) = ...
         (-4.875 + (5.839*SOC_p(init_time_node, space_node)) ...
       - (1.507*SOC_p(init_time_node, space_node)^3) ...
       + (0.533*SOC_p(init_time_node, space_node)^5)) ...
       /(SOC_p(init_time_node, space_node) - 1.03);
else
 U_eq_p(init_time_node, space_node) = ...
         (-4.656+ 88.669*(SOC_p(init_time_node, space_node))^2 ...
        - 401.119*(SOC_p(init_time_node,space_node))^4 ...
        + 342.909*(SOC_p(init_time_node, space_node))^6 ...
        - 462.471*(SOC_p(init_time_node, space_node))^8 ...
        + 433.434*(SOC_p(init_time_node, space_node))^10)/...
        (-1.0+18.933*(SOC_p(init_time_node, space_node))^2 ...
        - 79.532*(SOC_p(init_time_node, space_node))^4 ...
        + 37.311*(SOC_p(init_time_node, space_node))^6 ...
        - 73.083*(SOC_p(init_time_node, space_node))^8 ...
        + 95.96*(SOC_p(init_time_node, space_node))^10);
end

 eta_pos(init_time_node, space_node) = ...
           Us_p(init_time_node, space_node) ...
         - Ue_p(init_time_node, space_node) ...
         - U_eq_p(init_time_node, space_node);
```

```
 i0_p(init_time_node, space_node) = ...
        2 * K_p(init_time_node, space_node) ...
      * sqrt(Ce_p(init_time_node,space_node) ...
      * (Cs_max_p - Css_p(init_time_node, space_node)) ...
      * Css_p(init_time_node, space_node));

 J_p(init_time_node, space_node) = ...
      i0_p(init_time_node, space_node) ...
    * sinh((0.5*F*eta_pos(init_time_node, space_node)) ...
    / (R*celltmptr(init_time_node)));

 q_p(init_time_node, space_node) = ...
      i_app*23.7*(-(3*epss_pos * F ...
     * J_p(init_time_node, space_node)) ...
     / Rp_p * (eta_pos(init_time_node, space_node) ...
     - dudt*celltmptr(init_time_node)) ...
     - Ue_p(init_time_node, space_node) ...
     * Ie_p(init_time_node, space_node) ...
     + Us_p(init_time_node, space_node) ...
     * (I - Ie_p(init_time_node, space_node)));

 qp_lump(init_time_node, space_node) = ...
         (3 * epss_pos * F ...
        * J_p(init_time_node, space_node))/Rp_p ...
        * (U_eq_p(init_time_node, space_node) ...
        - (dudt * celltmptr(init_time_node)));
 space_node = space_node + 1;
end
init_soc = SOC_n(init_time_node,1);
```

```
count = 1;
Voltage(init_time_node) = Us_p(init_time_node, 1) ...
                        - Us_n(init_time_node, 1);
Current(init_time_node) = I;
if charge == true
 Q(count) = -I*dt;
 SOC(count) = (Q(count)/(R_Cap)) + init_soc;
else
 Q(count) = I*dt;
 SOC(count) = init_soc - (Q(count)/(R_Cap));
end
 count = count + 1;
 ocp(init_time_node) = U_eq_p(init_time_node, 1) ...
                     - U_eq_n(init_time_node, 1);
 Cs_n_avg(init_time_node) = sum(Cs_n(init_time_node,:))/N_n;
 SOC_Cs(init_time_node) = Cs_n_avg(init_time_node)/Cs_max_n;

if mode == 4

 delta(init_time_node) = ...
         ((alpha_ac*F*sum(eta_neg(init_time_node,:))/N_n) ...
        /(R*celltmptr(init_time_node)^2)) ...
        * ((6*sum(i0_n(init_time_node,:))/N_n)/(R*F)) ...
        * cosh((alpha_ac*F*sum(eta_neg(init_time_node,:))/N_n) ...
        /(R*celltmptr(init_time_node)));

 gamma(init_time_node) = ...
         ((3*epss_neg*F*dudt*sum(J_n(init_time_node,:))/Rp_n) ...
         + (3*epss_pos*F*dudt*sum(J_p(init_time_node,:)) ...
```

```
         /Rp_p))/rho_cp_avg;

 lambda_2(init_time_node) = ...
             (-I*(1+(2*alpha))+(2*alpha*I_max)) ...
            * rho_cp_avg/Voltage(init_time_node);


 lambda_1(init_time_node) = ...
            ((I*(1+(2*alpha))) - (2*alpha*I_max) ...
            + (lambda_2(init_time_node) ...
            * Voltage(init_time_node) ...
            / rho_cp_avg)) * zeta;
end
 celltmptr_rate(init_time_node) = 0;
```

Iterative Equations

```
% This is time iteration from second time step onwards.
% In each time step the space nodes are iterated.
for time_node = 2:max_time

% Calculations for Negative Electrode
% ********************************************************
% Inner iteration within each time step to reach convergence

% Boundary Values - Negative

 Ie_n(time_node, 1) = 0;
 Ie_n(time_node, N_n) = I;
 J_n(time_node, 1) =  (I/L_n)*(Rp_n/(3*epss_neg))*(1/F);
```

```
K_n(time_node, 1) = r_eff_n * exp(-30000 / R ...
                  * (1 / celltmptr(time_node - 1) ...
                  - 1 / T_amb));

De_n(time_node, 1) = diffu_E_n * exp(-10000/R ...
                   * (1/celltmptr(time_node-1) ...
                   - 1/T_amb))*0.21331;
Ce_n(time_node, 1) = Ce_init;


Cs_n(time_node, 1) = ((-3/Rp_n)*J_n(time_node - 1, 1) * dt) ...
                         + Cs_n(time_node - 1, 1);

Ds_n(time_node, 1) = diffu_S_n * exp(-20000 / R ...
                   * (1 / celltmptr(time_node-1) ...
                   - 1 / T_amb));

qs_n(time_node, 1) = ...
          -(((30*Ds_n(time_node, 1))/Rp_n^2) ...
          * qs_n(time_node-1, 1)*dt) ...
          - ((45/(2*Rp_n^2))*J_n(time_node-1, 1)*dt) ...
          + qs_n(time_node-1, 1);

Css_n(time_node, 1) = ...
           Cs_n(time_node, 1 ) ...
          +(((8*Rp_n)/35)*qs_n(time_node, 1)) ...
          -((Rp_n/(35*Ds_n(time_node, 1)))*J_n(time_node-1, 1));

SOC_n(time_node, 1) =Css_n(time_node, 1)/Cs_max_n;
```

```
Ke_n_0(time_node, 1)=(- 1.6018e-014)*Ce_n(time_node, 1)^4 ...
                     + 1.5094e-010*Ce_n(time_node, 1)^3 ...
                     - 4.7212e-007 * Ce_n(time_node, 1)^2 ...
                     + 0.0005007*Ce_n(time_node, 1)+0.041253;

Ke_n(time_node, 1) = Ke_n_0(time_node,1) * exp(-20000/R ...
                     *(1/celltmptr(time_node-1)-1/T_amb));
i0_n(time_node, 1) = 2 * K_n(time_node, 1) ...
                     * sqrt(Ce_n(time_node,1) ...
                     *(Cs_max_n - Css_n(time_node, 1)) ...
                     * Css_n(time_node, 1));

eta_neg(time_node, 1) = ((R*celltmptr(time_node-1))/(0.5*F)) ...
                     * asinh((J_n(time_node-1, 1)) ...
                     /(i0_n(time_node, 1)));

Ue_n(time_node, 1) = 0;

if charge == true && mode ~= 3
U_eq_n(time_node, 1) = 0.15 - 0.10*SOC_n(time_node, 1) ...
                     + (0.00578/SOC_n(time_node, 1));
else
U_eq_n(time_node, 1) = ...
       0.7222 + 0.1387*SOC_n(time_node, 1) ...
       + 0.029*(SOC_n(time_node, 1))^0.5 ...
       - (0.0172/SOC_n(time_node, 1)) ...
       + (0.0019/(SOC_n(time_node, 1))^1.5) ...
       + (0.2808*exp(0.90 - 15*SOC_n(time_node, 1))) ...
```

```
        - (0.7984*exp(0.4465*SOC_n(time_node, 1) ...
        - 0.4108));
       end

 Us_n(time_node, 1) = eta_neg(time_node, 1) ...
                    + Ue_n(time_node, 1) ...
                    + U_eq_n(time_node, 1);

 q_n(time_node, 1) = i_app*22.3*(-(3*epss_neg * F ...
                   * J_n(time_node, 1))/Rp_n ...
                   * (eta_neg(time_node, 1) ...
                   - dudt*celltmptr(time_node-1)));

 qn_lump(time_node, 1) = (3 * epss_neg * F ...
                       * J_n(time_node, 1))/Rp_n ...
                       * (U_eq_n(time_node, 1) ...
                       - (dudt * celltmptr(time_node - 1)));

% Looping in Internal Space Nodes
 for space_node = 2:N_n

% Ionic Current in Negative Electrode
 if space_node ~= N_n
 Ie_n(time_node, space_node) = ...
          ((3*epss_neg * J_n(time_node, space_node-1) ...
            * F*grid_n)/Rp_n) ...
            + Ie_n(time_node, space_node-1);
 end
```

```
De_n(time_node, space_node) = diffu_E_n * exp(-10000/R ...
                              *(1/celltmptr(time_node-1) ...
                              -1/T_amb))*0.21331;
if space_node ~= N_n
Ce_n(time_node, space_node) = ...
       ((De_n(time_node - 1, space_node)) ...
      *((Ce_n(time_node - 1,space_node + 1) ...
      - 2*Ce_n(time_node-1, space_node) ...
      + Ce_n(time_node-1, space_node - 1))/grid_n^2) + ...
       (t_plus*(Ie_n(time_node-1, space_node) ...
      - Ie_n(time_node - 1,space_node-1)) ...
      /(grid_n*F)))*dt ...
      + Ce_n(time_node - 1, space_node);

else
Ce_n(time_node, space_node) = (4/3)*Ce_n(time_node, N_n - 1) ...
                              - (1/3) * Ce_n(time_node, N_n - 2);

end

% Li+ Concentration in Negative Electrode

Cs_n(time_node, space_node) = ...
      ((-3/Rp_n)*J_n(time_node-1, space_node)*dt) ...
      + Cs_n(time_node-1, space_node);

Ds_n(time_node, space_node) = diffu_S_n * exp(-20000 / R ...
                            * (1 / celltmptr(time_node-1) ...
                                  - 1 / T_amb));
```

```
% Li+ Concentration Flux in Negative Electrode
 qs_n(time_node, space_node) = ...
        -(((30*Ds_n(time_node, space_node))/Rp_n^2) ...
        * qs_n(time_node-1, space_node)*dt) ...
        - ((45/(2*Rp_n^2)) ...
        * J_n(time_node-1, space_node)*dt) ...
        + qs_n(time_node-1, space_node);

% Li+ Solid/Electrolyte Concentration in Negative Electrode
 Css_n(time_node, space_node) = ...
         Cs_n(time_node, space_node) ...
       + (((8*Rp_n)/35) ...
       * qs_n(time_node, space_node)) ...
       - ((Rp_n/(35*Ds_n(time_node, space_node))) ...
       * J_n(time_node, space_node-1));

% State of Charge in Negative Electrode
 SOC_n(time_node, space_node) = ...
        Css_n(time_node, space_node)/Cs_max_n;

% Solid Phase Potential in Negative Electrode

 Us_n(time_node, space_node) = ...
            ((Ie_n(time_node, space_node-1) ...
              - I)/sigma_n)*grid_n ...
              + Us_n(time_node, space_node-1);

 Ke_n_0(time_node, space_node) = ...
        (-1.6018e-014) * Ce_n(time_node, space_node)^4 ...
```

```
        + 1.5094e-010 * Ce_n(time_node, space_node)^3 ...
        - 4.7212e-007 * Ce_n(time_node, space_node)^2 ...
        + 0.0005007 * Ce_n(time_node, space_node) + 0.041253;

 Ke_n(time_node, space_node) = Ke_n_0(time_node, space_node) ...
                             * exp(-20000/R ...
                             * (1/celltmptr(time_node-1)...
                             -1/T_amb));

 Ue_n(time_node, space_node) = ...
      ((-Ie_n(time_node, space_node-1) ...
      / Ke_n(time_node, space_node)) ...
      + (2*R*celltmptr(time_node-1)*(1-t_plus) ...
      * (log(Ce_n(time_node,space_node)) ...
      - log(Ce_n(time_node,space_node - 1))) ...
      /(F*grid_n)))*grid_n ...
      + Ue_n(time_node, space_node-1);

% Over-potential Calculation
 if charge == true && mode ~= 3
 U_eq_n(time_node, space_node) = ...
        0.15 - 0.10*SOC_n(time_node, space_node) ...
     + (0.00578/SOC_n(time_node, space_node));
 else
 U_eq_n(time_node, space_node) = ...
        0.7222 + 0.1387*SOC_n(time_node, space_node) ...
        + 0.029*(SOC_n(time_node, space_node))^0.5 ...
        - (0.0172/SOC_n(time_node, space_node)) ...
        + (0.0019/(SOC_n(time_node, space_node))^1.5) ...
```

```
        + (0.2808*exp(0.90 - 15 ...
        * SOC_n(time_node, space_node))) ...
        - (0.7984*exp(0.4465 ...
        * SOC_n(time_node, space_node) - 0.4108));
 end
 eta_neg(time_node, space_node) = ...
              Us_n(time_node, space_node) ...
            - Ue_n(time_node, space_node) ...
            - U_eq_n(time_node, space_node);


% Molar Ionic Flux [UNIT: A/m^2]
 K_n(time_node, space_node) = r_eff_n * exp(-30000/R ...
                           *(1/celltmptr(time_node-1)-1/T_amb));

 i0_n(time_node, space_node) = ...
        2 * K_n(time_node, space_node) ...
      * sqrt(Ce_n(time_node,space_node) ...
      * (Cs_max_n - Css_n(time_node, space_node)) ...
      * Css_n(time_node, space_node));

 J_n(time_node, space_node) = ...
       i0_n(time_node, space_node) ...
     * sinh((0.5*F*eta_neg(time_node, space_node)) ...
     /(R*celltmptr(time_node - 1)));

 q_n(time_node, space_node) = i_app*22.3*(-(3*epss_neg * F ...
                           * J_n(time_node, space_node))/Rp_n ...
                           * (eta_neg(time_node, space_node) ...
```

```
                          - dudt*celltmptr(time_node-1)));
qn_lump(time_node, space_node) = ...
          (3 * epss_neg * F ...
         * J_n(time_node, space_node))/Rp_n ...
         * (U_eq_n(time_node, space_node) ...
         - (dudt * celltmptr(time_node - 1)));
end


% ###################################################################
```

********* Calculation of Separator Region Parameters ************

```
% Boundary Condition Setup

De_s(time_node, 1) = diffu_E_s * exp(-10000 / R ...
                   * (1 / celltmptr(time_node-1) - 1 / T_amb));
Ue_s(time_node, 1) = Ue_n(time_node, N_n);
Ce_s(time_node, 1) = Ce_s(time_node - 1, 2)...
                   -((De_n(time_node, 1) ...
                   * grid_s/De_s(time_node,1))...
                   *(Ce_n(time_node, N_n) ...
                   - Ce_n(time_node, N_n-1))/grid_n);

q_s(time_node, 1) = 0;

Ke_s_0(time_node, 1) = (-1.6018e-014) * Ce_s(time_node, 1)^4 ...
                     + 1.5094e-010 * Ce_s(time_node, 1)^3 ...
                     - 4.7212e-007 * Ce_s(time_node, 1)^2 ...
                     + 0.0005007*Ce_s(time_node, 1) + 0.041253;
```

```
 Ke_s(time_node, 1) = Ke_s_0(time_node, 1) * exp(-20000/R ...
                     * (1/celltmptr(time_node-1)-1/T_amb));
 Ie_s(time_node, :) = I;

% Looping in internal Space nodes
 for space_node = 2:N_s - 1

 De_s(time_node, space_node) = diffu_E_s * exp(-10000 / R ...
                              * (1 / celltmptr(time_node-1) ...
                              - 1 / T_amb));

 Ce_s(time_node, space_node) = ...
      ((De_s(time_node-1, space_node) ...
     * (Ce_s(time_node-1,space_node+1) ...
     - 2*Ce_s(time_node-1, space_node) ...
     + Ce_s(time_node-1, space_node-1))/grid_s^2))*dt ...
     + Ce_s(time_node - 1, space_node);

% Electrolyte Phase Potential
 Ke_s_0(time_node, space_node) = ...
        (-1.6018e-014) * Ce_s(time_node, space_node)^4 ...
         + 1.5094e-010 * Ce_s(time_node, space_node)^3 ...
         - 4.7212e-007 * Ce_s(time_node, space_node)^2 ...
         + 0.0005007 * Ce_s(time_node, space_node) ...
         + 0.041253;

 Ke_s(time_node, space_node) = Ke_s_0(time_node, space_node) ...
                             * exp(-20000/R ...
                             *(1/celltmptr(time_node-1)-1/T_amb));
```

```
 Ue_s(time_node, space_node) = ...
        (-I/Ke_s(time_node, space_node) + ...
        (2*R*celltmptr(time_node-1)*(1-t_plus) ...
       *(log(Ce_s(time_node,space_node)) ...
       - log(Ce_s(time_node,space_node-1))) ...
       /(F*grid_s)))*grid_s ...
       + Ue_s(time_node, space_node-1);


 q_s(time_node, space_node) = ...
             -i_app*23.7*I*Ue_s(time_node, space_node);
 end

% Boundary Condition Setup

 De_s(time_node, N_s) = diffu_E_s * exp(-10000/R ...
                      *(1/celltmptr(time_node-1)-1/T_amb));
 Ce_s(time_node, N_s) = Ce_s(time_node - 1, N_s-1) ...
                      + ((De_p(time_node-1, N_p) ...
                      * grid_s/De_s(time_node,N_s)) ...
                      * (Ce_n(time_node, N_p) ...
                      - Ce_n(time_node, N_p-1))/grid_p);

 Ke_s_0(time_node, N_s) = ...
        (-1.6018e-014) * Ce_s(time_node, N_s)^4 ...
         + 1.5094e-010*Ce_s(time_node, N_s)^3 ...
         - 4.7212e-007 * Ce_s(time_node, N_s)^2 ...
         + 0.0005007 * Ce_s(time_node, N_s) ...
```

```
        + 0.041253;

Ke_s(time_node, N_s) = Ke_s_0(time_node, N_s) ...
                     * exp(-20000/R ...
                     * (1/celltmptr(time_node-1)-1/T_amb));
Ue_s(time_node, N_s) =  ...
      (-I/Ke_s(time_node, N_s) + ...
      (2*R*celltmptr(time_node-1)*(1-t_plus) ...
     * (log(Ce_s(time_node,N_s)) ...
     - log(Ce_s(time_node,N_s-1))) ...
     /(F*grid_s)))*grid_s ...
     + Ue_s(time_node, N_s-1);

q_s(time_node, N_s) = -i_app*23.7*I*Ue_s(time_node, N_s);

% ########################################################
```

********* Calculations for Positive Electrode ********** *Calculation is done from extreme positive end towards separator* ********** Boundary Values - Positive **********

```
Ue_p(time_node, 1) = 0;
Ie_p(time_node, 1) = 0;
Ie_p(time_node, N_p) = -I;
J_p(time_node, 1) =  -(I/L_p)*(Rp_p/(3*epss_pos))*(1/F);
Ce_p(time_node, 1) = Ce_init;
if charge == true
Ce_p(time_node, 1) = min(Ce_Hi_lim,Ce_p(time_node, 1));
else
```

```
Ce_p(time_node, 1) = max(Ce_Lo_lim,Ce_p(time_node, 1));
end
De_p(time_node, 1) = diffu_E_p * exp(-10000/R ...
                        * (1/celltmptr(time_node-1) ...
                        - 1/T_amb))*0.29585;

Ds_p(time_node, 1) = diffu_S_p * exp(-4000/R ...
                    * (1/celltmptr(time_node-1) ...
                    - 1/T_amb));

Cs_p(time_node, 1) = ((-3/Rp_p)*J_p(time_node-1, 1)*dt) ...
                    + Cs_p(time_node-1, 1);

qs_p(time_node, 1) = -(((30*Ds_p(time_node, 1))/Rp_p^2) ...
                    * qs_p(time_node-1, 1)*dt) ...
                    - ((45/(2*Rp_p^2)) ...
                    * J_p(time_node-1, 1)*dt) ...
                    + qs_p(time_node-1, 1);

Css_p(time_node, 1) = Cs_p(time_node-1, 1) ...
                     + (((8*Rp_p)/35) ...
                     * qs_p(time_node-1, 1)) ...
                     - ((Rp_p/(35*Ds_p(time_node, 1))) ...
                     * J_p(time_node-1, 1));

SOC_p(time_node, 1) = Css_p(time_node, 1)/Cs_max_p;

K_p(time_node, 1) = r_eff_p * exp(-30000 / R ...
                   * (1 / celltmptr(time_node-1) ...
```

```
                    - 1 / T_amb));

i0_p(time_node, 1) = 2 * K_p(time_node, 1) ...
                    * sqrt(Ce_p(time_node,1) ...
                    * (Cs_max_p - Css_p(time_node, 1)) ...
                    * Css_p(time_node, 1));

eta_pos(time_node, 1) = R*celltmptr(time_node-1)/(0.5*F) ...
                       * asinh((J_p(time_node-1, 1)) ...
                       /(i0_p(time_node, 1)));

if charge == true && mode ~= 3
U_eq_p(time_node, 1) = (-4.875 + (5.8399*SOC_p(time_node, 1)) ...
                      - (1.507*SOC_p(time_node, 1)^3) ...
                      + (0.533*SOC_p(time_node, 1)^5)) ...
                      /(SOC_p(time_node, 1) - 1.03);
else
U_eq_p(time_node, 1) = ...
                 (-4.656 + 88.669*(SOC_p(time_node, 1))^2 ...
                  - 401.119*(SOC_p(time_node,1))^4 ...
                  + 342.909*(SOC_p(time_node, 1))^6 ...
                  - 462.471*(SOC_p(time_node, 1))^8 ...
                  + 433.434*(SOC_p(time_node, 1))^10)/...
                 (- 1.0+18.933*(SOC_p(time_node, 1))^2 ...
                  - 79.532*(SOC_p(time_node, 1))^4 ...
                  + 37.311*(SOC_p(time_node, 1))^6 ...
                  - 73.083*(SOC_p(time_node, 1))^8 ...
                  + 95.96*(SOC_p(time_node, 1))^10);
end
```

```
Us_p(time_node, 1) = eta_pos(time_node, 1) ...
                   + Ue_p(time_node, 1) ...
                   + U_eq_p(time_node, 1);

q_p(time_node, 1) = i_app*23.7*(-(3*epss_pos * F ...
                  * J_p(time_node, 1))/Rp_p ...
                  * (eta_pos(time_node, 1) ...
                  - dudt*celltmptr(time_node-1)) ...
                  - Ue_p(time_node, 1) ...
                  * Ie_p(time_node, 1) ...
                  + Us_p(time_node, 1) ...
                  *(I - Ie_p(time_node, 1)));

qp_lump(time_node, 1) = (3 * epss_pos * F ...
                       * J_p(time_node, 1))/Rp_p ...
                       * (U_eq_p(time_node, 1) ...
                       - (dudt * celltmptr(time_node - 1)));
Ke_p_0(time_node, 1) = (-1.6018e-014) ...
                     * Ce_p(time_node, 1)^4+1.5094e-010 ...
                     * Ce_p(time_node, 1)^3 - 4.7212e-007 ...
                     * Ce_p(time_node, 1)^2+0.0005007 ...
                     * Ce_p(time_node, 1)+0.041253;

Ke_p(time_node, 1) = Ke_p_0(time_node, 1) * exp(-20000 / R ...
                   * (1 / celltmptr(time_node-1) ...
                        - 1 / T_amb));
% Looping in internal Space nodes
 for space_node = 2:N_p
```

```
% Ionic Current in Positive Electrode
 if space_node ~= N_p
 Ie_p(time_node, space_node) = ...
         ((3*epss_pos*J_p(time_node, space_node-1) ...
           * F*grid_p)/Rp_p) ...
        + Ie_p(time_node, space_node-1);
 end

 De_p(time_node, space_node) = diffu_E_p*exp(-10000/R ...
                                  * (1/celltmptr(time_node-1) ...
                                  - 1/T_amb))*0.29585;
 if space_node ~= N_p
 Ce_p(time_node, space_node) = ...
         ((De_p(time_node-1, space_node)) ...
        *((Ce_p(time_node-1,space_node + 1) ...
        - 2*Ce_p(time_node-1, space_node) ...
        + Ce_p(time_node-1, space_node-1))/grid_p^2) + ...
         (t_plus*(Ie_p(time_node-1, space_node) ...
        - Ie_p(time_node-1,space_node - 1))/(grid_p*F)))*dt ...
        + Ce_p(time_node - 1, space_node);
 else
 Ce_p(time_node, space_node) = ...
           (4/3)*Ce_p(time_node, N_p - 1) ...
         - (1/3) * Ce_p(time_node, N_p - 2);

 end
```

```
% Li+ Concentration in Positive Electrode
 Cs_p(time_node, space_node) = ...
           - 3*(dt/Rp_p)*J_p(time_node-1, space_node) ...
           + Cs_p(time_node-1, space_node);

 Ds_p(time_node, space_node) = diffu_S_p * exp(-20000 / R ...
                              * (1 / celltmptr(time_node-1) ...
                              - 1 / T_amb));

% Li+ Concentration Flux in Positive Electrode

 qs_p(time_node, space_node) = ...
           -(((30*Ds_p(time_node, space_node))/Rp_p^2) ...
           *qs_p(time_node-1, space_node)*dt) ...
           - ((45/(2*Rp_p^2)) ...
           * J_p(time_node-1, space_node)*dt) ...
           + qs_p(time_node-1, space_node);

% Li+ Solid/Electrolyte Concentration in Positive Electrode
 Css_p(time_node, space_node) = ...
            Cs_p(time_node, space_node) ...
            + (((8*Rp_p)/35) ...
            * qs_p(time_node, space_node)) ...
            - ((Rp_p/(35*Ds_p(time_node, space_node))) ...
            * J_p(time_node, space_node-1));

% State of Charge in Positive Electrode
 SOC_p(time_node, space_node) = ...
        Css_p(time_node, space_node)/Cs_max_p;
```

```
% Solid Phase Potential in Positive Electrode

 Us_p(time_node, space_node) = ...
                ((Ie_p(time_node, space_node) ...
                 - I)/sigma_p)*grid_p ...
                 + Us_p(time_node, space_node-1);

 Ke_p_0(time_node, space_node) = ...
        (-1.6018e-014) * Ce_p(time_node, space_node)^4 ...
       + 1.5094e-010 * Ce_p(time_node, space_node) ^ 3 ...
       - 4.7212e-007 * Ce_p(time_node, space_node)^2 ...
       + 0.0005007 * Ce_p(time_node, space_node)  ...
       + 0.041253;
 Ke_p(time_node, space_node) = Ke_p_0(time_node, space_node) ...
                              * exp(-20000 / R ...
                              * (1 / celltmptr(time_node-1) ...
                              - 1 / T_amb));

 Ue_p(time_node, space_node) = ...
        (-Ie_p(time_node, space_node-1) ...
        / Ke_p(time_node, space_node) + ...
        (2*R*celltmptr(time_node-1)*(1-t_plus) ...
        *(log(Ce_p(time_node,space_node)) ...
        - log(Ce_p(time_node,space_node-1))) ...
        /(F*grid_p)))*grid_p ...
        + Ue_p(time_node, space_node-1);
```

```
% Overpotential Calculation

if charge == true && mode ~= 3
U_eq_p(time_node, space_node) = ...
       (-4.875 + (5.8399*SOC_p(time_node, space_node)) ...
        - (1.507*SOC_p(time_node, space_node)^3) ...
        + (0.533*SOC_p(time_node, space_node)^5)) ...
        / (SOC_p(time_node, space_node) - 1.03);
else
U_eq_p(time_node, space_node) = ...
       (-4.656+ 88.669*(SOC_p(time_node, space_node))^2 ...
        - 401.119*(SOC_p(time_node,space_node))^4 ...
        + 342.909*(SOC_p(time_node, space_node))^6 ...
        - 462.471*(SOC_p(time_node, space_node))^8 ...
        + 433.434*(SOC_p(time_node, space_node))^10)/...
       (-1.0+18.933*(SOC_p(time_node, space_node))^2 ...
        - 79.532*(SOC_p(time_node, space_node))^4 ...
        + 37.311*(SOC_p(time_node, space_node))^6 ...
        - 73.083*(SOC_p(time_node, space_node))^8 ...
        + 95.96*(SOC_p(time_node, space_node))^10);
end

eta_pos(time_node, space_node) = ...
         Us_p(time_node, space_node) ...
       - Ue_p(time_node, space_node) ...
       - U_eq_p(time_node, space_node);

% Molar Ionic Flux [UNIT: A/m^2]
K_p(time_node, space_node) = r_eff_p * exp(-30000/R ...
```

```
                            *(1/celltmptr(time_node-1) ...
                            - 1/T_amb));
i0_p(time_node, space_node) = ...
      2 * K_p(time_node, space_node) ...
      * sqrt(Ce_p(time_node, space_node) ...
      * (Cs_max_p - Css_p(time_node, space_node)) ...
      * Css_p(time_node, space_node));

J_p(time_node, space_node) = i0_p(time_node, space_node) ...
                            * sinh((0.5*F ...
                            *eta_pos(time_node, space_node)) ...
                            / (R*celltmptr(time_node-1)));

q_p(time_node, space_node) = i_app*23.7*(-(3*epss_pos * F ...
                            * J_p(time_node, space_node))/Rp_p ...
                            * (eta_pos(time_node, space_node) ...
                            - dudt*celltmptr(time_node-1)) ...
                            - Ue_p(time_node, space_node) ...
                            * Ie_p(time_node, space_node) ...
                            + Us_p(time_node, space_node) ...
                            * (I - Ie_p(time_node, space_node)));

qp_lump(time_node, space_node) = ...
        ((3 * epss_pos * F ...
       * J_p(time_node, space_node))/Rp_p) ...
       * (U_eq_p(time_node, space_node) ...
       - (dudt * celltmptr(time_node - 1)));

end
```

```
% End of Node Point Calculations in one iteration

   Open Circuit Potential


ocp(time_node) = U_eq_p(time_node, 1) ...
               - U_eq_n(time_node, 1);
Voltage(time_node) = Us_p(time_node, 1) ...
                   - Us_n(time_node, 1);
```

Temperature Calculation

```
if charge == true
i_curr = I;
celltmptr(time_node) = celltmptr(time_node - 1) + ((-h * ...
                     (celltmptr(time_node - 1) - T_amb)) ...
                     + (sum(qn_lump(time_node, :)) * L_n) ...
                     + (sum(qp_lump(time_node, :)) * L_p) ...
                     + (i_curr * Voltage(time_node))) ...
                     *dt/rho_cp_avg;
else
i_curr = -I;
celltmptr(time_node) = celltmptr(time_node - 1) - ((-h * ...
                     (celltmptr(time_node - 1) - T_amb)) ...
                     + (sum(qn_lump(time_node, :)) * L_n) ...
                     + (sum(qp_lump(time_node, :)) * L_p) ...
                     + (i_curr * Voltage(time_node))) ...
                     *dt/rho_cp_avg;
end
```

```
celltmptr_rate(time_node) = (celltmptr(time_node) ...
                           - celltmptr(time_node-1))/dt;
```

Controller Settings

Maximum Charge

```
if charge == true
Q(count) = Q(count-1) - (I*dt);

SOC(count) = (Q(count)/(R_Cap)) + init_soc;

count = count + 1;

else
Q(count) = Q(count-1) + (I*dt);

SOC(count) = init_soc - (Q(count)/(R_Cap));

count = count + 1;

end
Current(time_node) = I;
Cs_n_avg(time_node) = sum(Cs_n(time_node,:))/N_n;
SOC_Cs(time_node) = Cs_n_avg(time_node)/Cs_max_n;
```

Post Processing

```
% Battery Simulation Selection - Mode 1: ...
  Charge, Mode 2 = Discharge, Mode
% 3: HPPC and Mode 4: Optimal Control.

 if mode == 1 || mode == 2 || mode == 3
 [I, charge] = load_current(time_node, i_app, mode, 1);
 else
 Control_Law;
 end

 SOC_n_CuSum = 0;
 SOC_p_CuSum = 0;
 for i = 1:N_n
 SOC_n_CuSum = SOC_n_CuSum + SOC_n(time_node, i);
 end
 for i = 1:N_p
 SOC_p_CuSum = SOC_p_CuSum + SOC_p(time_node, i);
 end
 SOC_n_avg = SOC_n_CuSum/N_n;
 SOC_p_avg = SOC_p_CuSum/N_p;
 if (time_node == (2 + (plot_step*time_stamp))) ...
                     && time_node <= max_time

 fprintf('Time Node = %d\n',time_node);
 fprintf('Open Circuit Potential = %f\n Cell Voltage = ...
                %f\n',ocp(time_node), Voltage(time_node));
```

```
time_stamp = time_stamp+1;
no_of_iter = no_of_iter + 1;
end
% End of Iteration within each time step for convergence
if charge == true
if SOC_Cs(time_node) > 0.90
break;
end
if (ocp(time_node) > 4.2 || Voltage(time_node) >= 4.3 || ...
Q(time_node) > (R_Cap-0.5)*3600 || ...
SOC_n_avg > 0.95 || SOC_p_avg < 0.09)


fprintf('Battery Fully Charged !!! SOC = %f\n', ...
                SOC(time_node));
break;
end
else
if SOC < 0.05
break;
end
if (ocp(time_node) < 2.6 || Voltage(time_node) <= 2.5 || ...
Q(time_node) > (R_Cap-0.5)*3600 || ...
SOC_p_avg > 0.99 || SOC_n_avg < 0.01)

fprintf('Battery Fully Discharged !!! SOC = %f\n', ...
          SOC(time_node));
break;
end
```

```
 end

Time Node = 2
Open Circuit Potential = 4.171340
 Cell Voltage = 4.157122

Time Node = 102
Open Circuit Potential = 4.126843
 Cell Voltage = 4.113110

Time Node = 202
Open Circuit Potential = 4.095992
 Cell Voltage = 4.082620

Time Node = 302
Open Circuit Potential = 4.068442
 Cell Voltage = 4.055356

Time Node = 402
Open Circuit Potential = 4.043195
 Cell Voltage = 4.030336

Time Node = 502
Open Circuit Potential = 4.019680
 Cell Voltage = 4.007002

Time Node = 602
Open Circuit Potential = 3.997559
 Cell Voltage = 3.985023
```

```
Time Node = 702
Open Circuit Potential = 3.976621
 Cell Voltage = 3.964194

Time Node = 802
Open Circuit Potential = 3.956736
 Cell Voltage = 3.944389

Time Node = 902
Open Circuit Potential = 3.937819
 Cell Voltage = 3.925525

Time Node = 1002
Open Circuit Potential = 3.919816
 Cell Voltage = 3.907551

Time Node = 1102
Open Circuit Potential = 3.902691
 Cell Voltage = 3.890430

Time Node = 1202
Open Circuit Potential = 3.886416
 Cell Voltage = 3.874137

Time Node = 1302
Open Circuit Potential = 3.870971
 Cell Voltage = 3.858651
```

```
Time Node = 1402
Open Circuit Potential = 3.856336
 Cell Voltage = 3.843951

Time Node = 1502
Open Circuit Potential = 3.842486
 Cell Voltage = 3.830012

Time Node = 1602
Open Circuit Potential = 3.829394
 Cell Voltage = 3.816806

Time Node = 1702
Open Circuit Potential = 3.817022
 Cell Voltage = 3.804291

Time Node = 1802
Open Circuit Potential = 3.805316
 Cell Voltage = 3.792413

Time Node = 1902
Open Circuit Potential = 3.794206
 Cell Voltage = 3.781097

Time Node = 2002
Open Circuit Potential = 3.783591
 Cell Voltage = 3.770238
```

```
Time Node = 2102
Open Circuit Potential = 3.773332
 Cell Voltage = 3.759690

Time Node = 2202
Open Circuit Potential = 3.763232
 Cell Voltage = 3.749250

Time Node = 2302
Open Circuit Potential = 3.753011
 Cell Voltage = 3.738627

Time Node = 2402
Open Circuit Potential = 3.742271
 Cell Voltage = 3.727408

Time Node = 2502
Open Circuit Potential = 3.730430
 Cell Voltage = 3.714994

Time Node = 2602
Open Circuit Potential = 3.716639
 Cell Voltage = 3.700505

Time Node = 2702
Open Circuit Potential = 3.699616
 Cell Voltage = 3.682620
```

```
Time Node = 2802
Open Circuit Potential = 3.677377
 Cell Voltage = 3.659288

Time Node = 2902
Open Circuit Potential = 3.646676
 Cell Voltage = 3.627153

Time Node = 3002
Open Circuit Potential = 3.601717
 Cell Voltage = 3.580209

Time Node = 3102
Open Circuit Potential = 3.530313
 Cell Voltage = 3.505815

Time Node = 3202
Open Circuit Potential = 3.397500
 Cell Voltage = 3.367700

Battery Fully Discharged !!! SOC = 0.065447

Simulation Completed

Total Time Consumed == 274.406849

end
time_consumed = toc;
fprintf('\nSimulation Completed\n');
fprintf('\nTotal Time Consumed == %f\n', time_consumed);
```

Plotting the Simulation Data

```
time_vec = 1:1:time_node;
figure(1);
[ax, p1, p2] = plotyy(time_vec, Voltage, time_vec, celltmptr-273);
ylabel(ax(1),'Cell Voltage (V)')                % label left y-axis
ylabel(ax(2),'Cell Temperature (DegC)')         % label right y-axis
xlabel(ax(2),'Time (Seconds)')                  % label x-axis
grid on;

if mode ~= 3
   Current = -Current;
end

figure(2);
[bx, p11, p22] = plotyy(time_vec, Voltage, time_vec, Current);
ylabel(bx(1),'Cell Voltage (V)')                % label left y-axis
ylabel(bx(2),'Load/Charge Current (A/m^2)')     % label right y-axis
xlabel(bx(2),'Time (Seconds)')                  % label x-axis
grid on;

figure(3);
plot(SOC*100, -Current);
ylabel('Load/Regen Current (A/m^2)')            % label y-axis
xlabel('SOC (%)')                               % label x-axis
grid on;

figure(4);
subplot(2,3,1);
```

```
mesh(SOC_n*100); title('SOC_n'); xlabel('N_n');ylabel('Time');zlabel('%')
subplot(2,3,2);
mesh(Ie_n); title('Ie_n'); xlabel('N_n');ylabel('Time');zlabel('A/m^2')
subplot(2,3,3);
mesh(Us_n); title('PhiS_n'); xlabel('N_n');ylabel('Time');zlabel('V')
subplot(2,3,4);
mesh(SOC_p*100); title('SOC_p'); xlabel('N_p');ylabel('Time');zlabel('%')
subplot(2,3,5);
mesh(Ie_p); title('Ie_p'); xlabel('N_n');ylabel('Time');zlabel('A/m^2')
subplot(2,3,6);
mesh(Us_p); title('PhiS_p'); xlabel('N_p');ylabel('Time');zlabel('V')



% samexaxis('abc','xmt','on','ytac','join','yld',1);



% ######################################################################

%%
% ######################################################################
%                           Optimal Controller
% ######################################################################
%
% Author :: Sourav Pramanik
%
% Course :: Master of Science - Thesis
%
% Date :: 20th November 2014
%
```

```
% Department :: Mechanical Engineering
%
% Institution :: Indiana University Purdue University Indianapolis
%
% Description :: This is the controller set up file for optimal
%                regeneration of the battery. The cost function is
%                solved using Hamiltonian method following
%                Pontryagin's Maximum Principle
%
% ########################################################################

%%



zeta = epss_neg*F*L_n;
alpha = 0.01;
beta = 5;
T_max = 40+273;


% ------------------------------------------------------------------
%             Control Law with Temperature
% ------------------------------------------------------------------

lambda_2(time_node)*Voltage(time_node)/rho_cp_avg;

lambda_1(time_node) = lambda_1(time_node-1);
```

```
delta(time_node) = ((alpha_ac*sum(eta_neg(time_node,:))/N_n)...
                   /((R*celltmptr(time_node))^2)) ...
                   * ((6*sum(i0_n(time_node,:))/N_n)) ...
                   *cosh((alpha_ac*F*sum(eta_neg(time_node,:)) ...
                   /N_n)/(R*celltmptr(time_node)));

gamma(time_node) = ((3*epss_neg*F*dudt*sum(J_n(time_node,:)) ...
                  /Rp_n) + (3*epss_pos*F*dudt*sum(J_p(time_node,:)) ...
                  /Rp_p)) / rho_cp_avg;

lambda_2(time_node) = ((((2*beta)*(T_max - ...
                          celltmptr(time_node - 1))) ...
                       + (lambda_2(time_node - 1)*(h/rho_cp_avg)) ...
                       - (lambda_2(time_node - 1) ...
                       * gamma(time_node - 1)) ...
                       - (lambda_1(time_node - 1) ...
                       * delta(time_node - 1)))*dt) ...
                       + lambda_2(time_node - 1);

I = I_max - (lambda_2(time_node)*Voltage(time_node) ...
             /rho_cp_avg)/(2*alpha);
```